THE UNIVERSITY OF ADELAIDE

Evolution of the basal Adelaidean in the northern Flinders Ranges: deposition, provenance and deformation of the Callanna and lower Burra Groups

Ashleigh Job

Supervisors:

Alan Collins

David Giles

Centre for Tectonic Resources and Exploration,

Department of Geology and Geophysics,

School of Earth and Environmental Sciences,

University of Adelaide, South Australia

Ashleigh.job@student.adelaide.edu.au

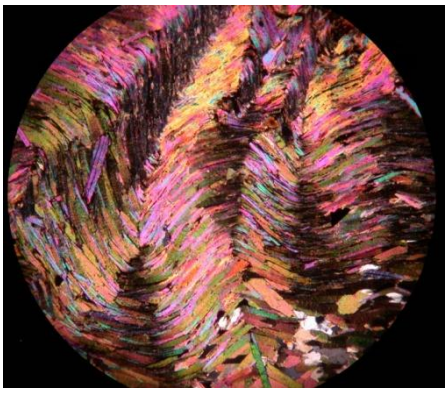

ABSTRACT

The rift and deformational evolution of the Adelaide Fold Belt's northern-most extent, the northern Flinders Ranges, has received comparatively little attention than that of the southern Adelaide Fold Belt. The Arkaroola area, located in the mid-north northern Flinders Ranges, exposes the lowermost Adelaidean stratigraphy of this rift complex, the Callanna and lower Burra Groups, in a near complete sedimentary sequence. The rift history of this stratigraphy is complex, with deposition being largely controlled by the northeast-southwest orientated Paralana Fault and similarly orientated local growth faults. Locally, the Paralana Fault deviates from its regional orientation and forms a north-south striking segment, which under a considered sinistral strike-slip regime during extension would potentially create localised transtension in a 'releasing bend' environment. Rifting in the Arkaroola area is therefore considered to be analogous to the formation of a pull-apart basin.

U-Pb dating of detrital zircons from the Paralana Quartzite, Humanity Seat Formation and Blue Mine Conglomerate from the Callanna and lower Burra groups yields ages that are comparable to local source regions the Gawler Craton, Mount Painter Basement Complex and the Curnamona Province, and suggest proximal derivation during early rift phases. Sm-Nd bulk rock analysis on the finer grained Woodnamoka Formation implies derivation from the Mount Painter Basement Complex or the upper Willyama Supergroup of the Curnamona Province, the latter of which potentially suggests a more distal provenance region outside of the Australian continent.

Deformation in the northern Flinders Ranges has previously been largely ascribed to the *ca*. 500 Ma Delamerian Orogeny. However, the Arkaroola area exhibits complex deformation not observed in the directly overlying gently folded stratigraphy. Reactivation of pull-apart rift structures during transpression is considered a possible mechanism for producing and localising such deformation. The possibility of an early Neoproterozoic deformational event occurring prior to deposition of the lesser-deformed overlying stratigraphy is also considered, but in lieu of an unequivocal orogenic unconformity, cannot be confidently ascribed. Temporal constraints defined by this study are too broad to accurately define the timing of deformation, and therefore its timing and potential relationship to the Delamerian Orogeny remains largely enigmatic.

Key Words: northern Flinders Ranges**,** Mount Painter Province, Arkaroola, Adelaidean, Rifting, Deformation, Provenance, Detrital U-Pb, Bulk rock Sm-Nd, Transtension, Transpression

1. Introduction

The Adelaide Fold Belt (AFB) is comprised of the Neoproterozoic-Cambrian aged Adelaidean sedimentary rocks, deposited in a complex of deeply subsided sedimentary basins, which have been subsequently deformed and now form the north-south trending uplifted topography of the Mount Lofty and Flinders Ranges (Preiss 1987; Wingate *et al.* 1998). Knowledge of the rift and deformational history of the northern Flinders Ranges remains limited, with published data largely focused on the AFB's southern extent.

The Arkaroola area, located in the Mount Painter Province (MPP) of the mid-northern Flinders Ranges, exposes the lowermost Adelaidean stratigraphy of the Callanna and Burra groups in a near complete sequence. Here the rift history has received relatively little attention; in particular the depositional environment and sediment provenance of these early rift sediments are poorly understood. Early rift sediments are proposed to have been deposited in an intracratonic rift setting (Preiss 1987; Powell 1994) and therefore sourced from surrounding cratonic provinces; however there is currently limited data available to support this inference. Deformation in the Arkaroola area is of particular interest as it exhibits a localised complexity that is not observed in the directly overlying sediments. Deformation and metamorphism in the northern Flinders Ranges have largely been assigned to the *ca*. 500 Cambro-Ordovician Delamerian Orogeny. However, the highly localised nature of such deformation in the Arkaroola area raises the possibility of a deformational event occurring prior to deposition of lesser deformed overlying sediments in the early Neoproterozoic.

This study aims to firstly address the nature of rifting in the Arkaroola area and investigate potential source regions of early rift sediments, using a combination of lithological analysis and geochronological and isotopic analytical methods.

Sedimentary provenance is of interest because it can help to constrain the proximity of potential source regions at the time of deposition, therefore assisting to construct a more accurate depositional history. The robustness of the Sm-Nd isotope system during diagenetic, sedimentary and metamorphic processes makes it ideal for sedimentary provenance (McCulloch and Wasserberg 1978). Nd model ages represent the average crustal residency time for components of the sediment, meaning they can be used to determine contributions of reworked crustal material and younger, mantle derived components. Isotopic εNd values are particularly useful as they represent deviation of the sample's

isotopic composition from the Bulk Earth (CHUR) and can be compared directly with possible source regions (McCulloch and Wasserberg 1978).

U-Pb detrital zircon data provide specific source rock ages. This method is useful because zircon is a stable heavy mineral with a high closure temperature that can withstand recycling events and is easily preserved in clastic sedimentary rocks (Cawood *et al.* 2003). Individual grains can be analysed to obtain age estimates that can then be directly correlated to potential source regions. The youngest detrital component of a rock can also provide a maximum age for deposition of the sedimentary unit which, when used in conjunction with a crosscutting event such as metamorphism or an intrusion, can aid in constraining the age of sedimentation (Fedo *et al.* 2003).Both of these analytical methods are employed in this study in conjunction with detailed lithological analysis to reconstruct the early stages of basinal evolution.

The second aim of this study is to investigate the nature and timing of deformation in the Arkaroola area. Extensive structural mapping and microstructural analysis are employed to firstly investigate the nature and possible mechanisms for such localised, complex deformation, and to secondly to explore if deformation is the result of Delamerian Orogenesis as previously ascribed, or the result of an early Neoproterozoic deformation. Mapping is focused on a ~4 x 4 km area adapted from Preiss (1987) immediately north of the Arkaroola Village, and covers local basement and the Callanna and lower Burra Group.

2. Geological Background and previous work

The Adelaide Fold Belt consists of Paleoproterozoic to Mesoproterozoic crystalline basement overlain by Neoproterozoic and Cambrian sedimentary rocks of the Adelaidean, deposited in a complex of deeply subsided sedimentary basins during which time Australia was part of the supercontinent Rodinia (Powell *et al*. 1994). The sediments have been subsequently deformed and now form the north-south trending uplifted topography of the Mount Lofty and Flinders Ranges (Preiss 1987; Wingate *et al*., 1998). It can be divided into four structural domains: the southern Adelaide Fold Belt, the Nackara Arc, the central Flinders Ranges, and the northern Flinders Ranges (Paul *et al*. 1999) (figure 2).

The Mount Painter Province (MPP) is located in the northern Flinders Ranges and consists of two exposed basement blocks, the Mount Painter and Mount Babbage Inliers. It is separated from the Paleoproterozoic-early Mesoproterozoic Curnamona Province to the east by the basement penetrating, steeply dipping Paralana Fault. To the west it is bounded

by the Late Archean-Early Proterozoic Gawler Craton and younger Stuart Shelf, and is separated by the Torrens Hinge Zone and more locally the Norwest Fault (figure 2a) (Paul *et al*. 1999; Payne *et al*. 2008). The crystalline basement forming the inliers is composed of Neoproterozoic-Mesoproterozoic metasedimentary rocks that have been intruded by Mesoproterozoic and Ordovician granites (McLaren *et al*. 2002). These units are overlain by 7-12 km of the Neoproterozoic and Cambrian Adelaidean sedimentary rocks, consisting of basal rift sequences unconformably overlain by younger, extensive sag phase sequences, which were deposited in the northern Flinders Ranges under ~ northeast-southwest extension (Preiss 1987; Powell *et al*. 1994).

The initial rift sequence is comprised of the early Cyrogenian Callanna group, which can be divided into the Arkaroola and Curdimurka subgroups. The Arkaroola Subgroup is regionally localised around the Paralana Fault, which is considered a primary growth structure (Preiss, 1987). Stratigraphically overlying these sediments are the voluminous mafic Wooltana Volcanics, which have stratigraphic equivalents throughout the AFB, the Curnamona Province and the Gawler Craton as well as in surrounding basins (Preiss 1987; Hilyard, 1990). Average tholeiitic compositions suggest they were extruded as extensive continental flood basalts (Hilyard 1990). The Gairdner Dyke Swarm, an equivalent recognised in the Stuart Shelf, has a $^{207}Pb/^{206}Pb$ age of 827 ± 6 Ma, which has been considered an emplacement age for the Wooltana Volcanics (Wingate *et al*. 1998).

The Curdimurka Subgroup is absent from the Arkaroola area. Disconformably overlying the Arkaroola Subgroup is the Burra Group, associated with the onset of sag phase sedimentation and a broader rift zone (Preiss 1987; Powell *et al*. 1994).The Gawler Craton and Curnamona Province, as well as local Mount Painter Basement, have been considered prominent source regions for these basal Adelaidean sediments (Preiss 1987; Turner *et al.* 1993; Powell *et al.* 1994)

This stratigraphy is unconformably overlain by the rift and sag phase Umberatana Group and the true sag phase Wilpena Group. Deposition of the Adelaidean continued until termination with the onset of the *ca.* 500 Ma Cambro-Ordovician Delamerian Orogeny (Paul *et al.* 1999).

The northern Flinders Ranges is characterised by thick skinned deformation involving the inversion of basement-penetrating growth faults. Both basement and cover are broadly deformed into upright, basement-cored east-northeast trending km scale folds which around the Mount Painter Inlier (MPI) swing northwards into the Paralana Fault (figure 1b)

(Sandiford *et al.* 1998; Paul *et al*. 1999). The Arkaroola area exhibits highly localised, intensified deformation that is notably more complex than the surrounding region.

The Paralana Fault appears to have largely controlled rifting and deformation in the Arkaroola area (Sandiford *et al*. 1998; Paul *et al*. 1990). Preiss (1987) and Paul et al. (1999) suggest it had a strike-slip displacement, however this remains poorly constrained.

An unusual style of metamorphism is observed in the MPP, which sees sediments rapidly grading from lower greenschist to amphibolites facies at the basement-cover contact. This has been attributed to extraordinarily high concentrations of heat-producing elements in the Mount Painter Basement (Sandiford *et al*. 1998; Mildren and Sandiford, 2007).

Deformation and metamorphism in the northern Flinders Ranges, and subsequently the Arkaroola area, have been largely ascribed to the Delamerian Orogeny due to a similarity in structural style to Delamerian-aged deformation and metamorphism in the southern AFB (Paul *et al.* 1999; Foden *et al*. 2002; Elburg *et al.* 2003). This is supported by a minor thermal event at ~ 495 Ma in the MPP (Elburg *et al*. 2003), with a major thermal pulse at 440 Ma also recognised (Elburg *et al.* 2003). However, there is no further geochronological evidence available to accurately constrain the timing of deformation in the MPP and its relationship to the Delamerian Orogeny.

$^{40}Ar/^{39}Ar$ and K/Ar thermochronology by McLaren *et al*. (2002) shows three cooling episodes affecting the MPP at 430, 400 and 330-320 Ma; the latter two of which are suggested to be the result of the 400-320 Ma Alice Springs Orogeny, a major intraplate tectonothermal event that took place throughout central Australia. This, and supplementary work by Pointon (2010) and Mitchell *et al.* (2002) suggests the MPP has also been the subject of an intracontinental orogenesis in relation to the Alice Springs Orogeny.

3. Structural and field relationships

3.1 Lithology

A geological map of the Arkaroola area is presented in figure 1 (see attached).

3.1.1 Mount Neill Granite Porphyry

The crystalline basement complex of the southernmost Mount Painter Inlier is composed of the Mount Neill Granite Porphyry, a massive granite composed of quartz, K-feldspar, biotite and minor muscovite. Locally, within the map area, it is characterized by ~ 1 cm pale blue quartz phenocrysts and abundant K-feldspar supported in a fine grained matrix. Within 30-50 m of the unconformity with the overlying Adelaidean sediments it shows the development of a strong, pervasive shear fabric sub-parallel to the contact. Initially, it is observed as a weak foliation, which develops into a strong proto-mylonitic shear fabric and finally to a micaceous mylonite associated with grain size reduction and ptygmatic veining at the contact (Figure 6a).

3.1.2 Paralana Quartzite

Unconformably overlying the Mount Neill Granite is the Paralana Quartzite. The basal member of this unit is variable within the Arkaroola area, most commonly commencing with a poorly sorted pink-pale grey quartzite. In other locations throughout the map area, it is observed to be a poorly sorted, impure, coarse pink to grey sandstone with heavy mineral lamination, rare ripple marks and cross laminations. The Paralana Quartzite then fines into a well-sorted medium grained pink to pale grey weathering quartzite. The basal Paralana Quartzite often shows reidel shear fractures at the contact with the Mount Neill Granite Porphyry. Striking across the Paralana Quartzite-basement contact to the east of the map area is 10-30 m of recrystallised quartz, potentially formed through hydrochemical action associated with metasomatism (Elburg *et al.* 2003).

The Paralana Quartzite shows an average thickness of 350 m in the map area, with changing facies distributions across the Paralana Fault to the east of the map area suggesting pene-contemporaneous faulting.

3.1.3 Wywyana Formation

The Paralana Quartzite grades conformably into the overlying Wywyana Formation, becoming increasingly calcic and less clastic with interbeds of quartz rich arenite and calcsilicate. The Wywyana Formation is composed of metamorphosed calcsilicates with minor interbedded evaporates, and is characterized in the field by its low topographic relief. The top of the formation is comprised of a distinctive thick dolomitic horizon that has been recrystallised in places to form <5mm dolomite “rhombs”, with secondary wholly crystallized actinolite and tremolite. Throughout the mapping area, the Wywyana Formation has been locally altered to a massive actinolitic rock with lesser biotite, epidote and tremolite, which often forms thick veins. The Wywyana Formation has a highly variable thickness due to local intense folding with an estimated average of ~ 200 m in the map area.

3.1.4 Wooltana Volcanics

Stratigraphically overlying the Wywyana Formation are the Wooltana Volcanics, which outcrop as blocky, grey weathering fine grained basic volcanics. The volcanics show various porphyroblastic and vesicular textures, and northwest of Dinnertime Hill exhibit an amygdaloidal texture, infilled with a pale white altered mineral, possibly quartz, stilbite or microcline. Locally the volcanics are scapolitized with common abundant secondary actinolite occuring on planar surfaces, also related to later metasomatism (Elburg *et al*. 2003).

3.1.5 Humanity Seat Formation

The Humanity Seat Formation is the basal unit of the Burra Group, and although not directly observed in the map area, disconformably overlies the Arkaroola Subgroup in a ~ 450 m thick wedge. It is a grey, medium grained quartz rich sandstone, interbedded with rare lenses of coarser grains and characterized by abundant heavy mineral lamination.

Overlying the Humanity Seat Formation is a ~165 m thick diamictic sedimentary breccia of the same material, which similarly forms a wedge and thins to the west. It is characterized by subangular to subrounded 2-8 cm diameter clasts of predominately quartzite and vein quartz. Rare chert and volcanic clasts occur, likely derived from the Wooltana Volcanics. It shows strong continuity with the Humanity Seat Formation, and has

therefore been considered a stratigraphic member and named the Arkaroola Creek Breccia Member.

3.1.6 Woodnamoka Formation

Conformably overlying the Arkaroola Creek Breccia Member is the Woodnamoka Formation, only present to the west of the Paralana Fault and whose thickness is hard to estimate due to strong folding and deformation.

The formation commences with a pale grey micaceous arenite. This rapidly grades into a distinctive ridge forming feldspar-rich arenite named the Mt Oliphant Arkose Member, estimated to be ~150 m thick. The arkose is moderately micaceous and preserves abundant cross lamination and ripple marks.

Situated stratigraphically above the Mt Oliphant Arkose Member is a significantly thicker pelitic horizon, consisting of laminated silty phyllite often characterised by abundant ripple marks.

The top of the Woodnamoka Formation is a gritty red-weathering arenite, characterised by heavy mineral laminations and minor interbedded silts. This horizon is considered to be transitional with the Blue Mine Conglomerate, as rare clasts associated with the overlying unit can be found within it near the contact.

The Woodnamoka Formation is variably metamorphosed, locally reaching amphibolite facies conditions from a mostly pelitic protolith, with the common development of andalusite and cordierite porphyroblasts largely dependent on the aluminium component. These porphyroblasts are most commonly associated with andalusite/cordierite-biotite schists, usually interbedded in 10-20 m thicknesses. Late thermal overprinting, likely related to the 440 Ma thermal pulse (Elburg *et al.* 2003), is evidenced by late overgrowth on surfaces by coarse muscovite, as well as the retrogression of porphyroblasts to fine grained sericite and pinite.

3.1.7 The Blue Mine Conglomerate

The Blue Mine Conglomerate is a ~ 150-750 m thick unit comprised of medium to fine grained arkosic sandstone with abundant clasts, interbedded with grits and blue-grey siltstones that are often heavily weathered to orange clays. It is characterised by heavy mineral lamination, ripple marks and tabular cross lamination.

The clast population across the unit is heterogeneous. To the east, clasts are composed of quartzite, vein quartz, fresh K-feldspar, minor red cherts and various lithic fragments, supported by a medium grained sandstone matrix. Toward the west it becomes almost clast supported with abundant 0.5-1 cm clasts composed predominately of rounded pale blue quartz and K-feldspar, suggesting a proximal derivation from the Mount Neill Granite.

3.1.8 Opaminda Formation

The Opaminda Formation marks the base of the 'upper Burra Group' and is notably more extensive than the underlying lithologies. It is comprised of actinolite rich dolomitic shales that grade into a well bedded dark grey siltstone with preserved ripple marks and mudcracks. The lower boundary of the Opaminda Formation in the west of the map area forms an angular unconformity, with the Opaminda Formation steeply juxtaposed against older stratigraphy. To the east, this contact with the Blue Mine Conglomerate is largely eroded by tributaries and is only truly observed in one location. Here it is abrupt but conformable, with the Blue Mine Conglomerate folding sharply into the boundary with apparent continuation of folding across the contact.

3.1.9 Late igneous intrusions

A number of late igneous intrusions occur in the Adelaidean cover. These include the coarsely crystalline sodic leucogranites that form the Pinnacles and Sitting Bull (Elburg *et al.* 2002),the Arkaroola Pegmatite to the north of the map area, and several smaller intrusions of similar composition. A small mafic intrusion also occurs to the east of Sitting Bull in the Opaminda, possibly of doleritic composition. Ages for these intrusives vary between 514-485 Ma, as well as 440 Ma (Elburg *et al.* 2003; Farrand and Preiss 1995).

3.2 Structure

Section lV-lV' (figure 4d) and figure 6a illustrate lithologies to the east of the map area showing comparatively little deformation and dipping uniformly to the south. Elsewhere the lithologies are heavily affected by deformation.

3.2.1 Fabrics

The Woodnamoka Formation, due to its rheology and metamorphic grade, preserves multiple deformational events that have affected the area and is therefore useful in determining relationships between fabrics and folding. A structural type section in the phyllite member to the eastern side of Mount Oliphant is used to demonstrate these relationships, where they are excellently preserved.

The Woodnamoka Formation is characterised by a continuous to zonal pervasive foliation that is defined by the alignment of platy minerals ands consistently exhibits a low angle to bedding (~10-20°). This fabric is often seen crenulating a shallowly dipping earlier fabric, 'S_1', also defined by the alignment of micas (figure 5a). Measured intersections between bedding (S_0) and the later schistosity 'S_2' form a 'streaky' intersection lineation ($L_{Z\text{-}0}$) and show a predominant southwest plunge (figure 7d). When observed in the same outcrop, both 'S_1' and 'S_2' appear to share the same intersection lineation (figure 5b, c). This, as well as the similarity of their character, indicates they were formed progressively, and have therefore been considered a composite foliation and named S_Z. Heterogeneously developed c-s fabrics (figure 6c, d) suggest a component of non-coaxial shear. Elongate porphyroblasts and rare mineral stretching lineations also suggest a component of extension within the foliation plane (figure 6e). When unfolded S_Z is sub-horizontal (figure 7g).

S_Z is associated with the common growth of andalusite and cordierite porphyroblasts. When viewed under a handlense the fabric appears to largely wrap around the porphyroblasts, which often feature inclusions of an earlier fabric, suggesting their growth is syntectonic with fabric development. The porphyroblasts commonly show developed strain shadows, indicative of a later deformational event.

The mylonitic fabric in the Mount Neill Granite, assigned S_B, suggests a highly localised shear zone along the basement contact. Reidel shears in the basal Paralana Quartzite suggest shear was differentially accommodated by the basement and Adelaidean. The fabric displays excellent kinematic indicators, with developed c-s fabrics as well as more

resistant quartz phenocrysts forming sigma clasts (figure 6b). Kinematics taken from the basement near the contact to the east of the map area suggest top-block to the southwest, and to the west show top-block to the northeast. A mineral stretching lineation associated with the fabric plunges northeast-southwest into the basement contact (figure 7e).

A third cleavage (S_3) is observed as an upright asymmetric crenulation cleavage produced by the microfolding of S_Z, and is developed primarily in fold hinges and most readily observed in the Woodnamoka Formation's phyllite member. It is associated with a mm scale 'corrugation' like crenulation intersection ($L_{3\text{-}Z}$), which has a northwest plunge, similar to $L_{Z\text{-}0}$ (Figure 7f).

A distinct pressure solution cleavage is observed in coarser rheologies. The Mount Oliphant Arkose Member exhibits this cleavage at a high angle to bedding, indicating a hinge zone. A single cleavage seen in the Blue Mine Conglomerate and Humanity Seat Formation is similar in nature but at a low angle to bedding. The often low angle of this cleavage to bedding suggests it is potentially associated with S_Z, however, its axial planar orientation to a prominent fold set named F_3, discussed in the following section, suggests it is a different cleavage, and has been named F_3. A lack of preservation of S_Z in coarser rheologies suggests it was not expressed in mica-poor formations, or has been overprinted.

3.2.2 Folds

The most prominent fold set affecting the map area is of a northeast-southwest hinge plunge orientation, with folds of < 500 m wavelength. The structural type section intersects an upright syncline of this generation, which folds S_0 as well as S_Z, indicating it is the result of an event post dating S_Z (Figure 7h). S_3 is developed as a crenulation cleavage in the hinge zones of these folds and is largely axial planar. Fold hinge orientations are also comparable to the shallow southwest plunge of $L_{3\text{-}Z}$, and therefore folds have been assigned to F_3. Numerous smaller scale folds, well formed and tight in the Wywyana and Woodnamoka Formations (figure 5d) and more open and poorly developed in coarser rheologies, have a similar orientation and are considered to be parasitic.

Sections I-I' and II-II' (figure 4a,b) highlight a broad syncline that dominates the western side of the map area, trending northwest-southeast with a broad hinge zone located in the Woodnamoka Formation (figure 6g; figure 7b). It is largely responsible for the observed map pattern to the west, seeing older stratigraphy being exposed by the fold's

limbs suggesting a shallow plunge to the east-southeast. The fold's hinge appears to 'die out' to the west of the Mt Oliphant peak, as highlighted by section lV-lV' (figure 4d).

Observed cleavages could not be attributed to this fold, possibly due to its broad, open nature resulting in no fabric generation. Both $L_{Z\text{-}0}$, basement mineral lineations and $L_{3\text{-}Z}$ show folding around a northwest-southeast axis that correlate with the syncline's approximate hinge, therefore the fold has been assigned F_4 (figure 7d, e, f).

F_3 and F_4 produce a classic type 1 dome and basin fold interference pattern (Ramsay, 1962) (figure 3). The interaction of the F_4 sycline and an F_3 syncline to the west of the Mount Oliphant Peak forms a prominent 'basin' structure, which is responsible for both the eastern and western ends of the syncline plunging shallowly in toward the middle (figure 7c). Immediately to its east stratigraphy 'pops up' due to interference between the F_4 syncline and an F_3 anticline, named the Mt Oliphant Anticline.

Prominent F_3 folds appear to be truncated by the Opaminda Formation. Intense, tight folding is observed at its base, suggesting it has accommodated some shortening. However, the described deformational structures of the Arkaroola area are not apparent in the overlying Wortupa Quartzite.

Despite being readily apparent, S_Z could not clearly be associated with any of the observed folds.

3.2.3 Faults

A number of faults in the map area were recognised using crush breccia, slickenslides, growth fibres and offset criteria.

A northeast-southwest striking fault occupies the northwest corner of the map area, coinciding with the basement contact, and is informally referred to as the 'top-northwest fault' (figure 3). The map pattern shows that the Arkaroola Subgroup thickens significantly toward it, suggesting it is a growth fault and was a primary control of deposition. It is characterised by a strong fabric, heavily reduced grain size and extreme muscovite retrogression, indicating a fluid rich history.

A second predominant fault bounds the east of the map area, named the Arkaroola Bore Fault, and juxtaposes the Humanity Seat Formation against an outcrop of the Wooltana Volcanics immediately east of the map area (figure 3). The Humanity Seat Formation thickens eastward towards this fault, suggesting it largely controlled deposition and therefore likely dips to the northwest.

The third major fault recognised in the map area is the Sitting Bull Fault (figure 3). The Blue Mine Conglomerate thickens up toward and is bounded by this fault structure, suggesting it was a primary normal growth fault and controlled deposition of this unit to its south, and therefore likely dips to the southeast. An overturned anticline in the Woodnamoka Formation to the north of the fault creates a geometry that could be likened to ramping on a footwall and "drag" in the overlying sediments, suggesting the Sitting Bull Fault potentially dips to the northwest and has been rotated from its original orientation (figure 4c). The nature of this fault is poorly constrained, so a northwest dip is favoured because of its fit with the overturned anticline geometry. It must also be noted that the overturned anticline could possibly be the result of fold interference with the eastern limb of the Mount Oliphant Anticline to the northeast.

Numerous minor faults are observed throughout the map area and appear to be the result of later brittle zone deformation, with both oblique and reverse offset observed.

3.3 Micro-structure

Three orientated samples were taken from various locations within the Woodnamoka Formation for thin section analysis to further investigate the nature of S_Z and S_3. Microstructural observations are presented below, with additional images displayed in appendix 2.

3.3.1 AARK01

The AARK01 sample was collected from the lowermost Woodnamoka Formation to the east of the map area, where S_Z is prominent. The sample shows zonal cleavage domains of concentrated micas, predominately biotite and muscovite, which are separated by microlithons of largely unfoliated quartzofeldspathic material (figure 8a). The transition between cleavage domains and microlithons is largely gradational, with commonly elongate quartz crystals lengthened within the foliation plane suggesting solution transfer (figure 8b). An earlier foliation is rarely observed in microlithons as elongate mica crystals orientated at a low angle to the cleavage domains, supporting field evidence of an earlier fabric 'S_1', developed at a low angle to the predominant 'S_2' foliation (figure 8c).

3.3.2 AARK03

Sample AARK03 was collected from the summit of Mount Oliphant where the S_3 crenulation cleavage is present . Thin sections show predominant cleavage domains with only minor, thin microlithons. The cleavage domains are symmetrically, to slightly asymmetrically microfolded, with the hinge of the microfold developed at a high angle to 'S_2' (figure 8d). The crenulations are not associated with the growth of new micas parallel to fold hinges and do not show concentrations of quartz in hinge areas. This suggests they were formed at lower metamorphic conditions and form microfolds, rather than true metamorphic crenulation cleavage. Overgrowth by large muscovite crystals suggests late thermal overprinting, consistent with outcrop observations (figure 8e).

3.3.3 AARK07

Sample AARK07 was taken from the western side of the Woodnamoka Formation's phyllite member. Thin sections show predominant cleavage domains similar to AARK03, and feature ~1-3 mm porphyroblasts. Their blocky, anhedral habit and grayish-blue colour under crossed-polars suggests they are cordierite (figure 8f). Strong alteration to fine grained pinite, developed along cracks and grain margins, as well as to coarser aggregates of various alteration minerals (figure 8f), makes accurate mineral identification difficult. Cleavage domains largely wrap around the porphyroblasts, suggesting pre-kinematic growth (figure 8g). figure 7h shows a porphyroblast that appears to record an earlier internal foliation, suggesting it is possibly syn-kinematic. It should be noted that it is possible that two closely spaced porphyroblasts are depicted, rather than one, which show rotation. These kinematic relationships support field evidence, which suggests that S_Z is associated with pre-syn kinematic porphyroblast growth.

4 U-Pb geochronology of Callanna and lower Burra groups

4.1 Analytical methodology

Analytical techniques for U-Pb isotopic dating of detrital zircon follow those of Payne *et al.* (2006) and are outlined in appendix 1 along with normalisation values. Samples were taken from across the Callanna and lower Burra Groups, and included the Paralana, Humanity Seat and Blue Mine Conglomerate. The Wortupa Quartzite was also sampled but did not yield sufficient detrital zircons.

U-Pb analysis was undertaken using a New Wave 213nm Nd-YAG laser in a He ablation atmosphere, coupled to an Agilent 7500cs LA-ICPMS (Laser Ablation Inductively Coupled Plasma Mass Spectrometer). U-Pb calculations were untaken using the real time correction program GLITTER version 4.0, following the processes outlined by Griffin *et al.* (2008).

4.2 Results

U-Pb Detrital zircon morphologies and description are displayed in table 1 and data displayed in appendix 4.

4.2.1 Paralana Quartzite

Sample ARK002 for the Paralana Quartzite was taken from the Arkaroola Waterhole. 59 grains were analysed, with 49 grains being less than 10% discordant. The detrital zircon probability density plot of ^{207}Pb /^{206}Pb ages (figure 9a) is dominated by one broad peak at ~1610 Ma with individual zircon ages falling between 1800 and 1425 Ma, and a minor peak at ~1758 Ma. Minor populations plot at ~1860 and ~1154 Ma. The youngest zircon grain gives an age of 1154 ± 28 Ma which can be considered the maximum depositional age of the formation. Limited sampling for this sample means that the absence of younger age detrital zircons does not prove their non-existence.

4.2.2 Humanity Seat Formation

Sample ARK004 was collected from the southern lower part of the unit. 81 detrital zircon grains were analysed, with 70 found to be within 10% concordance. Major detrital $^{207}Pb/^{206}Pb$ zircon peaks occur at ~1570 and ~1645 Ma (figure 10a). Minor populations include small peaks at 1876 and 1818 Ma, as well as single grain ages of ~2400 and ~2080 Ma. The youngest zircon grain is 1473 ± 27 Ma, but five of the youngest grains were included in a weighted average which produced a maximum depositional age of 1528 ± 22 Ma (MSWD = 0.13).

4.2.3 Blue Mine Conglomerate

The Blue Mine Conglomerate Formation sample, ARK005, was taken in the Arkaroola Creek from the eastern side of the unit. 103 grains were analysed, 64 of which were within 10% discordance. A dominate detrital $^{207}Pb/^{206}Pb$ zircon peak occurs at ~1585 Ma, with minor populations at around ~1278 and ~1146 Ma (figure 11a). A mean weighted average of the three youngest grains yields an age of 1129 ± 34 (MSWD = 0.72) and can be considered the maximum depositional age.

5. Sm-Nd isotopic analysis of the Woodnomoka Formation

5.1 Analytical methodology

Analytical techniques for whole rock Sm-Nd isotopic analysis and normalisation values are listed in appendix 1. Three samples from the Woodnamoka Formation were selected and then analysed for their Sm and Nd isotopic compositions on a Finnigan MAT 262 Thermal Ionisation Mass Spectrometer (TIMS).

5.2 Results

Sm-Nd isotopic results are presented in table 2 and figure 12. The three samples from the Woodnomoka Formation show highly evolved isotopic signatures with εNd values calculated at 780 Ma of -10.39 to -11.7 and T_{DM} values varying between 2356 and 2051 Ma.

6. Discussion

6.1 U-Pb and Sm-Nd analyses and sediment provenance

The age of the Callanna Group is poorly constrained, with the only current age constraint being given by the 827 ± 6 Ma Wooltana Volcanics (Wingate *et al.* 1998). Detrital zircon grains analysed from the Paralana Quartzite Formation yield a maximum depositional age of 1154 ± 28 Ma. However, given the 827 ± 6 Ma age of given for the Wooltana Volcanics, the true time of deposition and rifting initiation is considered to be closer to ~850 Ma.

Due to the intracratonic nature of rifting, neighbouring basement provinces of the Gawler Craton, Curnamona Province and Mount Painter Basement Complex (MPBC), are investigated as potential sources. Table 5 compares these regions with $^{207}Pb/^{206}Pb$ age ranges for the analysed samples.

The Paralana Quartzite shows a broad range of ages that largely fall between 1800-1425 Ma, which correlate with both the Gawler Craton and MPBC.

The predominant peak at ~ 1610 Ma suggests contribution of < 1603 ± 3 material of the 1605 – 1556 Ma MPBC (Kromkhun, 2010). This is consistent with localisation of Paralana Quartzite around the top-northwest fault, which is bounded by the MPBC. Benton (1993) and O'Halloran (1992) highlight this relationship using εNd mixing models, which show strong compatibility between εNd values of the Paralana Quartzite and the MPBC. This is consistent with lithological observations of a basal unit of the Paralana Quartzite present to the west of the map area, the Shanahan Conglomerate, containing basement-derived clasts (Preiss 1987; Benton 1993).

The broad ~ 1610 Ma Paralana Quartzite population is comprised of a significant portion of > 1603 Ma ages. These are largely comparable to ages of the Gawler Craton, indicating it too provided a significant source (table 5). A lesser peak at ~ 1758 Ma is similar to the 1760-1740 Ma Wallaroo Group (Myers *et al.* 1996), the 1763-1738 Moonta Porphyry (Belousova *et al.* 1999) and the *ca*. 1750 Ma Moody Suite (Dutch *et al.* 2008). The oldest zircon population at ~1860 Ma could be attributed to the *ca.* 1850 Donington Suite (Belousova *et al*. 2009). A discordant grain in the Paralana Quartzite also yielded a ~2400 Ma age, compatible with the late Archean Sleaford and Mulgathing complexes (Swain *et al.* 2005).

The Humanity Seat shows greater correlation with the MPBC than the Paralana Quartzite, and a dominant population peak at ~1570 Ma can be strongly correlated with 1603- 1556 Ma units from the MPBC. Ages > 1603 + 3 Ma, the oldest given age of the MPBC,

can be correlated with the Gawler Craton, suggesting it provided a significant proportion of source material. A prominent population peak at ~1645 Ma is similar in age to the *ca*. 1670-1640 Ma Tarcoola Formation (Howard *et al.* 2011) and the 1656 ± 7 St Peter Suite (Flint *et al.* 1990). A lesser population at ~1876 Ma could potentially be correlated to the *ca*. 1850 Ma Donington Suite (Belousova *et al.* 2009). Correlations with a similarly populated peak at 1818 Ma are less clear. A single zircon grain age of 2080 Ma could correspond with ages given for the 2015 ± 25 Miltalie Gneiss (Fanning *et al.* 1998). A second single grain yielded a 2400 Ma age, which can be correlated with the Sleaford and Mulgathing Complexes (Swain *et al.* 2005).

There is less geochronology from the Curnamona Province available compared to the Gawler Craton, however, both the Paralana Quartzite and Humanity Seat Formation also show potential age correlations with the upper and lower Willyama Supergroup (table 5). The Willyama Supergroup is comprised of metasediments and minor volcanics, and detrital zircon U-Pb analysis by Page et al (2000) yields age populations at 2700-2400 Ma, 2300-2000 Ma, 1870-1850 Ma, *ca*. 1820 Ma and *ca*. 1780 Ma. These correlate with a proportion of the Paralana Quartzite's broad 1800-1425 Ma population, as well as older populations in the Humanity Seat Formation of ~ 1876 Ma and ~ 1818 Ma, as well as ~2400 Ma and ~ 2080 Ma, meaning material being shed from the Curnamona Province into the Arkaroola rift basin remains a possibility.

Sources for the lower Willyama Supergroup are suggested to be the late Archean to Paleoproterozoic Gawler Craton, as well as the Northern Australian Craton, including the Paleozoic Arunta Region and late Archean to early Paleoproterozoic rocks of the Mount Isa, Tanami and McArthur region (Barovich and Hand 2008). The upper Willyama Supergroup is associated with the introduction of a significantly more juvenile source. Barovich and Hand (2008) suggest that the juvenile source terrain of *ca*. 1650 Ma interpreted for the upper Willyama Supergroup is unknown in Australia. Pre-Rodinian reconstruction models place eastern Australia proximal to southwestern Laurentia (Moores 1991; Brookfield 1993; Li *et al.* 1995; Wingate *et al.* 2002), which Barovich and Hand (2008) suggests contains rocks of appropriate geochemical and isotopic signatures that therefore could have therefore supplied such juvenile felsic material into the Willyama Basin. Although source regions outside of the Australian continent have not been considered in this study, a potential correlation between basal Adelaidean sediments and the upper Willyama Supergroup suggest such distal source contributions are a possibility. It must be noted that the various sources comprising the upper and lower parts of the Willyama Supergroup makes direct

comparisons with it ambiguous, and reflects the limitations of using U-Pb dating of detrital zircon based comparisons with potential metasedimentary sources.

The Blue Mine Conglomerate sample does not contain detrital zircon grains older than 1700 Ma (discordant grains record up to 1900 Ma ages). Its dominant narrow peak at ~1585 Ma is similar to the Gawler Craton's 1595-1575 Ma Hiltaba Suite (Flint *et al.* 1993) and 1580 Ma Munjeela Granite (Ferris *et al.* 2004), as well as the 1586 ± 45 Box Bore and 1590 ± 5 Mount Neill Granites of the MPBC (Kromkhun 2010). The high presence of fresh Mount Neill Granite Porphyry material in the Blue Mine Conglomerate support the latter correlation, suggesting exposure of the local basement during rifting and proximal sediment derivation. The sample analysed was selected from the western side of the formation, so includes a greater proportion of fine grained matrix likely derived from more distal sources, which is supported by a relatively minor proportion of ages > 1590 Ma.

Youngest zircon populations in the Paralana Quartzite, Humanity Seat Formation and the Blue Mine Conglomerate of 1280-1140 Ma are significantly younger than the investigated source regions. It is possible that they originate from the Musgrave Province, situated at the northwestern corner of South Australia. This province is dominated by the 1,200-1,140 Ma Pitjantjatjura Supersuite (Wade *et al.* 2008), which correlates with the youngest ages analysed in the Arkaroola samples. Given the interval between 1140 Ma and the onset of rifting ~ 850 Ma, such transport of grains is probable. It must be noted that the minor ~1278 Ma population of the Blue Mine Conglomerate cannot be accounted for by derivation from the Musgrave Province, and its source remains unknown.

Neodymium isotopic data for the Woodnamoka Formation shows model ages between 2356 and 2051 Ma and εNd values of -11.7 to -10.4 calculated at 780 Ma, suggesting the Woodnamoka Formation contains a major component of recycled older crustal material (table 2).

Table 3 compares the Woodnamoka with T_{DM} values for surrounding source regions. It most strongly correlates with T_{DM} values calculated for average early-Proterozoic basement, of 2000-2400 Ma, which includes the MPBC and the Olary and Broken Hill blocks of the Curnamona Province (McCulloch 1987).

Figure 12 shows the isotopic evolution of the Woodnamoka Formation is considerably less evolved than the average Archean and Proterozoic Gawler Craton. Their evolution correlates with the MPBC as well as the *ca.* 1670-1640 Ma upper Willyama Supergroup, suggesting both could be primary sources. Given the localised nature of rifting,

derivation from the MPBC is most probable. However, the Woodnamoka Formation is considerably finer grained than other Arkaroola lithologies, suggesting it could be derived from more distal sources. Direct derivation from the Willyama Supergroup into the developing rift complex therefore cannot be ruled out. Alternatively, the Woodnamoka Formation could be derived from the same sources as the upper Willyama Supergroup, suggesting a source region located outside of the Australian continent as previously discussed. Such distal sources would suggest a broadening of the drainage area into the depocentre.

Interestingly, the Woodnamoka has a considerably more evolved εNd signature than other lithologies from the Callanna and lower Burra Groups (table 4). Samples from the Callanna and lower Burra Group are potentially derived directly from the MPBC, however, some appear to have had also had input from a more juvenile source, potentially the Wooltana Volcanics, giving them a more juvenile isotopic character. This would suggest that the Woodnamoka did not have access to such a juvenile source during deposition.

6.2 Early rift development and deposition of the Callanna and Lower Burra Groups

Early rift development in the Arkaroola area is relatively poorly understood. Local analysis of rifting and depositional environment can provide insight into the earliest phases of basin formation during deposition of the Adelaidean, which can be applied regionally to the northern Flinders Ranges.

The Callanna Group records the first evolutionary stages of extension and rifting in the northern Flinders Ranges. Hilyard (1990) and Wingate *et al*. (1998) suggest the development of early rifting in the AFB was driven by regional domal uplift, associated with dynamic mantle upwelling. Hilyard (1990) proposes broad ‘sag basins’ were formed along the crest of the dome with localised minor rifting along major crustal structures such as the Paralana Fault.

Localised deposition of the Arkaroola Subgroup around the Paralana Fault, characterised by changing facies thicknesses across it, suggests it was an active primary growth fault. The Arkaroola Subgroup is not preserved elsewhere in the northern Flinders Ranges, supporting the notion it was deposited away from the Paralana Fault as thin veneers in shallow basins away from the Paralana Fault, which have since been eroded.

In the Arkaroola area, deposition of the Arkaroola Subgroup appears to have been controlled by the top-northwest fault and thickens toward it, suggesting a half-graben geometry. The poorly sorted nature of the lowermost Paralana Quartzite suggests a variable energetic environment, consistent with minor alluvial fans being shed from the top-northwest fault scarp. Heavy mineral laminations and ripple marks indicate these sediments were deposited into a shallow body of water with limited tidal influence (figure 13a). A rapid change to well sorted quartzite in the upper Paralana Quartzite indicates a minor transgression, and the mature nature of sediments suggests a longer residence time. Deposition of the Paralana Quartzite was followed by a highly gradational transition into the Wywyana Formation reflecting a lowering of clastic source.

The ensuing Wooltana Volcanics appear to thicken toward fault structures in the map area, and are regionally localised around the Paralana Fault, suggesting their eruption was facilitated by fault structures. A lack of significantly thick sequences at the level of the volcanics suggests rifting was still relatively minor (figure 13b).

The overlying lower Burra Group is characterised by more voluminous, typical rift-valley type sedimentation, indicating the onset of active extension associated with greater rift development. The Humanity Seat Formation is shown in the Geological Survey of South Australia, Department of Mines, Adelaide: Mount Painter Province 1:125,000 Sheet (Coats *et al.* 1969) to be deposited in greater thicknesses to the east of the Paralana Fault, with only a small wedge present in the Arkaroola area. Here the Humanity Seat Formation is bounded by the Arkaroola Bore and Echo Camp Faults, suggesting these structures localised the formation of a minor depocentre. The depositional wedge of sediment thickens eastward, indicating downfaulting on the Arkaroola Bore Fault was comparatively greater and resulted in deeper subsidence. Lenses of coarser material and the relatively poorly sorted nature of the Humanity Seat Formation are consistent with deposition as an alluvial fan. The eastward increase in clast size and population of the Arkaroola Creek Breccia, as well as its depositional thickness, suggests it was rapidly shed as a mass flow as the result of further downfaulting along the Arkaroola Bore Fault. Sedimentary features for both facies suggest sediments were shed into moderately energetic shallow water environment (figure 13c).

The significantly thicker Woodnamoka Formation is exclusive to the Arkaroola area. The map pattern suggests its base represents a depositional unconformity, as it appears to directly overlie older stratigraphy, including the Humanity Seat Formation. Its exclusiveness to the west of the Paralana Fault suggests a major depocentre was generated by this fault structure (figure 13d). Deposition of the Humanity Seat is considered to have continued on

the eastern side of the fault during deposition of the Woodnamoka Formation, making the Woodnamoka Formation a deeper water equivalent (Preiss 1987). This is consistent with a finer grained protolith, as well as evidence of tidal influence.

A renewed phase of rifting associated with the generation of a depocentre along the Sitting Bull Fault resulted in the deposition of the Blue Mine Conglomerate (figure 13e). A gradational contact between the Blue Mine Conglomerate and the Woodnamoka Formation suggests the Sitting Bull Fault became active as the topmost Woodnamoka Formation was being deposited. The well stratified nature of clasts and minor imbrication suggests transport was dominated by fluvial processes, rather than debris flows. Gravelly braided stream-alluvial fan deposits likely drained into a standing body of water, with some tidal influence evidenced by tabular crossbedding. Clast composition, particularly to the west of the unit, indicates it was largely derived from the Mount Neill Granite, consistent with U-Pb analysis, suggesting localised uplift of basement.

The Opaminda Formation, as well as the overlying Wortupa Quartzite, are laterally more extensive than older stratigraphy, suggesting a more broadly confined depositional zone. Shallow marine sedimentary features indicate a transgressive environment.

Sections l-l' and ll-ll' (figure 4a,b) show the Opaminda Formation is steeply juxtaposed against older stratigraphy to the west, creating an angular unconformity. This juxtaposition could potentially be explained by three proposed models: a) deformation of the Arkaroola Subgroup and Lower Burra Group occurring prior to the deposition of the Opaminda Formation, resulting in the tilting of older stratigraphy; b) broad folding of stratigraphy by a later fold event, which is later discussed, or c) early rift processes resulted in the tilting of stratigraphy prior to deposition of the Opaminda Formation.

The rift tilting model can be explained as follows: during deposition of the Woodnamoka Formation, a tilt block was thrown down on the western side of the Paralana Fault, exposing older stratigraphy to the west of the map area at higher elevations; as the Sitting Bull Fault became active, upward motion of its top north-western footwall block could have further tilted up this stratigraphy. This would have resulted in the very south-western basement and Callanna Group being exposed at further increased elevations. Onlap of the Opaminda Formation onto this angled stratigraphy could explain the current angular geometry. This exposure of the south-western basement could have also provided the local basement source for the Blue Mine Conglomerate, consistent with the predominance of basement material to the west of the facies. It must be noted that the Sitting Bull Fault is a

relatively minor growth structure, making the considerable fault block movement required for this model questionable.

U-Pb analyses show marked variability in potential source region contributions to the Paralana Quartzite, Humanity Seat Formation and the Blue Mine Conglomerate. This is consistent with active emergent faulting producing impediments to sediment dispersal and resulting in the fragmentation of source regions.

Preiss (1987) and Powell *et al*. (1993) have regionally considered the northern Flinders Ranges to have an intracratonic rift setting. This is consistent with the Arkaroola area, with restricted shallow water depositional environments suggesting the basin was not opened up to the sea to the south east during early basin formation.

Regionally within the northern Flinders Ranges the Callanna and lower Burra Groups appear to be most voluminous along the Paralana Fault in the Arkaroola area, suggesting a mechanism for the localisation of rifting during the time of their deposition.

The Paralana Fault has a regional northeast-southwest trend, but in the Arkaroola area has a local ~ north-south orientation (figure 16). Movement along this fault is poorly constrained, with Paul *et al.* (1999) suggesting dextral strike-slip displacement during rifting, as evidenced by changing facies thicknesses across it (Preiss 1987), induced from regional northeast-southwest extension. If this is so, the local north-south deviation of the Paralana Fault in the Arkaroola area from its regional trend could create localised transtension, analogous to a 'dilational jog' at a releasing bend in a fault system, resulting in the localisation of rifting.

Recognised growth faults in the Arkaroola area, being the top-northwest, Arkaroola Bore, Echo Camp and Sitting Bull Faults, are all orientated oblique to the local Paralana Fault segment and therefore subparallel to the regional Paralana Fault trend. The faults have left-stepping en echelon geometries, and it is therefore possible they splay from the Paralana Fault at depth as an imbricate fault array. Assuming regional strike-slip offset along the Paralana Fault, local growth faults could generate components of oblique and strike-slip displacement, generating minor fault bounded "pull apart" depocentres analogous to the deposition of the Humanity Seat Formation. Oblique-normal faulting across the Paralana Fault would generate downthrow along it and the generation of a greater depocentre, consistent with the deposition of the Woodnamoka Formation.

Such localised transtension associated with rift development is analogous to the formation of a pull-apart basin. Pull-apart basins are typically defined as deep depressions

bounded by two subparallel, overlapping strike-slip faults, which are linked at their ends by perpendicular or diagonal transfer faults (Gubuz 2010). They evolve progressively from narrow grabens bounded by oblique-slip link faults to wider, rhombic basins associated with terraced inner fault systems (Dooley and McClay 1997) and are characterised by deep sedimentation as well as longitudinal basin asymmetry associated with abrupt facies changes and local unconformities (Loganson 2005). A pull-apart basinal model is highly analogous to the Arkaroola area: Initial minor half-graben development during the deposition of the Arkaroola Subgroup was followed by the complex development of migrating depocentres during deposition of the lower Burra Group, resulting in a highly asymmetric, abrupt basinal pattern. Assuming growth faults splay from the Paralana Fault at depth, such rifting is comparable to a negative 'tulip structure' commonly associated with pull-apart basins (figure 14b) (Woodcock and Fischer 1986).

Given a lack of constraint on the Paralana Fault, a pull-apart basin as the result of transtension along a locally north-south orientated fault segment is considered an affective mechanism for localising rifting during deposition of the Callanna and lower Burra Groups in the Arkaroola area.

6.3 Nature of deformation

The nature of deformation in the Arkaroola area remains largely enigmatic. By determining the relationships between deformational components, its evolution can be reconstructed to create insight into its regional context. The nature of individual deformational components are briefly summarised below:

The planar, shallow-to-bedding nature of S_Z suggests that it originally formed as a sub-horizontal foliation, and was produced by flattening generated by vertical principal stresses, mostly likely due to burial beneath a significantly thick sedimentary pile. The fabric is not axial planar to any observed folds, but the presence of folds not seen at this scale of mapping cannot be ruled out. Its progressive nature, associated with subsequent development of rotating composite foliations and a component of non-coaxial shear, also evidenced by both pre and syn-kinematic-porphyroblasts growth, suggests that the fabric was potentially produced during the initiation of deformation and is associated with prograde metamorphism.

The spatially restricted shear foliation, S_B, is constrained to the boundary zone between the ~ 1590 Ma Mount Neill Granite Porphyry and the basal Adelaidean succession. The shear fabric was formed under non-coaxial strain, with a high muscovite component and extensive quartz veining indicating that fluid flow was an important mechanism in localising shear. Pervasive mineral stretching lineations suggest northeast-southwest orientated extension. For an in depth discussion on the nature of S_B, refer to Hansberry (2011).

F_3 folds and S_3 crenulation cleavages deform S_Z, demonstrating that their generation unequivocally post-dates S_Z. Metamorphic zonation is also folded by F_3 in the Arkaroola area, but this does not necessarily imply that folding occurred after the formation of metamorphic zonation. The ductile deformational nature of F_3 implies that it was produced at considerable mid crustal depths, below the brittle-ductile boundary.

F_4 is suggested to post date F_3, on the basis of $L_{3\text{-}Z}$ and $L_{Z\text{-}0}$ being folded by a northwest-southeast axis comparable to its own. Its ductile nature suggests it too was formed whilst at considerable depth.

Asymmetric F_3 crenulations, formed at a high angle to S_Z, imply that maximum principle stresses associated with their formation were orientated at a low angle to the plane of S_Z, and suggest that during the formation of F_3 principal stresses were no longer vertical. F_3 fold hinges are sub-parallel to growth faults in the Arkaroola area, suggesting that reactivation of these fault structures was associated with thrust related folding and buttressing against normal fault scarps. Growth faults appear to partition deformation, as directly evidenced by the F_3 and F_4 fold interference 'bowl' geometry, which is confined to between the top-northwest fault and Echo Camp Fault.

Paul *et al.* (1999) suggests that during deformation of the northern Flinders Ranges, the Paralana Fault was associated with a switch from dextral to sinistral strike-slip displacement. This would effectively produce transpression in a pre-existing zone of transtension, which Jones *et al.* (1997) and Woodcok and Fischer (1986) suggest can produce highly localised deformation. The inversion of transtensional structures in the Arkaroola area under a transpressional regime could therefore be a potential mechanism for producing and localising the complex deformation observed in the Arkaroola area.

Considering a transpressional regime in the Arkaroola area, two possible scenarios for the progression of deformation are proposed:

Double Strain Model:

Two subsequent strain models are considered to have contributed to the observed deformation. The first strain model is associated with the formation of S_Z and S_B during northeast-southwest extension and dextral strike-slip displacement along the Paralana Fault. As the basin formed and sediments accumulated, S_Z was developed progressively under sub-vertical compression, associated with prograde metamorphism. A component of extension within the foliation plane of S_Z could represent a degree of lateral shortening accommodation.

Extension evidenced by S_B is parallel to that of S_Z, and is orientated sub-parallel to the northeast-southwest direction of extension proposed under a transtensional regime. It is therefore possible S_B was produced during later phases of rift development as a ductile extensional shear fabric. Hansberry (2011) discusses specific mechanisms for the localisation and nature of this fabric at the basement cover contact, concluding that fluid flow is a significant contributing factor. Basin formation and extension was then followed by a switch to sinistral strike-slip displacement along the Paralana Fault, generating transpressional basin inversion and a second strain model. Transpression was associated with oblique compression and F_3 was subsequently produced as a response to shortening, and accommodated compression vertically by thrusting and folding parallel to bounding faults (Figure 16a).

Single strain model:

Deformation was produced under a single progressively evolving strain model, which was associated with transpression generated by sinistral strike-slip displacement along the Paralana Fault, and post-dates phases of extension. S_Z was formed during the initiation of deformation by sub-vertical compression similarly to that as described in the double strain model. As a transpressional regime developed, an increasing predominance of horizontal stresses resulted in a transition to oblique compression, and F_3 was subsequently produced.

Jones *et al.* (1997) suggests that in a laterally unconfined transpressional zone, horizontal shortening across the zone can be balanced by upward and downward vertical thickening, as produced by F_3, as well as by lateral extrusion. Lateral extrusion is defined as horizontal stretch within an orogenic zone (Jones *et al.* 1997), and can result in extension at low angles to the deformational boundary (Grujic and Mancktelow 1994; Jones *et al.* 1997).

Fossen and Tikoff (1998) and Grujic and Mancktelow (1994) suggest that when folds 'lock' up and buckling ceases to be an affective shortening mechanism, or when orogenic

boundary conditions change, lateral extrusion can become favourable to the accommodation of shortening. Dewey *et al.* (1988) suggests that under these conditions it is possible to develop components of localised constrictional strain. Localised constriction can develop because of a marked tendency for simple-shear and pure-shear to be spatially partitioned within transpressional zones; in particular, non-coaxial strain is commonly partitioned into discrete narrow zones of simple shear (Jones *et al.* 1997). It is therefore possible that under an increasing component of lateral extrusion, a narrow zone of non-coaxial shear could form, localised by fluid flow, which is analogous to S_B. Constriction associated with lateral extrusion would produce extension sub-parallel to bounding faults in a northeast-southwest direction, as observed in S_B. Following this model, it is therefore possible that S_B is an 'extensional fabric' that was generated through transpression, rather than transtension (figure 16b).

In both models F_4 is considered to have been produced subsequent to F_3. Its shallower, broader nature than that of F_3, as well as its differing fold hinge orientation, suggests it was potentially produced by a later, different phase of deformation. This is, however, poorly constrained.

Both discussed models are considered potential scenarios for the evolution of deformation in the Arkaroola area. Due to a lack of constraint on the development of S_B, a double strain model scenario incorporating both transtension and transpression is favourable; however, a singular strain model scenario, involving only transpression to account for observed deformation in the Arkaroola area, is also possible and cannot be discounted.

6. 4 Timing of deformation

The timing of deformation and metamorphism in the northern Flinders Ranges has been previously assigned to the Delamerian Orogeny (Preiss 1987; Paul *et al.* 1999; Elburg *et al.* 2003), based on similarities in structural style to the southern AFB and its association with metamorphism. However, available geochronological data does not effectively constrain the age of deformation and metamorphism.

Despite the often highly localised nature of transpression (Jones *et al.* 1997), it is unclear whether this alone would facilitate the sharp contrast in shortening observed

between the Callanna and lower Burra Groups, and the overlying upper Burra Group. Both S_Z and F_3 are not apparent in the overlying Wortupa Quartzite and younger stratigraphy, which exhibit only broad, gentle folding associated with the km scale folds of the northern Flinders Ranges. Such non-continuity raises the possibility that deformation potentially occurred prior to deposition of the upper Burra Group, and that the base of this group represents an orogenic unconformity. The possibility of deformation being assigned to an earlier deformational event in the early Neoproterozoic, rather than the largely ascribed Delamerian Orogeny, is discussed. Timing constraints on S_Z, F_3 and F_4 are firstly briefly summarised below:

An absolute constraint the formation of S_Z is that it post-dates deposition of the Woodnamoka Formation. The maximum depositional age of the Humanity Seat Formation, considered a partly regional lateral equivalent, is 1528 ± 22, however the true age of the Woodnamoka Formation is considered more likely to be ~780 Ma. The fabric's association with cordierite porphyroblasts provides a more useful constraint on its formation: Paul *et al.* (1999) suggests that observed cordierite-bearing assemblages imply temperatures in excess of 500°C and, although poorly constrained by quantitative barometry, pressure estimates of ~ 3 kbars, which correspond to depths of ~ 10 km. Such burial would not likely have been achieved by sedimentation until the late Neoproterozoic-early Cambrian (Paul *et al.* 1999).

S_Z is not observed in lithologies overlying the Woodnamoka Formation or to the east of the Paralana Fault, but is also non-apparent, or has been overprinted, in older stratigraphy. This could largely be due to a lack of facies possessing the same fine grained protolith and developed metamorphic grade as the Woodnamoka Formation, required to produce such a fabric. S_Z is therefore not a diagnostic tool for ascribing the extent of deformation.

The age of F_3 is poorly constrained; folding is confined to the Callanna and lower Burra Groups, and is therefore absolutely constrained to after their deposition.

As previously mentioned, F_4 is considered to potentially be the result of a younger deformational event. The orientation and broad nature of F_4 is notably similar to the east-northeast km scale folding of the northern Flinders Ranges. This regional folding is also poorly constrained, so their association does not aid the constraint of deformation in the Arkaroola area.

$^{40}Ar/^{39}Ar$ and K/Ar thermochronology undertaken by various workers in the MPP provides an absolute upper constraint on the timing of deformation. McLaren *et al.* (2003),

supplemented by the work of Mitchell *et al.* (2002) and Pointon (2010), shows cooling ages of 430 Ma, 400 Ma and 330-320 Ma, which are implied to be the result of exhumation and denudation of up to 6-7 km. The ductile nature of deformation in the Arkaroola area suggests deformation must have occurred at depth and therefore before such exhumation.

Given the considered time constraints, the possibility of both an early Neoproterozoic deformational event occurring prior to the deposition of the upper Burra Group, and a younger deformational event, including the Delamerian Orogeny, are considered.

Early Neoproterozoic deformation:

Pressure and temperature constraints associated with S_Z suggest significant burial was required to produce such a fabric, not likely to have been reached prior to deposition of the upper Burra Group. It is possible that such sedimentary thicknesses could have been actively emplaced prior to this time by crustal-scale low-angle thrusting. Regionally, however, there is no evidence to suggest such large scale thrusting, or the erosion of a significantly thick sedimentary pile prior to deposition of the Opaminda Formation. A second possibility is that the deformation observed in the Callanna and lower Burra Groups produced enough local thickening to generate the required burial and metamorphic conditions. Given the relatively limited thicknesses of these sediments, burial of up to ~ 10 km produced by their shortening seems unlikely, but cannot be discounted. It should be noted that S_Z pre-dates F_3, which is responsible for producing a considerable amount of the shortening involved, and so provides a further complication.

The restriction of deformation to the Callanna and lower Burra Groups implies an orogenic unconformity at the base of either the Opaminda Formation or the Wortupa Quartzite. The Wortupa Quartzite is conformable with the Opaminda Formation (Preiss, 1987), so an unconformity at the base of the Opaminda Formation is considered. This notion is supported by the angular unconformity to the west of the map area, implying deformation and tilting of older stratigraphy occurred prior to deposition of the Opaminda Formation. However, the Opaminda Formation and Blue Mine Conglomerate are considered to be conformable to the west of the Arkaroola area; it is therefore hard to attribute an orogenic unconformity to the contact. It must be noted, however, that this contact was only truly observed in one location, making the nature of the contact difficult to confidently ascribe. Therefore an orogenic unconformity cannot be discounted.

Deformation post-dating deposition of the upper Burra Group

The estimated burial of the Woodnamoka Formation required to produce S_Z is suggested to not have been accumulated until the late Neoproterozoic-early Cambrian (Paul *et al.* 1999), implying that deformation did not occur until at least this time. This is consistent with relatively continuous deposition of sediments in the Arkaroola area, and the angular unconformity at the base of the Opaminda Formation being associated with early rift-tilting. The angular unconformity can also potentially be explained by later broad-scale folding, such as a fold corresponding to F_4, resulting in the tilting of all stratigraphy, as well as the Sitting Bull Fault from its original normal south dipping orientation, to generate the present day geometry (figure 14). Deformation post dating deposition of the Opaminda Formation is also consistent with the presence of tight, complex folding at the base of the formation and folding of the boundary itself, suggesting that it too experienced a component of shortening.

The problem still remains of a sharp contrast in the amount of shortening observed between the Callanna and lower Burra Groups, and the upper Burra Group. This can potentially be explained by the Opaminda Formation acting as a décollement horizon: due to its inherent weakness, the formation could have accommodated shortening through slip, resulting in lateral displacement of deformation in the upper Burra Group, as well as the detachment of fold structures in the lower stratigraphy. This could is consistent with buttressing of F_3 folds proximal to this contact (figure 2). Regionally, there is no evidence to support such displacement of deformation in the upper Burra Group; this, however, does not prove its non-existence.

If a later deformational event is considered, within the ascribed time window for deformation between the late Neoproterozoic and the 430 Ma, 400 Ma and 330-320 Ma cooling ages associated with exhumation (McLaren *et al.* 2002), the Delamerian Orogeny is a potential orogenic event. This is consistent with a minor thermal pulse in the MPP at ~ 495 Ma, associated with the emplacement of the pinnacles and the Arkaroola Pegmatite in the cover sequences (Elburg *et al.* 2003). Work by McLaren *et al.* (2002), Mitchell *et al*. (2002) and Pointon (2010) suggest the MPP has also been subject to intracontinental orogenesis associated with the 400-320 Ma Alice Springs Orogeny, which also falls between given time constraints. Temporal constraints assigned by this study are broad, and without further evidence neither of these orogenic events can be confidently ascribed to deformation in the Arkaroola area.

The timing of deformation in the Arkaroola area and therefore its relationship to regional deformation remains enigmatic. Further work, focused on directly dating deformation, is required before it can be more accurately constrained, and the possibility of early Neoproterozoic or younger deformation can be further investigated.

6.5. Future Research

To further constrain contributions of source regions to the Callanna and lower Burra Groups in the northern Flinders Ranges, employing a wider range of provenance tools would supplement and expand on currently available data. Lu-Hf analysis would complement Sm-Nd and U-Pb analyses, as well as whole rock geochemical analysis, which would be particularly useful in determining the contributions of volcanic material to the sediments.

The direct dating of deformation in the Arkaroola area is crucial in constraining its timing and therefore its regional context. S_Z was likely produced under conditions significant enough to produce monazite growth. U-Pb in-situ dating of such monazite would yield ages that reflect the fabric's development, and would consequently place a significant temporal constraint on the timing of deformation.

$^{49}Ar/^{39}Ar$ thermochronology focused on the Arkaroola area, following on from McLaren *et al.* (2002), could also be employed to date cooling as a proxy to exhumation, to further constrain deformation and gain greater understanding of the evolution of the Arkaroola area.

7. Conclusion

1. The basal Adelaidean in the Arkaroola area shows a complex rift history, associated with minor rifting during deposition of the Callanna Group followed by the onset of significant rifting associated with the lower Burra Group. Assuming dextral strike-slip displacement along Paralana Fault, the local north-south segment in the Arkaroola area could generate localised transtension and the facilitate the formation of a minor pull-apart basin. This model of basin formation is considered analogous to rifting and sedimentation in the Arkaroola area.

2. U-Pb analysis suggests the Callanna and lower Burra Groups in the Arkaroola area are comprised of locally derived source material from the Mount Painter Basement Complex, Gawler Craton and Curnamona Province, and reflects the heterogeneous nature of rifting. Sm-Nd analysis suggests direct derivation of the Woodnamoka Formation from either the Mount Painter Basement Complex or the upper Willyama Supergroup of the Curnamona Province. Potential derivation from the same sources as the upper Willyama Supergroup sources suggests distal source regions beyond the Australian continent, in southwestern Laurentia.

3. The reactivation of early rift structures of the Arkaroola area under transpression is considered an effective mechanism for localising the complex deformation in the Arkaroola area. Two models for the development of deformation are proposed, and are considered potential alternatives:

1) A primary burial fabric and localised shear fabric at the basement-cover contact were generated during later phases of transtension, and a subsequent switch to transpression generated the observed folding and shortening.

2) A burial fabric was generated during the initiation of deformation, and as transpression and horizontal principal stresses became increasingly predominant, folding and shortening ensued. Progressive accommodation of shortening by lateral extrusion resulted in localised constriction, which generated an ‘extensional’ fabric at the basement-cover contact, localised by fluid flow.

4. The timing of deformation remains enigmatic. Early Neoproterozoic deformation prior to deposition of the upper Burra Group cannot be confidently ascribed due to the lack of an unequivocal orogenic unconformity, but cannot be discounted. A younger deformational event also remains a possibility, but there is no available evidence to constrain it further. Further work focused on directly dating deformation is therefore highly recommended.

8. Acknowledgements

I would like to firstly thank my supervisors Alan Collins and David Giles for giving me the opportunity to spend this year working in and on the truly amazing Arkaroola area. A big thanks to Steve Hore, for all of his help during field work and for providing us with a few much needed laughs, and a huge thanks to the amazing Katie Howard, for her all of her help and incredible patience throughout the year no matter what crazy situations we managed to throw at her, and also to David Bruce for dedicating so much of his time to my project. A big thankyou to the Sprigg family for their hospitality, and also to the staff at Adelaide Microscopy for all of their help. And last but not least, an enormous thanks to everyone in the honours crowd this year for making this year such a good one! And of course, I must also acknowledge the beautiful Arkaroola area for providing such amazing views, wacky rocks, cool rock wallabies, stinky plants and overall an amazing experience - and to the merciless Mount Oliphant for making sure we worked hard for it.

9. References

AITKEN. A. R. A and BETTS, P. G., 2009. Constraints on the Proterozoic supercontinent cycle from the structural evolution of the south-central Musgrave Province, central Australia. *Precambrian Research* **168**, 284-300.

BAROVICH, K. M. and Hand, M., 2008. Tectonic setting and provenance of the Palaeoproterozoic Willyama Supergroup, Curnamona Province, Australia: geochemical and Nd isotopic constraints on contrasting source terrain components., *Precambrian Research* **166**, 318-337.

BELOUSOVA, E. A., GRIFFIN, W. L, O'REILLY, S. Y., 1999, Cathodoluminsescence and geochemical properties of kimberlitic and lamproitic zircons. *The 7th International Kimberlite Conference Proceedings, Cape Town,* 23-29

BELOUSOVA, E. A., REID, A. J., GRIFFIN, W. K., O'REILLY, S. Y., 2009. Rejuvenation versus recycling of Archean Crust in the Gawler Craton, South Australia: Evidence from U-Pb and Hf-isotopes in detrital zircon. *Lithos* **113**, 570-582

BENTON, J. S., 1993. Sedimentology, deformation and isotopic investigation of the Paleo and Neoproterozoic sequences of the Mount Painter Inlier. University of Adelaide Honours Thesis. (Unpubl).

BETTS, P. G., VALENTA, R. K. and FINLAY, J., 2003. Evolution of the Mount Woods Inlier, northern Gawler Craton, South Australia: an integrated structural and aeromagnetic analysis. *Tectonophysics* **366**, 83-111.

BROOKFIELD, M. E., 1993. Neoproterozoic Laurentia-Australia fit. *Geology* **21**, 683-686.

CAWOOD, P. A., NEMCHIN, A. A., FREEMAN, M., SIRCOMBE, K., 2003. Linking source and sedimentary basin: detrital zircon record of sediment flux along a modern river system and implications for provenance studies. *Earth and Planetary Sciences Letters* **210**, 259– 268.

CLARKE, L. G. and POWELL, R., 1987. Basement-Cover interaction in the Adelaide Foldbelt, South Australia: the development of an arcuate foldbelt. *Tectonophysics* **158**, 209-226.

COLIN, H. P. and Preiss, W. V., 2008. Understanding the 1720-1640 Ma Palaeoproterozoic Willyama Supergroup, Curnamona Province, Southeastern Australia: implications for tectonics, basin evolution and ore genesis. *Precambrian Research* **166**, 297-317.

COMPSTON, W., CRAWFORD, A. R. and BOFINGER, V.M., 1966. A radiometric estimate of the duration of sedimentation in the Adelaide Geosyncline, South Australia. *Australian Journal of Earth Sciences* **13,** 229-276.

CRAWFORD, A. R., 1960. The geology of the Wooltana volcanic belt, South Australia, University of Adelaide Honours Thesis (unpubl.)

DALY, S. J., FANNING, C. M. and FAIRCLOUGH, M. C., 1998. Tectonic evolution and exploration potential of the Gawler Craton, South Australia. *Journal of Australian Geology and Geophysics* **17**, 145-168.

DEWEY, J. F., HOLDSWORTH, R. E. and STRACHAN, R. A., 1998. Transpression and transtension zones. *Geological Society of London, special publications* **135** 1-14.

DOOLEY, T and MCCLAY, K., 1997. *Analogue modelling of pull-apart basins* **81**, 1804-1826

DOOLEY, T., 2008. 4D analogue modelling of transtensional pull-apart basins. *Marine and Petroleum Geology* **26**

DREXEL, J.F., PREISS, W. V. and PARKER, A.J., 1993. The geology of South Australia, Volume 1, *Geological Survey of South Australia*, Bulletin **54**

DUTCH, R., HAND, M. and KINNY, P. D., 2008. High-grade Paleoproterozoic reworking in the southeastern Gawler Craton. *South Australia Australian Journal of Earth Sciences* **55**, 1063-1081.

DYMOKE, P. and SANDIFORD, M., 1992. Phase relationships in Buchan facies series pelitic assemblages: calculations with application to andalusite-staurolite paragensis in the Mount Lofty Ranges, South Australia. *Contributions to Mineralogy and Petrology* **110**, 121-132.

ELBURG, M. A., BONS, P. D., DOUGHERTY-PAGE, J., JANKA, C. E., NEWMAN, N and SCHAEFER, B. Age and metasomatic alteration of the Mt Neill Granite at Nooldoonooldoona Waterhole, Mt Painter Inlier, South Australia. *Australian Journal of Earth Sciences* **48**, 721 – 730

ELBURG, M.A., BONS, P. D., FODEN, J., BRUGGER, J., 2003. A newly defined late Ordovician magmatic-thermal event in the Mount Painter Province, northern Flinders Ranges, South Australia. *Australian Journal of Earth Sciences* **50** 611-631.

FARRAND, M. G and PREISS, W. V., 1995. Early and middle Paleozoic orogenisis: Delamerian igneous rocks. *South Australian Geological Survey* **2**, 54-57

FERRIS, G. M., SCHWARZ, M., 2004. Definition of the Tunkillia Suite, western Gawler Craton. *MESA Journal* **34**, 32-41

FERGUSSON, C. L., HENDERSON, R. A., FANNING, C. M. and WITHNALL, I.W., 2007. Detrital zircon ages in Neoproterozoic to Ordovician siliclastic rocks, northeastern Australia: implications for the tectonic history of the East Gondwana continental margin. *Journal of the Geological Society, London* **164**, 215-225.

FLETCHER, J. M. and BARTLEY, J. M., 1993. Constrictional strain in a non-coaxial shear zone: implications for fold and rock fabric development, central Mojave metamorphic core complex, California. *Journal of Structural Geology* **16**, 555-570.

FLINT, R. B., BLISSET, A. H., CONOR, C.H. H., COWLEY, W. M., CROSS, K.C., CREASER, R. A., DALY, S. J., KREIG, C. W., MAJOR, R. B., TEALE, G.S., PARKER, A. J., 1993. Mesoproterozoic. In: Drexel, J.F., Preiss, W.V., Parker, A.J (editors), *The geology of South Australia, Volume 1, The Precambrian* Bulletin **54**, 106-169

FLINT, R. B., RANKIN, L. R. and FANNING, C. M., 1998. The Paleoproterozoic St Peter Suite of the western Gawler Craton. *Geological Survey of South Australia, Quarterly Notes* **114**, 2-8.

FLOTTMAN, T., JAMES, P., ROGERS, J. and JOHNSON, T., 1994. Early Palaeozoic foreland thrusting and basin reactivation at the Palaeo-Pacific margin of the southeastern Australian Precambrian Craton: a reappraisal of the structural evolution of the Southern Adelaide Fold-Thrust Belt. *Tectonophysics* **234**, 95-116.

FLOTTMAN, T. and JAMES, P., 1997. Influence of basin architecture on style of inversion and fold thrust-belt tectonics – the Southern Adelaide Fold-Thrust Belt, South Australia. *Journal of Structural Geology* **19,** 1093-1110

FLOTTMAN, T., JAMES, P., ROGERS, J. and JOHNSON, T., 1994. Early Palaeozoic foreland thrusting and basin reactivation at the Palaeo-Pacific margin of the southeastern Australian Precambrian Craton: a reappraisal of the structural evolution of the Southern Adelaide Fold-Thrust Belt. *Tectonophysics* **234,** 95-116

FODEN, J., BAROVICH, K., JANE, M. and O'HALLORAN, G., 2001. Sr-isotopic evidence for Late Neoproterozoic rifting in the Adelaide Geosyncline at 586 Ma: implications for a Cu ore forming fluid flux. *Precambrian Research* **106**, 291–308.

FODEN, J., ELBURG, M. A., DOUGHERTY-PAGE, J. and BURRT, A., 2006. The timing and duration of the Delamerian Orogeny: Correlation with the Ross Orogen and implications for Gondwana assembly. *The Journal of Geology* **114,**198-210.

FODEN, J., ELBURG, M. A., TURNER, S. P., SANDIFORD, M., O'CALLAGHAN, J., MITCHELL, S., 2002. Granite production in the Delamerian Orogen, South Australia. *Journal of the Geological Society* **159,** 557-575.

FOSSEN, H. and TIKOFF, B., 1998. Extended models of transpression and transtension, and application to tectonic settings. Continental transpressional and transtensional tectonics. *Geological Society of London, Special Publications***135**

FEDO, C. N., SIRCOMBE, K.M., RAINBIRD., R. H, 2003. Detrital zircon analysis of the sedimentary record. *Reviews in Mineral and Geochemistry* **53**, 277-303

FOSTER, D.A., MURPHY, J. M. and GLEADOW, A. J. W., 1994. Middle Tertiary hyrdrothermal activity and uplift of the northern Flinders Ranges, South Australia: insights from apatite fission-track thermochronology. *Australian Journal of Earth Sciences* **14**, 11-17

FRASERA, G., MCAVENEYB, S., NEUMANN, N., SZPUNAR, M., and REID, A., 2010. Discovery of early Mesoarchean crust in the eastern Gawler Craton, South Australia*. Precambrian Research* **179**, 1-21.

GRUJIC, D and MANCKTELOW, N. S., 1995. Folds with axes parallel to the extension direction: an experimental study. *Journal of Structural Geology* **17**, 279-291.

GEUYDAN, F., LEROY, W. M. and JOLIVET, L., 2004. Mechanics of low-angle extensional shear zones at the brittle-ductile transition. *Journal of Geophysical Research* **109.**

GRUBUZ, A., 2010. Geometric characteristics of pull-apart basins. *Lithosphere* **2**, 199-206.

HAINES, P. W. and FLOTTMAN, T., 1998. Delamerian Orogeny and potential foreland sedimentation: a review of age and stratigraphic constraints. *Australian Journal of Earth Sciences* **45**, 559-570.

HILYARD, D., 1990. Willourian Basic Province: Stratigraphy of late Proterozoic flood basalts, Adelaide Geosyncline, South Australia. *Geology Society Special Publication* **16**, 34-48.

HORE, S., FIDLER, R., MCINNES, R. and RAGLESS, J., 2005. Mount Painter Geochemistry - an old terrain revisited with new science. *MESA* **38**, 8-14.

HOWARD, K. E., HAND, M., BAROVICH, K. and BELOUSOVA, E., 2011. Provenance of late Paleoproterozoic cover sequences in the central Gawler Craton: Exploring stratigraphic correlations in eastern Proterozoic Australia using detrital zircon ages, Hf and Nd isotopic data*. Australian Journal of Earth Sciences* **58**, 475-500.

HOWARD, H. M., HAND, M., BAROVICH, K. M., REID, A. and WADE, B.P., 2009. Detrital zircon ages: Improving interpretation via Nd and Hf isotopic data. *Chemical Geology* **15,** 277-292.

IDNURM, M. and HEINRICH, C., 1993. A Palaeomagnetic study of the hydrothermal activity and uranium mineralisation of Mt Painter, South Australia. *Australian Journal of Earth Sciences* **40**, 87-101.

IRELAND, T.R., FLOTTMAN, T., FANNING, C.M., GIBSON, G. M. and PREISS, W. V., 1998. Development of the early Palaeozoic Pacific margin of Gondwana from detrital-zircon ages across the Delamerian orogen. *Geology* **26,** 243-246.

JENKINS, R. J. F. and SANDIFORD, M., 1992. Observations of the tectonic evolution of the Southern Adelaide Fold Belt*. Tectonophysics* **214**, 27-36.

JONES, R.R., HOLDSWORTH, R.E. and BAILEY, W., 1997. Lateral extrusion in transpression zones: the important of boundary conditions. *Journal of Structural Geology* **19**, 1201-1217.

KIRSCHNER, D. L. and TIEXELLE, A., 1996. 3 dimensional geometry of kink bands in slates and its relationship with finite strain. *Tectonophysics* **262,** 195-211.

KROMKHUN, K., 2010. Petrogenesis of high heat producing granite: implication for Mt Painter Province, South Australia. University of Adelaide pHD (unpubl.)

LALLEMAND, S., LIU, C., DOMINGUEZ, S., SCHNURLE, P. and MALAVIELLE, J., 1999. Trench parallel stretching and folding of forearc basins and lateral migration of the accretionary wedge in the southern Ryukyus: A case of strain partition caused by oblique convergence. *Tectonic*s **18**, 231-247.

LEVY, F. and JAUPART, C., 2010. Folding in regions of extension. *Geophysical Journal International* **185**, 1120-1134.

LINDSAY, J.F., KORSCH, R.J. and WILFORD, J.R., 1987. Timing of the breakup of a Proterozoic supercontinent: Evidence from Australian intracratonic basins. *Geology* **15**, 1061-1064.

LOGANSON, L., I., 2005. Pull-apart basins: a review. *Geotectonics* **39**, 156-168.

MCBRIDE, J. H., 1994. Investigating the crustal structure of a strike-slip “step-over” zone along the Great Glen fault. *Tectonics* **13** 115-1160.

MCCULLOCH, M. T and WASSERBURG, G. J., 1978. More anomalies from the Allende meteorite: Samarium, *Geophysical Research Letters* **7**

MCCULLOCH, M. T., 1987. Sm-Nd isotopic constraints on the evolution of Pre-Cambrian crust in the Australian continent. In: Kroner, A (Editor) *Proterozoic Lithospheric Evolution*, *Am, Geophys. Union, Geodynamic Series* **17** 115-130.

MCLAREN, S., DUNLAP, W.J., SANDIFORD, M. and MCDOUGALL, I., 2002. Thermochronology of high heat-producting crust at Mount Painter, South Australia: Implications for tectonic reactivation of continental interiors. *Tectonics* **21**.

MCLAREN, S., SANDIFORD, M., POWELL. R., NEUMANN, N. and WOODHEAD, J., 2006. Palaeozoic intraplate crustal anatexis in the Mount Painter Province, South Australia: Timing, thermal budgets and the role of crustal heat production. Journal of Petrology **47**, 2281-2302.

MILDREN, S.D. and SANDIFORD, M., 1995. Heat refraction and low-pressure metamorphism in the northern Flinders Ranges, South Australia. *Australian Journal of Earth Sciences* **42**, 241-247.

MITCHELL, M. M., KOHN, B. P., O'SULLIVAN, P. B., HARTLEY, M. J. and FOSTER, D. A., 2002. Low temperature thermochronology of the Mt Painter Province, South Australia. *Australian Journal of Earth Sciences* **49,** 551-563.

MOORES, E. M., 1991. Southwest U.S.-East Antarctic (SWEAT) connection: A hypothesis. *Geology* **19,** 425-428.

MYERS, J. S., SHAW, R. D., TAYLOR, I. M., 1996. Tectonic evolution of Proterozoic Australia. *Tectonics* **15**, 1431-1446

O'HALLORAN, G., 1992. The sedimentology and Nd isoptic geochemistry of some early Adelaidean rocks from the northern Flinders Ranges, South Australia. University of Adelaide Honours Thesis (unpubl).

PAGE, R.W., CONOR, C. H. H., STEVENS, B. P. J., GIBSON, G. M., PREISS, W. V., SOUTHGATE, P. N., 2005. Correlation of Olary and Broken Hill Domains, Curnamona Craton: possible relationship to Mount Isa and other north Australia Pb-Zn-Ag-bearing successions*. Economic Geology* **87,** 663-676.

PAGE, R.W., STEVENS, B. P. J., GIBSON, G. M. and CONOR, C. H. H., 2000. Geochronology of Willyama Supergroup rocks between Olary and Broken Hill, and comparison to northern Australia. Broken Hill Exploration Initiative: *abstracts of papers presented at the may 2000 conference in Broken Hill.*

PAUL, E., FLOTTMAN, T. and SANDIFORD, M., 1999. Structural geometry and controls of basement-involved deformation in the Northern Flinders Ranges, Adelaide Fold Belt, South Australia. *Australian Journal of Earth Sciences* **46**, 343-354

PAYNE, J.L., BAROVICH, K. M. and HAND, M., 2006. Provenance of metasedimentary rocks in the northern Gawler Craton, Australia: implications for palaeoproterozoic reconstructions. *Precambrian Researc*h **148,** 275-291.

PAYNE, J.L., HAND, M., BAROVICH, K. M. and WADE, B.P., 2008. Temporal constraints on the timing of high-grade metamorphism in the northern Gawler Craton: implications for assembly of the Australian Proterozoic. *Australian Journal of Earth Sciences* **55,** 623-640.

POWELL, M. C., PREISS, W. V., GATEHOUSE. C. G., KRAPEX, B., LI, Z. X., 1994. South Australian record of a Rodinian epicontinental basin and its mid-Neoproterozoic breakup (~ 700 Ma) to form the Palaeo-Pacific Ocean. *Tectonophysics* **237,** 113-140.

PREISS, W.V., 1987. The Adelaide Geosyncline - Late Proterozoic Stratigraphy, Sedimentation, Palaeontology and Tectonics*. Geological survey of South Australia* Bulletin **53.**

PREISS, W. V., 2000. The Adelaide Geosyncline of South Australia and its significance in Neoproterozoic continental reconstruction. *Precambrian Research* **100**, 21-63.

PREISS, W. V. and FORBES, B. G., 1981. Stratigraphy, correlation and sedimentary history of Adelaidean (late Proterozoic) basins in Australia. *Precambrian Research* **15,** 255-304

RAMSAY, J,G., 1962. Interference patterns produced by the superposition of folds of similar type. *The Journal of Geology* **70**, 466-481.

RAMSAY, J.G. and WOOD, D.S., 1973. The geometric effects of volume change during deformational processes. *Tectonophysics* **16**, 263-277.

REID, A., HAND, M., JAGODZINKSKI, E., KELSEY, D. and PEARSON, N., 2008. Palaeoproterozoic orogenesis in the southeastern Gawler Craton*. South Australia Australian Journal of Earth Sciences* **55**, 449-471.

RICHERT, J.P., 1976. Thrust faulting in northern Flinders Range, South Australia. *Australian Journal of Earth Sciences* **23,** 361-366.

RUTHERFORD, L., HAND, M. and MAWBY, J., 2006. Delamerian-aged metamorphosed in the southern Curnamona Province, Australia: implications for the evolution of the Mesoproterozoic Olarian Orogeny. *Terra Nova* **18,** 138-146.

SANDIFORD, M., PAUL, E. and FLOTTMAN., T., 1998. Sedimentary thickness variations and deformation intensity during basement inversion in the Flinders Ranges, South Australia. *Journal of Structural Geology* **20,** 1721-1731

STEVENS, B. P. J., PAGE, R. W. and CROOKS, A., 2008. Geochronology of the Willyama Supergroup metavolcanics, metasediments and contemporaneous intrusions, Broken Hill, Australia*. Australian Journal of Earth Sciences* **55**, 301-330.

SWAIN, G., WOODHOUSE, A., HAND, M., BAROVICH, K. M., SCHWARTZ, M., FANNING, C. M., 2005. Provenance and tectonic development of the late Archaean Gawler Craton, Australia; U–Pb zircon, geochemical and Sm–Nd isotopic implications. *Precambrian Research* **141**, 106-136.

THOMPSON, B. P., 1965. The lower boundary of the Adelaide system and older basement relationships in South Australia. *Australian Journal of Earth Sciences* **13**, 203-228.

TURNER, G. R., 1976. The stratigraphy, structural geology and metamorphism of the Callanna beds and base of the Burra Group in the Arkaroola Village area, South Australia. University of Adelaide Honours Thesis (Unpubl.)

TURNER, S., FODEN, J., SANDIFORD, M. and BRUCE, D., 1992. Sm-Nd isotopic evidence for the provenance of sediments from the Adelaide Fold Belt and southeastern Australia with implications for episodic crustal addition*. Geochimica et Cosmochimica Acta* **57**, 1837-1856

VON DER BORCH, C.C., 1980. Evolution of late Proterozoic to early Paleozoic Adelaide Foldbelt, Australia: Comparisons with post-Permiam rifts and passive margins. *Tectonophysics* **70**, 115-134.

WILLIAMS, P. F., 1990. Differentiated layering in metamorphic rocks*. Earth-Science Reviews* **29**, 267-281.

WINGATE, M. T. D., CAMPBELL, I. H., COMPSTON, W. and GIBSON, G. M., 1998. Ion microprobe U-Pb ages for Neoproterozoic basaltic magmatism in south-central Australia and implications for the breakup of Rodinia. *Precambrian Research* **87**, 135-159.

WINGATE, M. T. D., PISAREVSKY, S.A. and EVANS, D.A.D., 2002. Rodinia connections between Australia and Laurentia: no SWEAT, no AUSWUS? *Terra Nova* **14**, 121-128.

WOODCOCK, N.H. and FISCHER, M., 1986. Strike slip duplexes. *Journal of Structural Geology* **8**, 725-735.

ZHAO, J. and MCCULLOCH, M. T., 1993. Sm-Nd mineral isochron ages of late Proterozoic dyke swarms in Australia: evidence for two distinctive events of mafic magmatism and crustal extension. *Chemical Geology* **109**, 341-354.

ZHAO, J., MCCHULLOCH, M. T. and KORSCH, R. J., 1992. Characterisation of a plume-related ~ 800 Ma magmatic event and its implications of basin formation in central South Australia. *Earth and Planetary Science Letters* **121**, 349-367.

10. Figure and Table Captions

Tables

1. Description of zircon morphologies

2. Sm-Nd isotope data for selected Woodnamoka Formation samples [a] $^{143}Nd/^{144}Nd$ CHUR (0) = 0.512638, $^{147}Sm/^{144}Nd$ CHUR (0) = 0.1966, [b] T_{DM} calculated using the single stage model of Goldstein et al. (1994)

3. T_{DM} of potential proximal and distal source provenances as well as values for Willourian Volcanics taken from (McCulloch 1987)[a]. Early Proterozoic basement includes the Mount Painter Basement Complex, as well as the Olary and Broken Hill Blocks of the Curnamona Craton.

4. T_{DM} and ƐNd values for the Arkaroola Subgroup and lower Arkaroola Subgroup taken from O'Halloran (1992) and (denoted by *) Foden et al (2001). Bracketed figures represent ages used for calculation.

5. Possible correlations between $^{207}Pb/^{206}Pb$ defined age ranges for analysed samples (individual ages within indicate population peaks) and potential source provenances. Known age determinations are given for geological units within the source provenances.
[a] and references therein

Figures

1. Geological map of the Arkaroola area (see attached fold out). Inset: schematic showing major recognised faults

2. a) Location map of the Adelaide Fold Belt, South Australia, b) Regional map of the Adelaide Fold Belt: SAFB = southern Adelaide Fold Belt, CAFB = central Adelaide Fold Belt. The Torrens Hinge is shown as a dashed line. Thick solid lines in the MPP represent the Norwest Fault (west) and the Paralana Fault (east), c) schematic image of the Mount Painter Inlier and location of the Arkaroola Resort.

3. Schematic adaption of the Arkaroola geological map, highlighting fault and fold structures, as well as geographic features. Cross-section transects are also indicated.

4. Schematic structural cross-sections transecting the Arkaroola area. a, b) Sections l and ll, cross the mid and western portions of the map area, highlighting the F4 syncline and the angular unconformity at the base of the Opaminda Formation. Section l includes a thin band of Wooltana Volcanics which outcrop to the south between the upper and lower Paralana and have been projected to cut up stratigraphy into the Wywyana Formation, c) Section lll transects the mid-west of the map area, highlighting the north dipping Sitting Bull Fault the overturned anticline geometry in the hanging wall, as well as the intrusive Arkaroola Pegmatite, d) Section lV transects the eastern side of the map area, showing the

relatively uniform south-dipping stratigraphy to the east of the map area. Topography was generated using the Government of South Australia, Wooltana 6737-2 1:50000 Sheet (second edition).

5. Type section in the Woodnamoka Formation phyllite member: a) composite shear fabric S_Z comprised of S_1 and steeper S_2 which crenulates both S_0 and S_1, b) S_0 surface exhibiting an intersection lineation shared by both S_1 and S_2, ($L_{Z\text{-}0}$), c) cartoon schematic of the outcrop showing the relationship between S_1 and S_2 with S_0, with topmost arrows representing their intersection lineation

6. a) Basement-Paralana Quartzite contact, indicated by the white dashed line. The basement, left of the line, shows an increasingly mylonitic fabric toward the contact, b) Mylonitic fabric of the Mount Neill Granite Porphyry near the basement-cover contact. Note quartz phenocrysts forming sigma clasts, c) C-S fabrics formed by S_1 being crenulated by S_2, d) Schematic of c), e) Elongation of porphyroblasts with $L_{Z\text{-}0}$, f) F_3 parasitic folding in the Woodnamoka Formation, g) F_4 syncline, shown by white dashed line, observed from the summit of Mt Oliphant looking west.

7. Lower hemisphere equal area stereographic projections: a) poles to bedding taken from all stratigraphy to the east of the F_4 syncline, demonstrating a predominately southern dip, b) poles to bedding of the western third of the map area, highlighting folding around a northwest-southeast to north-south axis, c) poles to bedding in the western Woodnomoka highlighting shallow dipping planes toward the centre of the fold interference 'bowl' geometry, d) $L_{Z\text{-}0}$ showing a predominately south-western plunge, e) basement mineral stretching lineatons, f) $L_{3\text{-}Z}$ showing a predominately south-western plunge. Small crosses represent poles to S_3, which are largely axial planar, g) unfolded $L_{Z\text{-}0}$ (unfolding achieved by assuming bedding planes were originally horizontal), h) poles to S_0 (dots) and poles to S_z (crosses) associated with structural type section in the eastern Woodnamoka Formation, show folding around an east-west axial plane associated with F_3.

8. Microphotographs of Woodnamoka Formation thin sections. Scale bare is 1 mm: a, b, c) sample AARK01, d, e) sample AARK03, f, g, h) sample AARK07.

9. Paralana Quartzite: a) $^{207}Pb/^{206}Pb$ weighted average plot, b) concordia plot of all zircon analyses, c) CL image showing subrounded euhedral zircon grains exhibiting growth zoning and minor rims.

10. Humanity Seat Formation: a) $^{207}Pb/^{206}Pb$ weighted average plot, b) concordia plot of all zircon analyses, c) CL image showing subrounded euhedral zircon grains exhibiting complex growth zoning and xenocrystic cores, d) subangular zircon grains showing complex zoning patterns

11. Blue Mine Conglomerate: a) $^{207}Pb/^{206}Pb$ weighted average plot, b) concordia plot of all zircon analyses, c) CL image showing subrounded euhedral grains exhibiting varying development of growth zoning and minor rims.

12. **ε**Nd *vs* time for Woodnamoka Formation samples compared with the average Archean and > 1700 Ma Proterozoic Gawler Craton. Average Archean and Proterozoic bands are taken from Howard et el. (2011)[a]. Samples from the upper and lower Willyama Supergroup are included (Barovich and Hand, 2008), as well as values from igneous units from the Mount Painter Basement Complex (Kromkhun, 2010), and values from the the Callanna and lower Burra Groups (O'Halloran, 1992; Foden et al., 2001). The dashed line represents the evolution of the Woodnamoka Formation samples. Note that the average Gawler Craton bands must be used with precaution due to large variability in isotopic ranges of some rocks, not all data from the Archean and Paleoproterozoic Gawler Craton will lie within these bands. [a] and references therein.

13. Schematic reconstructions of basin development in the Arkaroola area during deposition of the Arkaroola Subgroup and lower Burra Group: a) deposition of the Paralana Quartzite, b) deposition of the Wywyana Formation and Wooltana Volcanics, c) deposition of the Humanity Seat. Note that the Arkaroola Subgroup is represented by pale grey, d) deposition of the Woodnamoka Formation. Note the western extent of nature of deposition is uncertain, e) deposition of the Blue Mine Conglomerate. Note that deposition east of the Paralana Fault has not been included. See text for discussion.

14. a) Schematic of extension and rift development of the northern Flinders Ranges, adapted from Paul et al. (1999). Major growth faults are orientated sub-parallel to the Norwest Fault and are suggested to splay from the Paralana Fault at depth, analogous to growth faults in the Arkaroola area. The Muloorina Ridge is the postulated northern most extent of Adelaidean sedimentation, b) Cartoon schematic of a "negative tulip structure" formed from subsidence along faults which splay from a major strike-slip fault at depth, adapted to the north-south Paralana Fault segment in the Arkaroola area. White arrows indicate the northeast-southwest direction of extension of the Northern Flinders Ranges. Adapted from Woodcock and Fischer, 1986.

15. Schematic of broad folding and tilting of Blue Mine Conglomerate, Woodnamoka and Opaminda Formations and the Sitting Bull Fault, resulting in the apparent angular unconformity to the west of the map area: a) Sub-horizontal stratigraphy folded by F_3. Note that the Sitting Bull Fault dips to the southeast. The red line represents the present-day topography, and the red arrow indicates the direction of folding required to generate the angular unconformity, b) The present day orientation of stratigraphy, as the result of tilting of stratigraphy on the limb of a broad fold.

16. Schematic reconstructions of the evolution of deformation considering a double strain model scenario. See text for discussion. For simplification, stratigraphy overlying the lower Burra Group is not inluded: a) transtension, resulting in the generation of S_B, illustrated as horizontal black lines in the basement (grey). Extension direction is indicated by white arrows. This was followed by the generation of S_Z, as illustrated as horizontal black lines in the Woodnamoka Formation (yellow), under sub-vertical principal stresses produced by burial, as indicated by solid black arrow. b) Subsequent transpression associated with the generation of F_3. Solid black arrows indicate suggested direction of principal stresses.

17. Schematic reconstructions of the evolution of deformation considering a single strain model scenario. See text for discussion. For simplification, stratigraphy overlying the lower Burra Group is not inluded: a) Onset of transpression with predominant vertical stresses, as indicated by solid black arrow, resulting in the generation of $S_{Z,}$ illustrated as horizontal black lines in the Woodnamoka (yellow) formation, b) Increasingly predominant horizontal stresses, as indicated by solid black arrows, resulting in the generation of F_3, c) Lateral extrusion resulting in extension parallel to fold hinges, as indicated by white arrows, and the generation of S_B, illustrated by horizontal black lines in the basement (grey).

11. Tables

Table 1

Sample	Formation	Size (μm)	Aspect ratio	Colour	Shape and morphology	CL description
ARK001	Paralana Quartzite	80-170	2:1 to 4:1	Pink to colourless	Subangular to rounded, commonly euhedral and elongate. Frosted, pitted appearance indicating degree of transport	Vary between complex growth zoning and no zoning, common xenocrystic cores, few minor rims
ARK002	Humanity Seat Formation	70-200	2:1 to 4:1	Yellow to colourless	Subangular to subrounded, commonly euhdral and less commonly needle shaped. Frosted, pitted appearance indicating degree of transport	Complex growth zoning, common xenocrystic cores, few minor rims and late developed domains. Rare reabsorbed grains with no zonation
ARK003	Blue Mine Conglomerate	50-150	3:1 to 4:1	Pink to colourless, commonly exhibit dark red staining	Subangular to subrounded, euhedral to anhedral	Complex growth zoning and common xenocrystic cores, few minor rims, rare fracturing.

Table 2

Sample	Sm (ppm)	Nd (ppm)	$^{147}Sm/^{144}Nd$	$^{143}Nd/^{144}Nd$	2SE	εNd (0) [a]	εNd (T) [b]	T_{DM}	Age
ARK010	4.0876	20.0780	0.12310	0.511731	8	-17.7	-10.39	2356 Ma	780 Ma
ARK011	5.3477	32.5313	0.09940	0.511596	8	-20.32	-10.65	2051 Ma	780 Ma
ARK012	6.4502	34.4909	0.11307	0.511612	8	-20.02	-11.70	2301 Ma	780 Ma

Table 3

	Archean Gawler Craton	Early Proterozoic basement[a]	Musgrave Province	Wooltana Volcanic Formation	Gairdner Dyke Swarm
T_{DM}	-2.7 to - 2.9	-2 to -2.4	-1.8 to -1.9	+ 1.5	+ 2.9

Table 4

	Paralana Quartzite	Wywyana Formation	Humanity Seat Formation	Blue Mine Conglomerate	Opaminda Formation
T_{DM}	1.9	1.9	2.3	2.1	2
εNd	-8.4 (850)	-7.1 (840)	-6.8 (830)	-9.1 (800)	-8.6 (790)
	-8.6* (835)	-7.3* (830)	-7* (790)	-9.4* (765)	-8.9*(760)

Table 5

Sampled formations			Known age determinations (Ma)	Geological Unit			References [a]
Paralana Quartzite	Humanity Seat Formation	Blue Mine Conglomerate		Gawler Craton	Curnamona Province	Mount Painter Basement Complex	
			2558 ± 27	Mulgathing and Sleaford complexes			Daly et al. (1998)
			2560 – 2500				
	2400 Ma						
	2080 Ma		2015 ± 28	Miltalie Gneiss			Fanning et al. (1988)
1860 Ma	1876 Ma		*ca.* 1850	Donington Suite			Belousova et al. (2009)
	1818 Ma						
			1760 – 1740	Wallaroo group			Myers et al. (1996)
			1763 – 1738	Moonta Porphyry			Belousova et al. (2009)
			ca. 1750	Moody Suite			Dutch et al. (2008)
1758 Ma			1737 ± 7	Middle Camp Granite			Reid et al. (2008)
		1700 Ma	~1715 – 1670		lower Willyama Supergroup		Barovich and Hand (2008)
			~1670 – 1640		upper Willyama		
			~1670 – 1640	Tarcoola Formation	Supergroup		Barovich and Hand. (2008)
			1656 ± 7	St Peter Suite			Flint et al. (1990)
	1645 Ma		1631-1627	Nuyts Volcanics			Flint et al. (1990)
1610 Ma			1603 ± 19			Pepegoona Volcanics	Kromkhun (2010)
			1595-1575	Hiltaba Suite			Flint et al. (1993)
			ca 1590	Gawler Range Volcanics			Howard et al. (2011)
			1590 ± 5			Mount Neill Granite	Kromkhun (2010)
		1585 Ma	1586 ± 45			Box Bore Granite	Kromkhun (2010)
			ca 1580	Munjeela granite			Ferris et al. (2004)
	1570 Ma		1569 ± 20			Terapinna Granite	Kromkhun (2010)
			1562 ±7			Wattleowie Granite	Kromkhun (2010)
			1556 ± 20			Yerila Granite	Kromkhun (2010)
			ca. 1500	Spilsby suite			Howard et al. (2011)

12. Figures

Figure 2

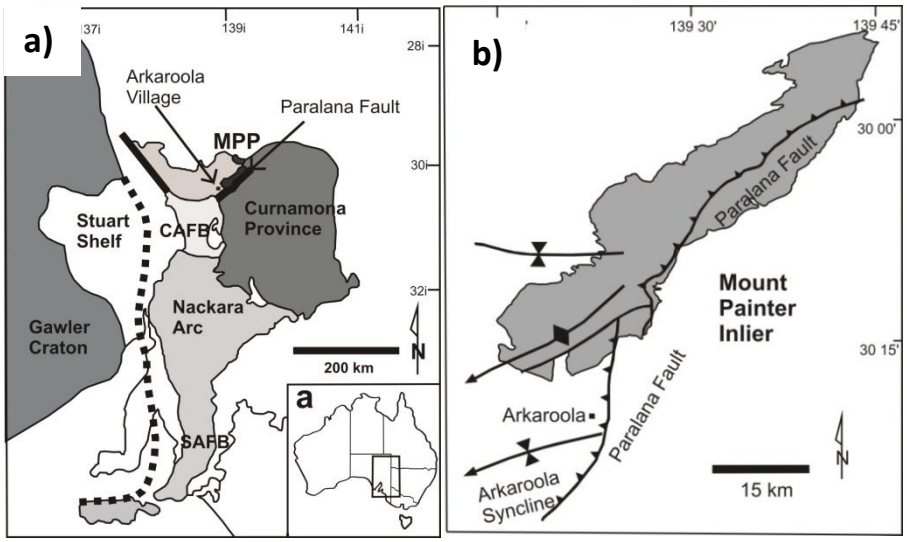

Figure 3

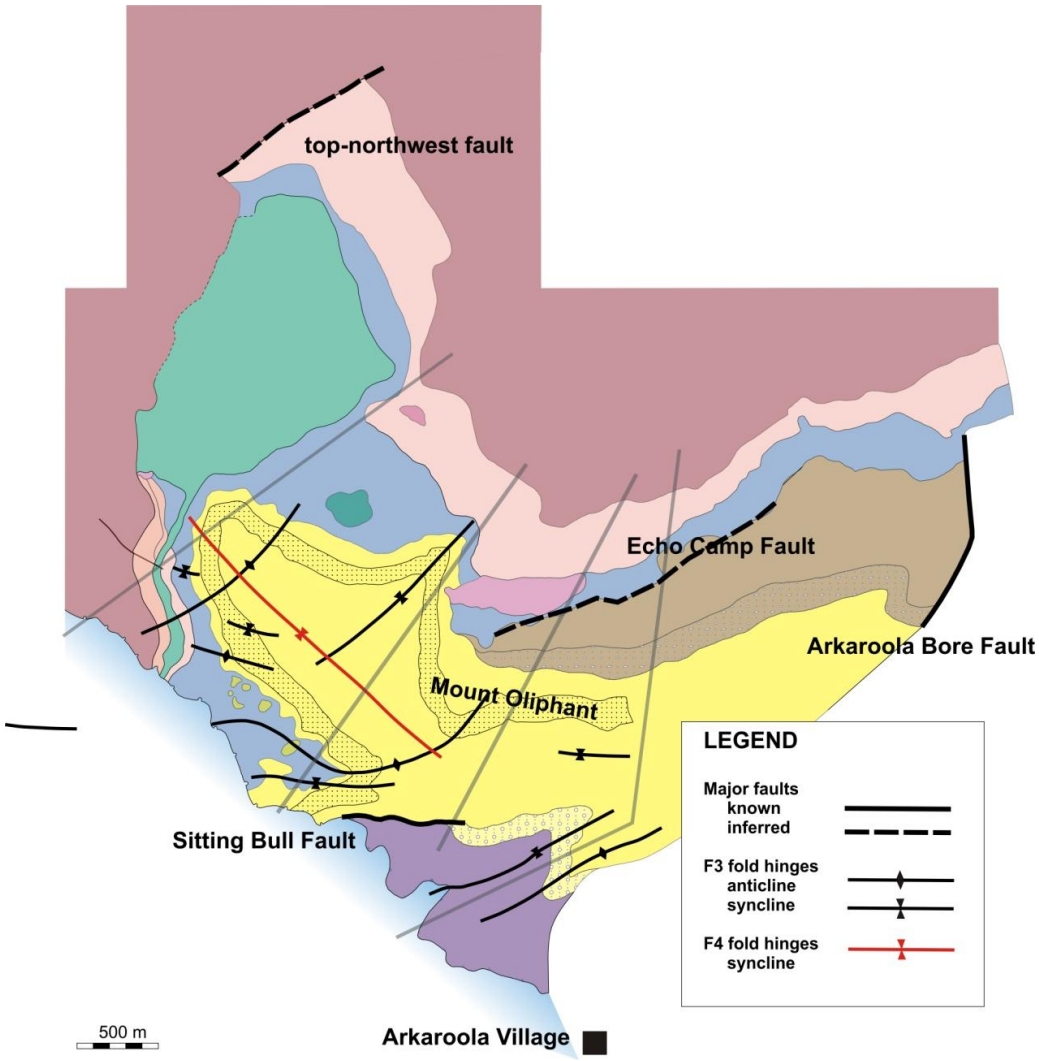

Figure 4

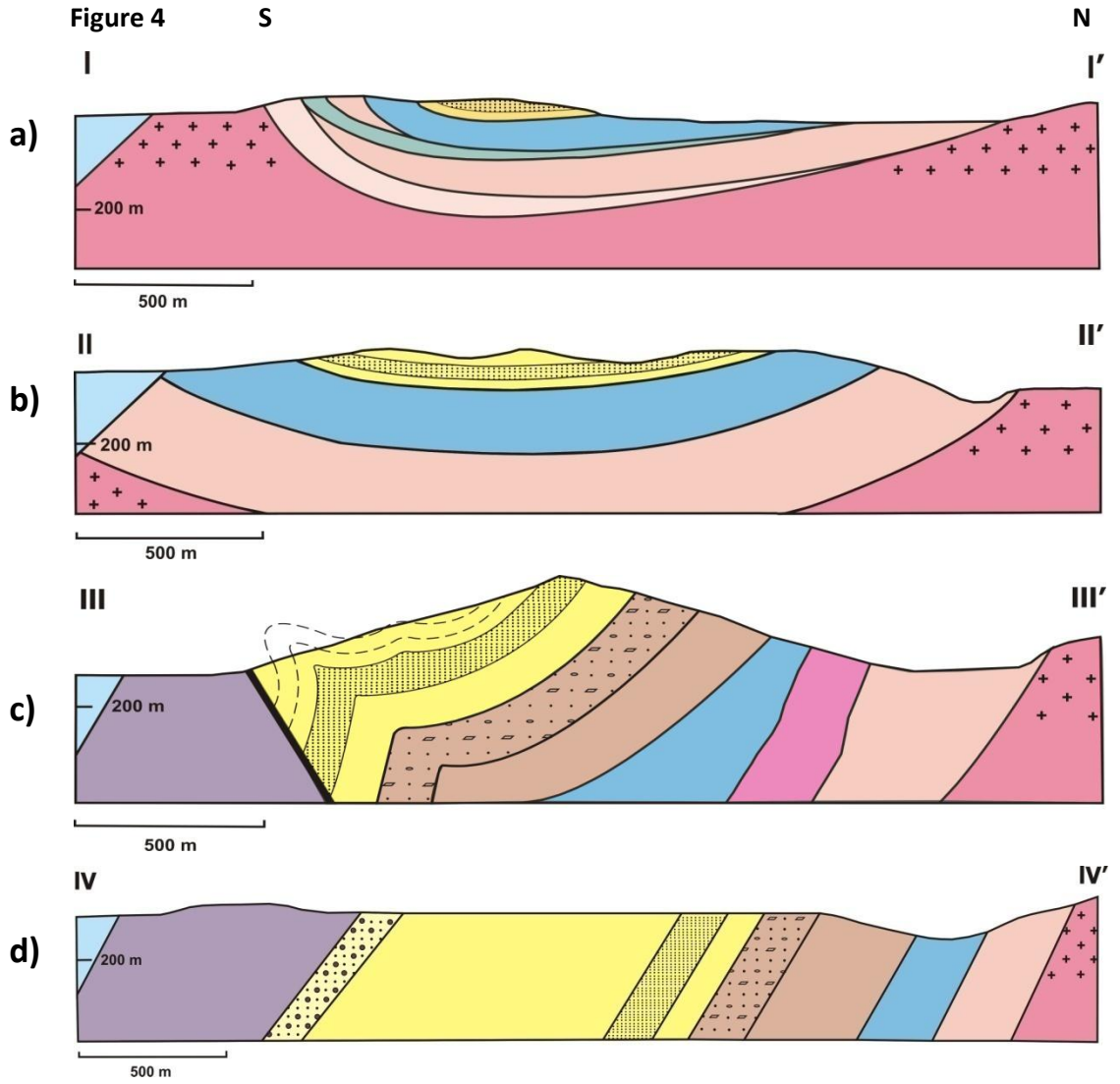

Figure 5

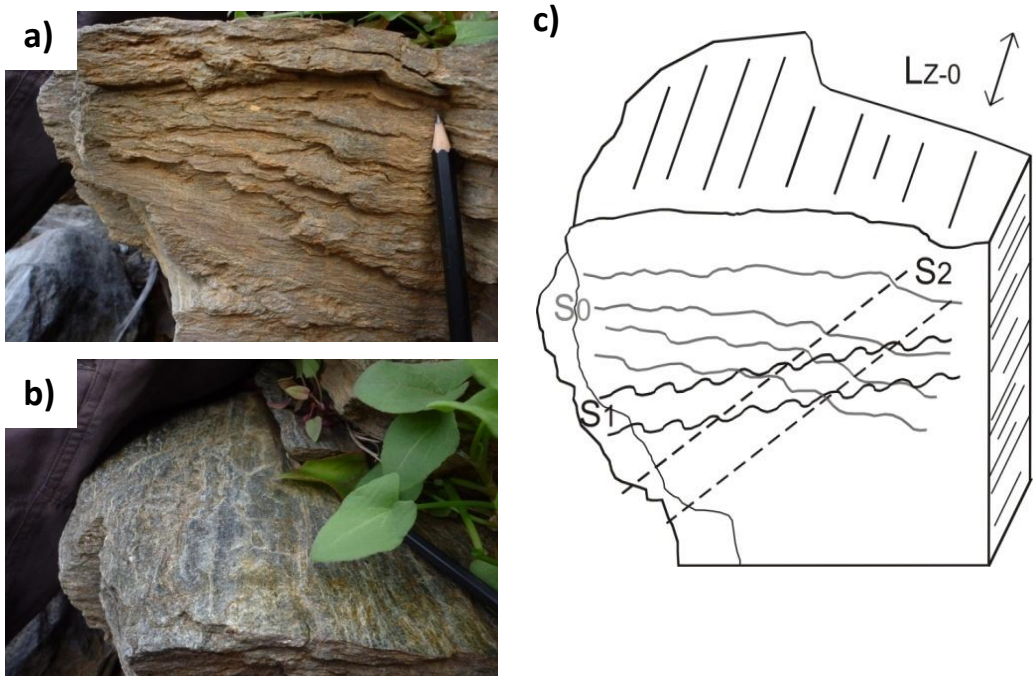

Figure 6

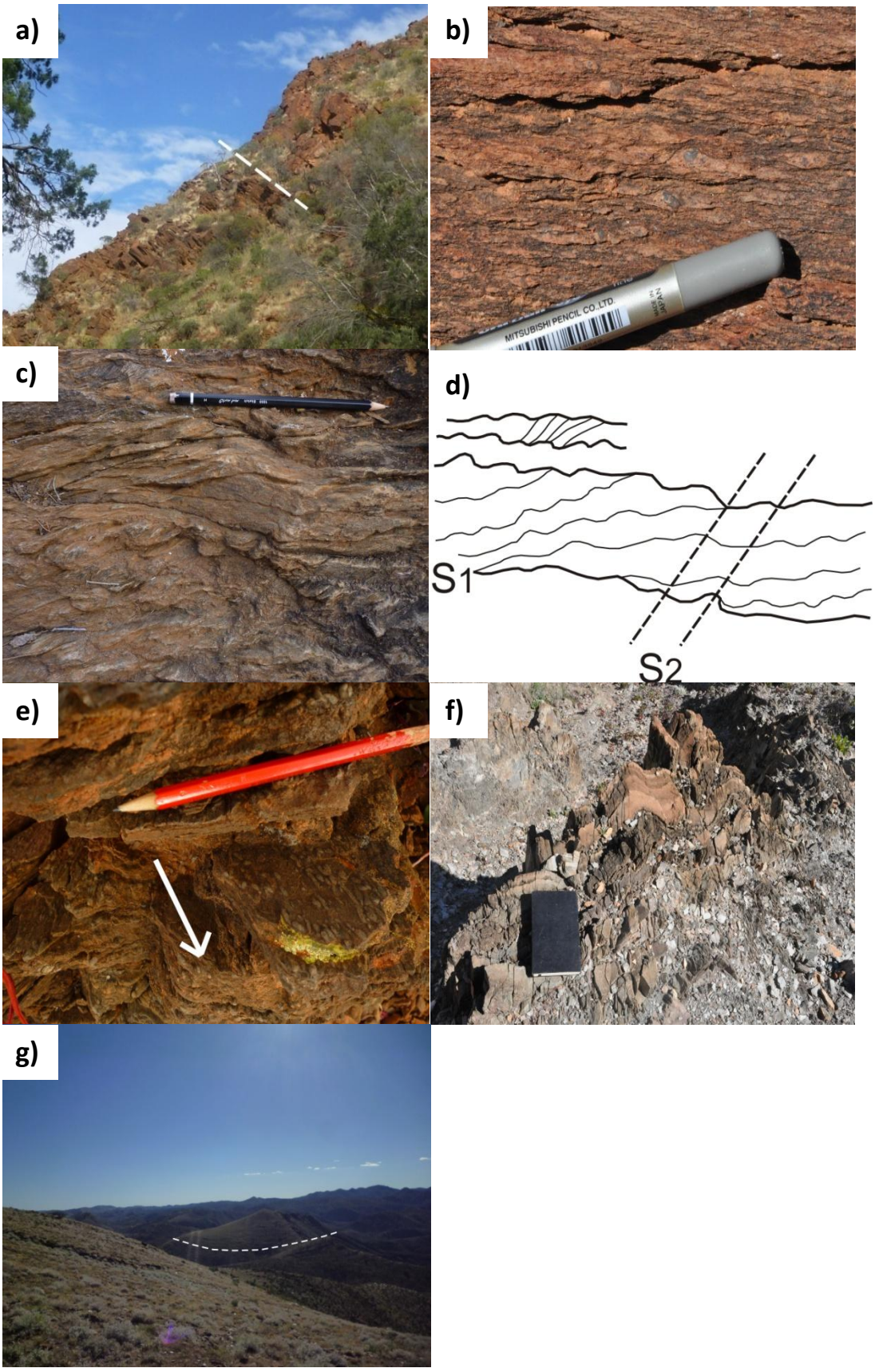

Figure 7

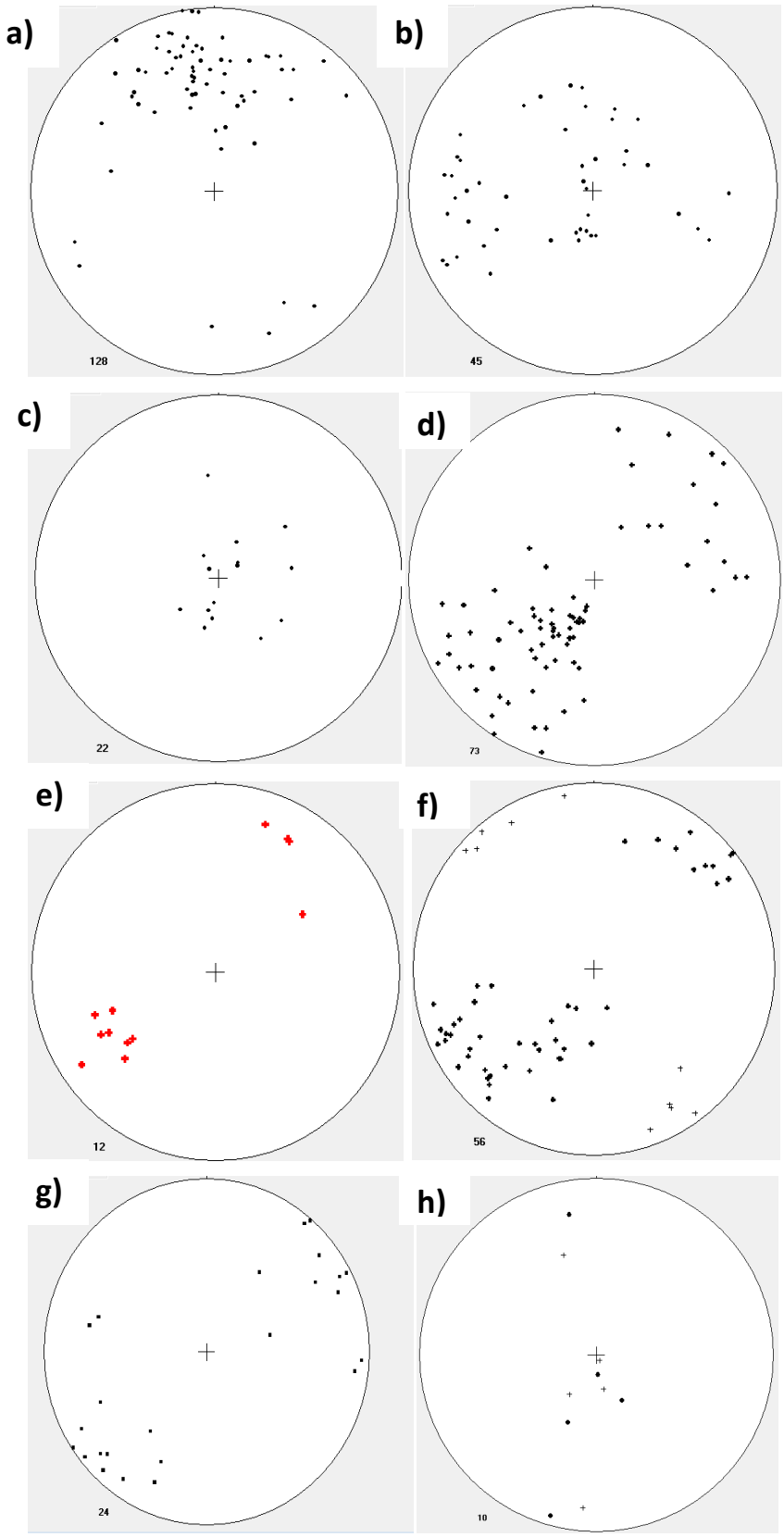

Figure 8

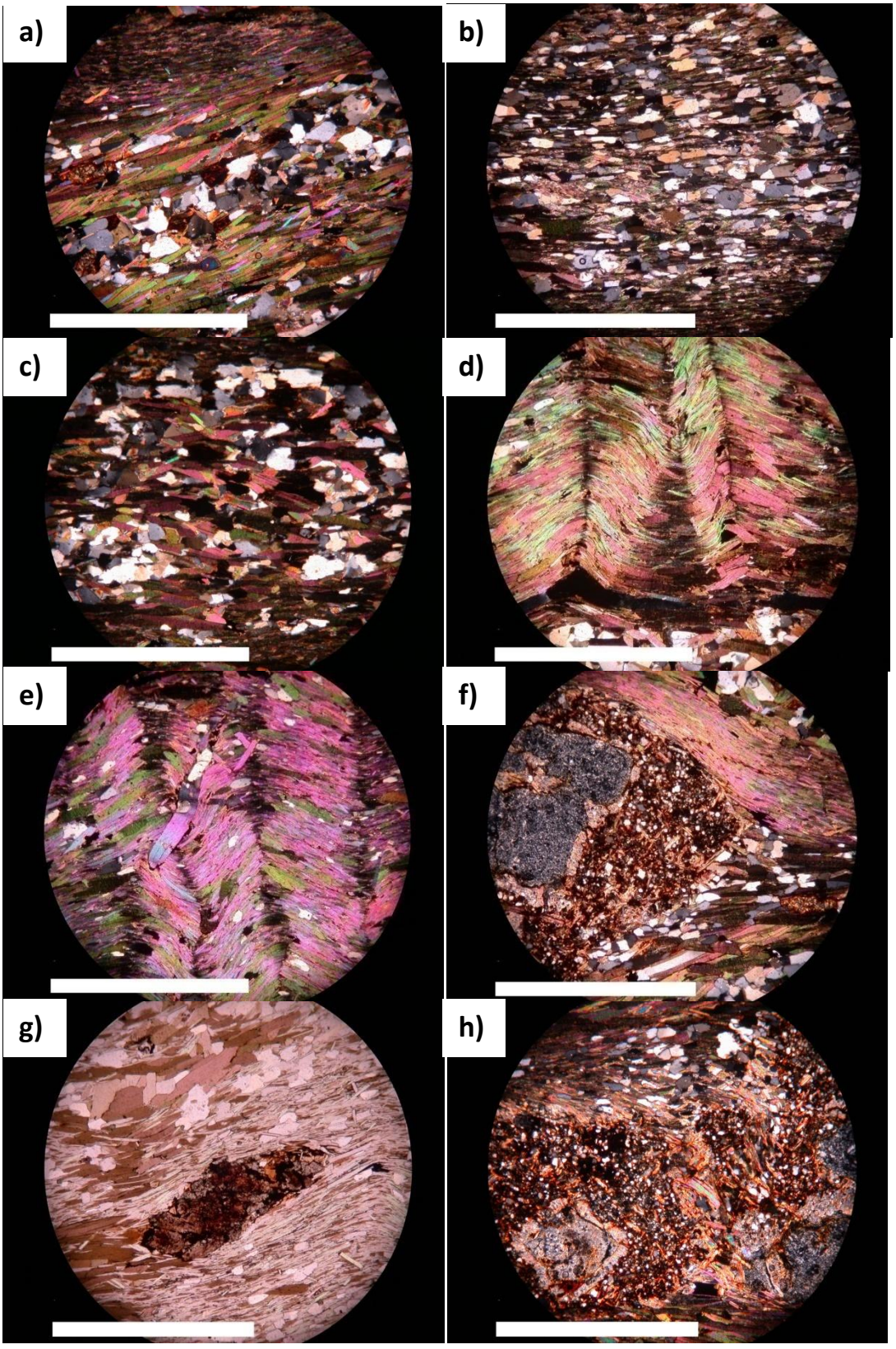

Figure 9

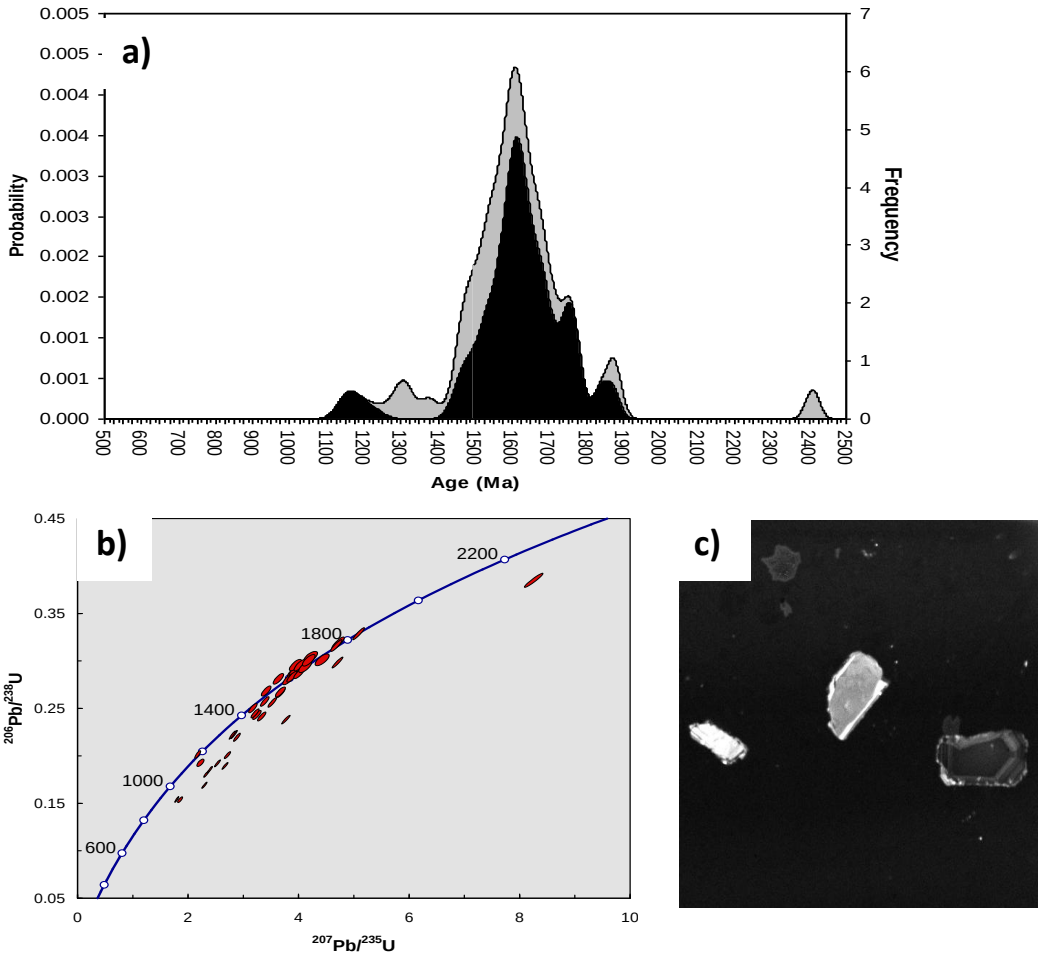

Figure 10

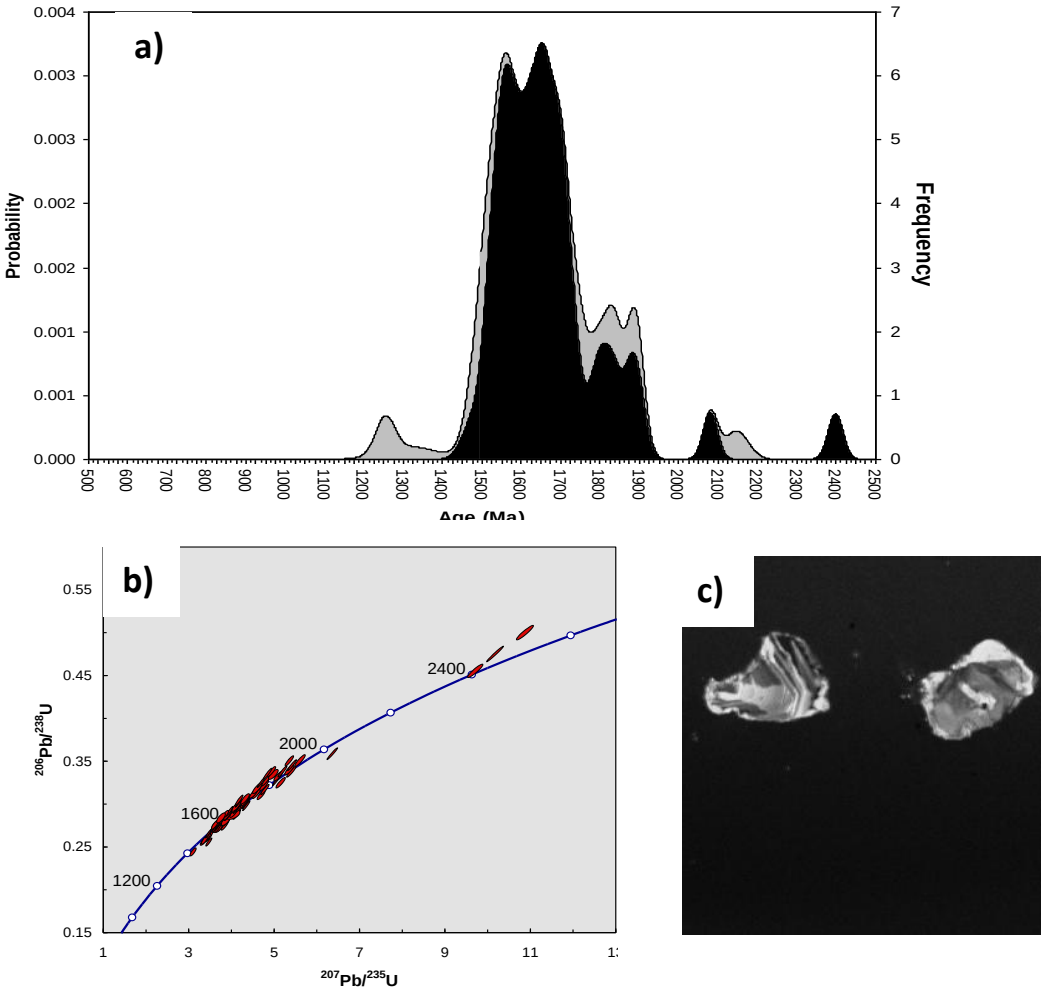

Figure 11

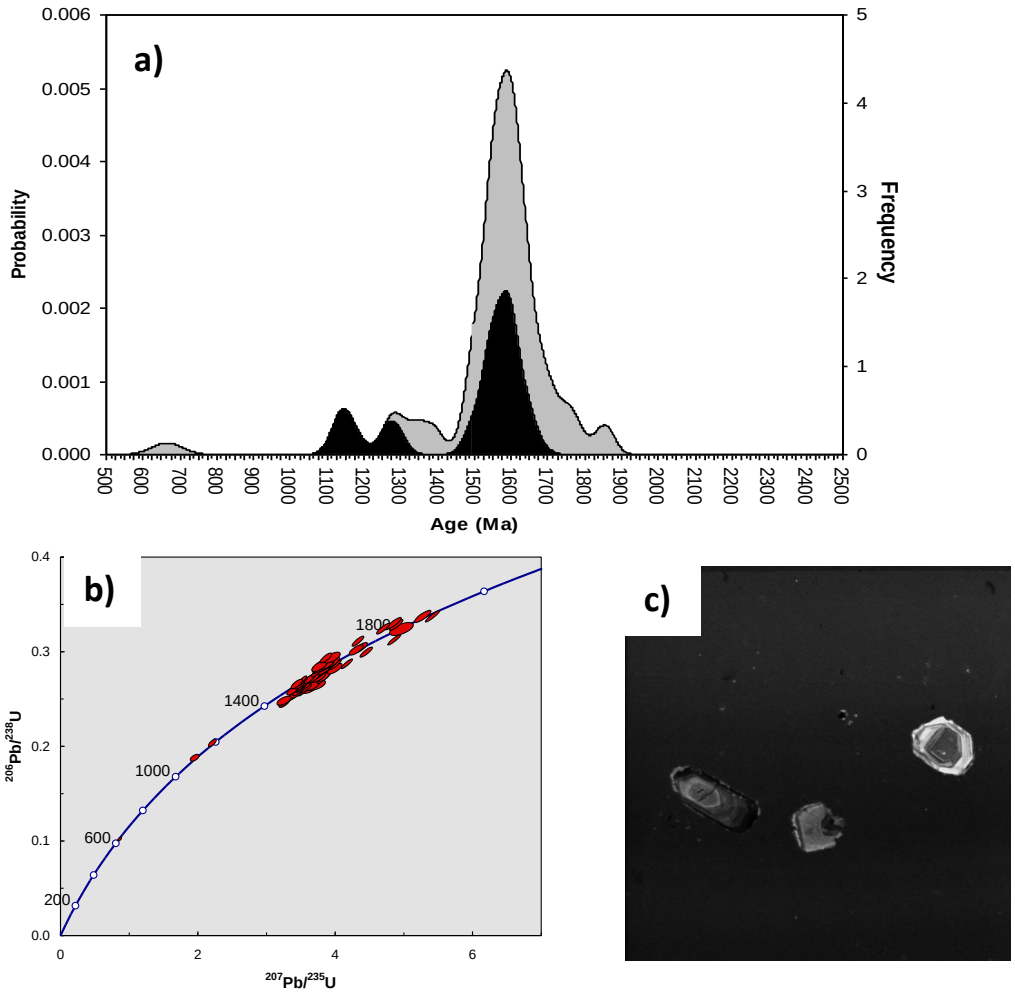

Figure 12

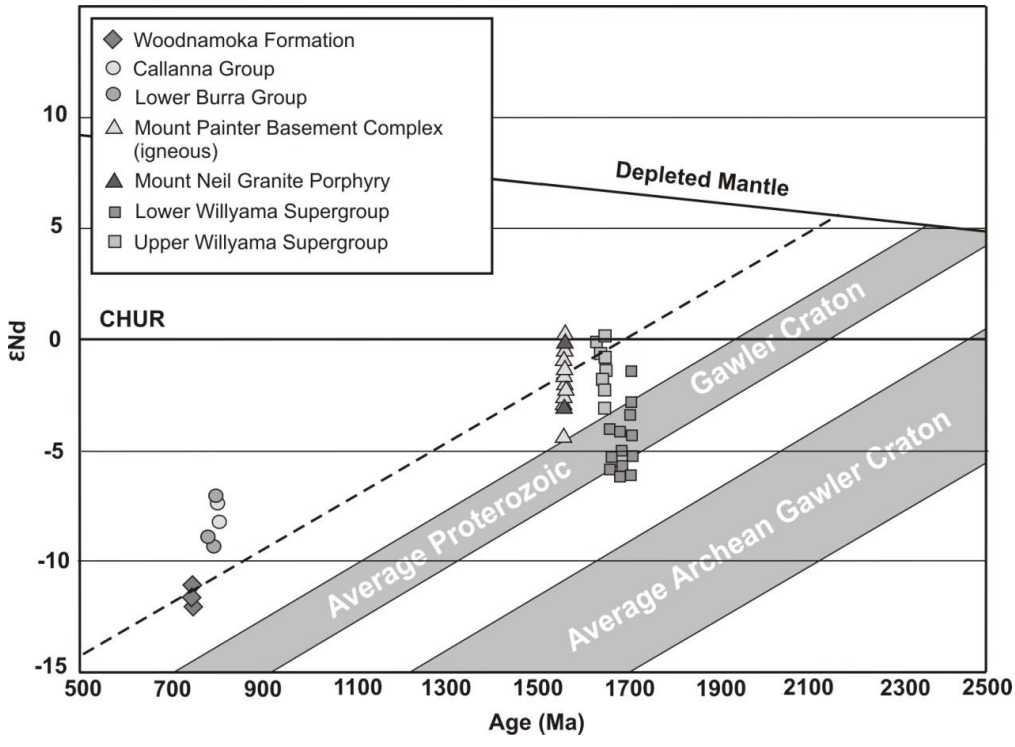

Figure 13

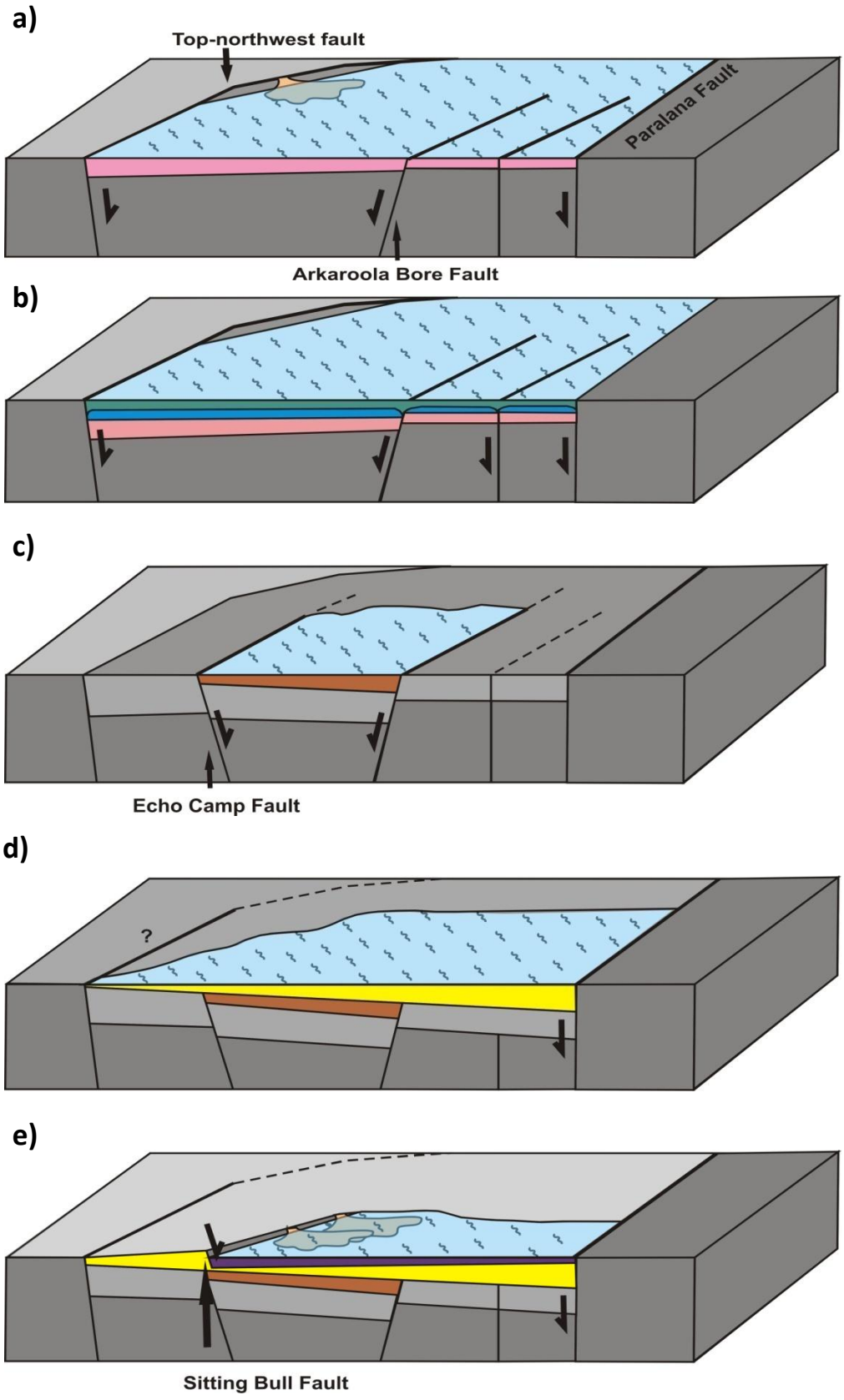
a)
Top-northwest fault
Paralana Fault
Arkaroola Bore Fault
b)
c)
Echo Camp Fault
d)
?
e)
Sitting Bull Fault

Figure 14

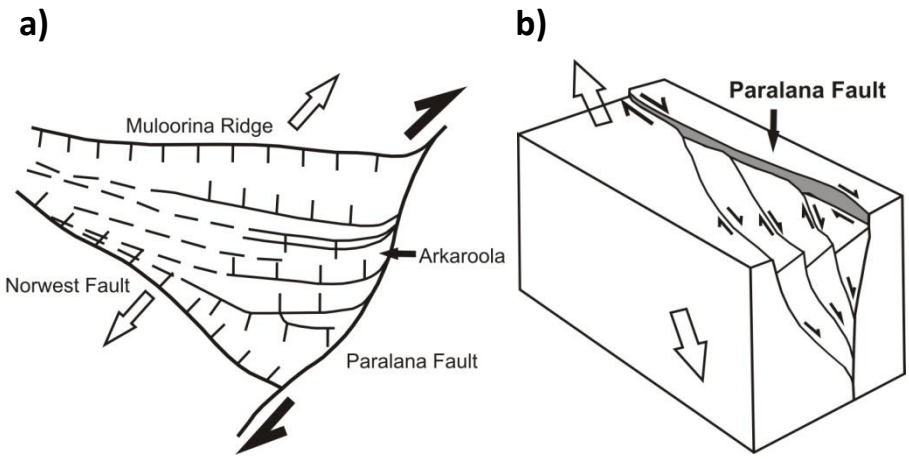

Figure 15

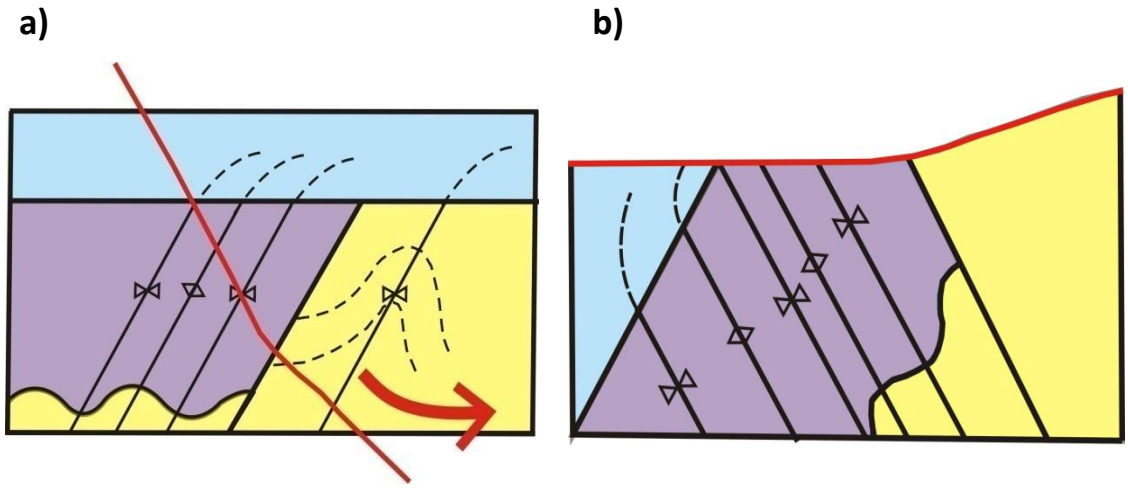

Figure 16

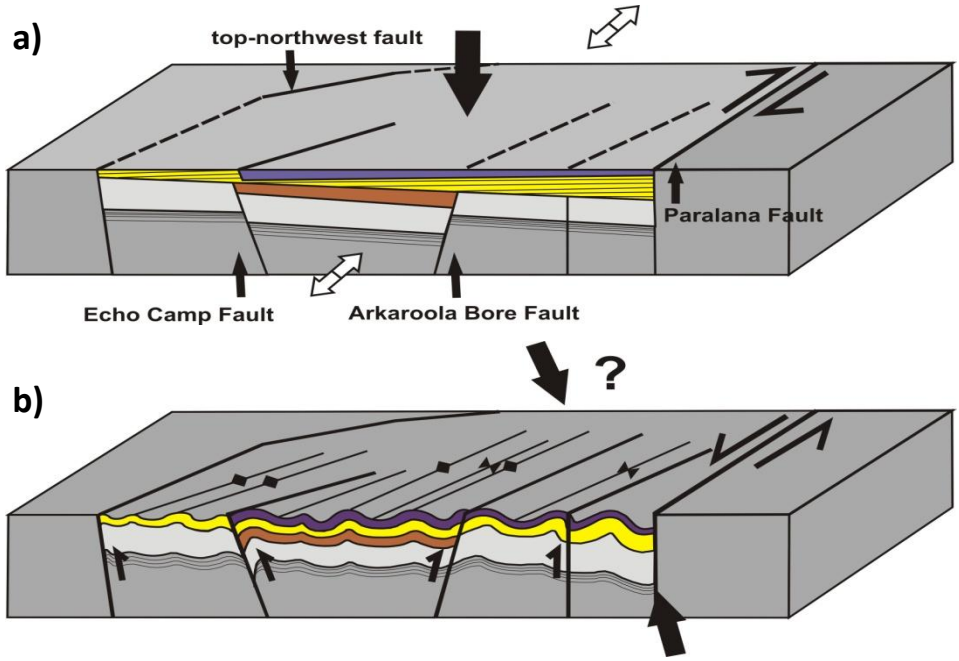

Figure 17

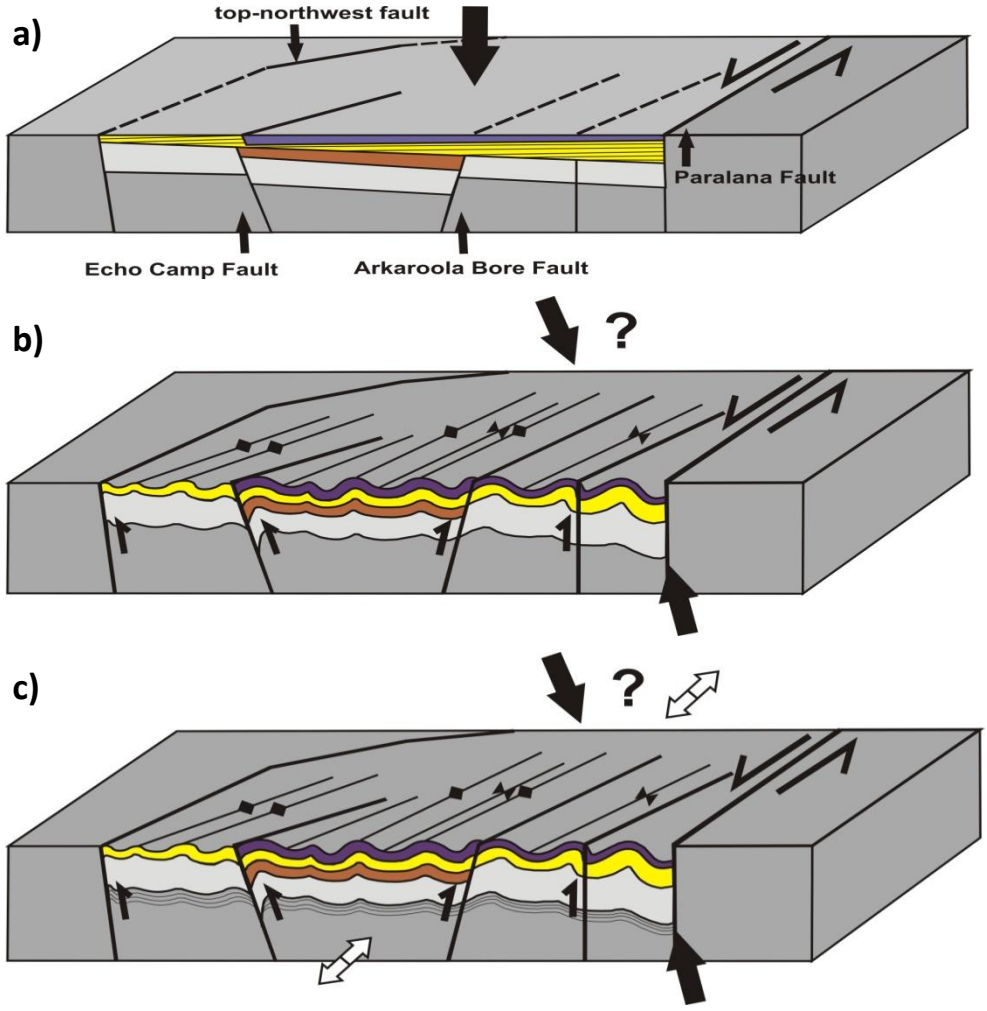

13. Appendices

Appendix 1: Analytical methods

U-Pb analytical methods

Four samples for geochronological investigation were crushed in a stainless steel jaw crusher and a 79-425 µm fraction separated using a tungsten-carbide ring mill and sieve shaker. Separates were obtained by hand panning, Franz, and heavy liquid methods, which were then handpicked and mounted into epoxy resin. The Wortupa sample did not yield sufficient zircon grains so was excluded from the analysis.

Zircon grains were imaged using CL on a Phillips XL-20 SEM with attached Gatan Cathode Luminescence.

U-Pb analysis was then undertaken using a New Wave 213nm Nd-YAG laser in He ablation atmosphere, coupled to a Agilent 7500cs LA-ICPMS.

U-Pb fractionation was corrected using the GEMOC GJ-1 zircon (TIMS normalisation data $^{207}Pb/^{206}Pb$ = 608.3 Ma, $^{206}Pb/^{238}U$ = 600.7 Ma and $^{207}Pb/^{235}U$ = 602.2 Ma; Jackson et al., 2004). Accuracy was checked with the Plešovice zircon standard mean ID-TIMS U-Pb age of 337.13 ± 0.37 Ma (Howard et al., 2011). Detrital cores were targeted using 30 μm spot size at 75% power rating with smaller grains targeted with a 25 μm spot size at 80% power rating.

A <10% discordancy threshold was used to filter the data. Average normalized ages over the duration of the study for GJ-1 are: 609.6 ± 9.4, 602.6 ± 1.3, 603.3 ± 5 (σ2, n = 98), and Plešovice: 341 ± 14, 341 ± 4.8, 342 ± 4 for $^{207}Pb/^{206}Pb$, $^{206}Pb/^{238}U$, $^{207}Pb/^{235}U$ (σ2, n = 82).

Sm-Nd analytical methods

Samples were spiked with a $^{150}Nd/^{147}Sm$ solution and dissolved in PFA vials using HF and HF-HNO_3. These were then converted to chloride using 6N HCl. REE were separated in Biorad Polyprep columns and further separated in HDEHP-impregnated Teflon-powder columns to isolate Sm and Nd. The resulting Sm and Nd samples were loaded onto double tantalum and rhenium filaments and analysed for their isotopic compositions on a Finnigan MAT 262 Thermal Ionisation Mass Spectrometer (TIMS). Data blocks of 10 scans were run until acceptable within-run statistics were achieved. A running average appropriate to the duration of the analysis for mass spectronometer standard JNdi-1 is 0.512081 ± 0.008.

Appendix 2

Thin section analysis microphotographs

Microphotographs for AARK01

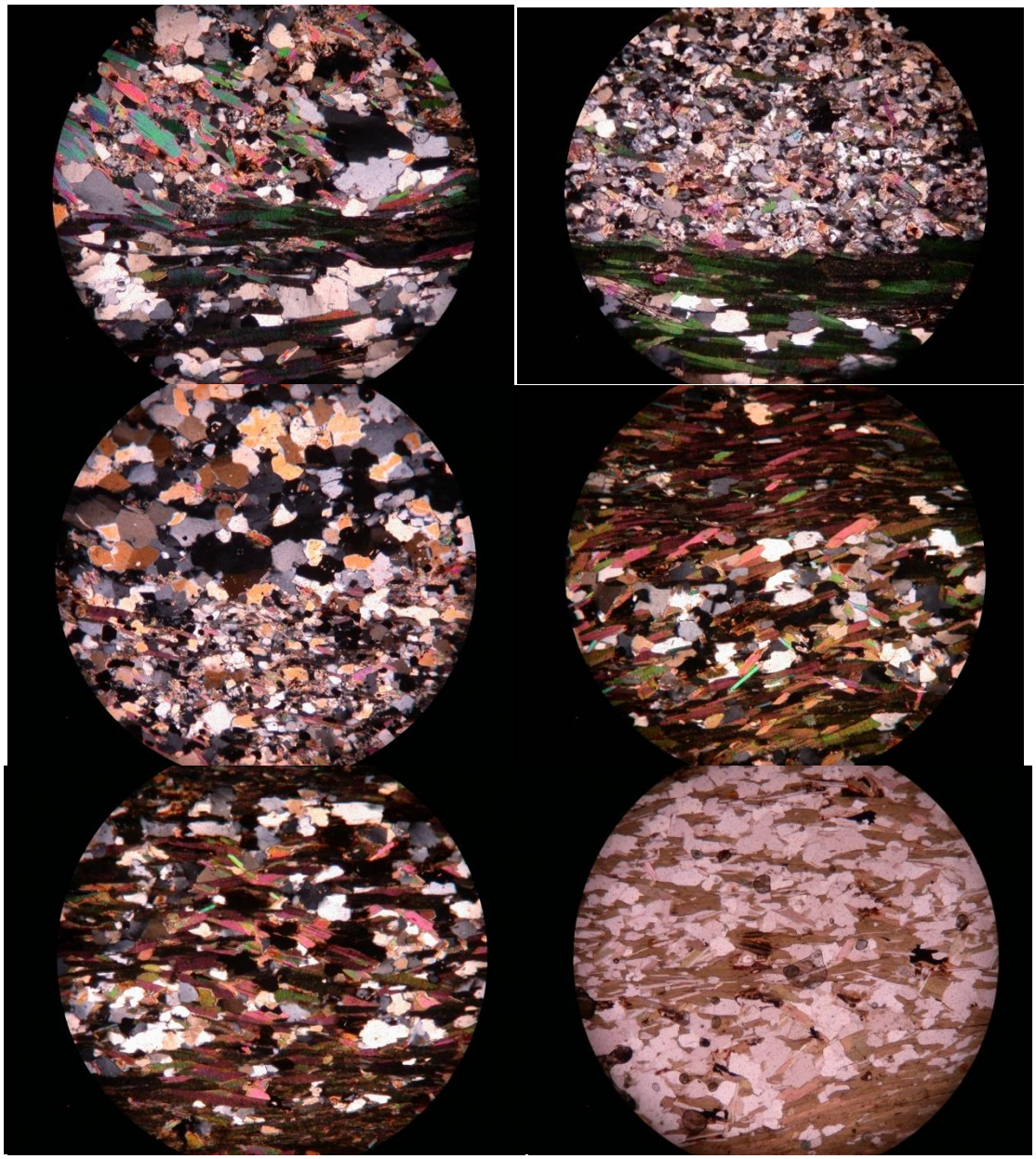

Photomicrographs for AARK03

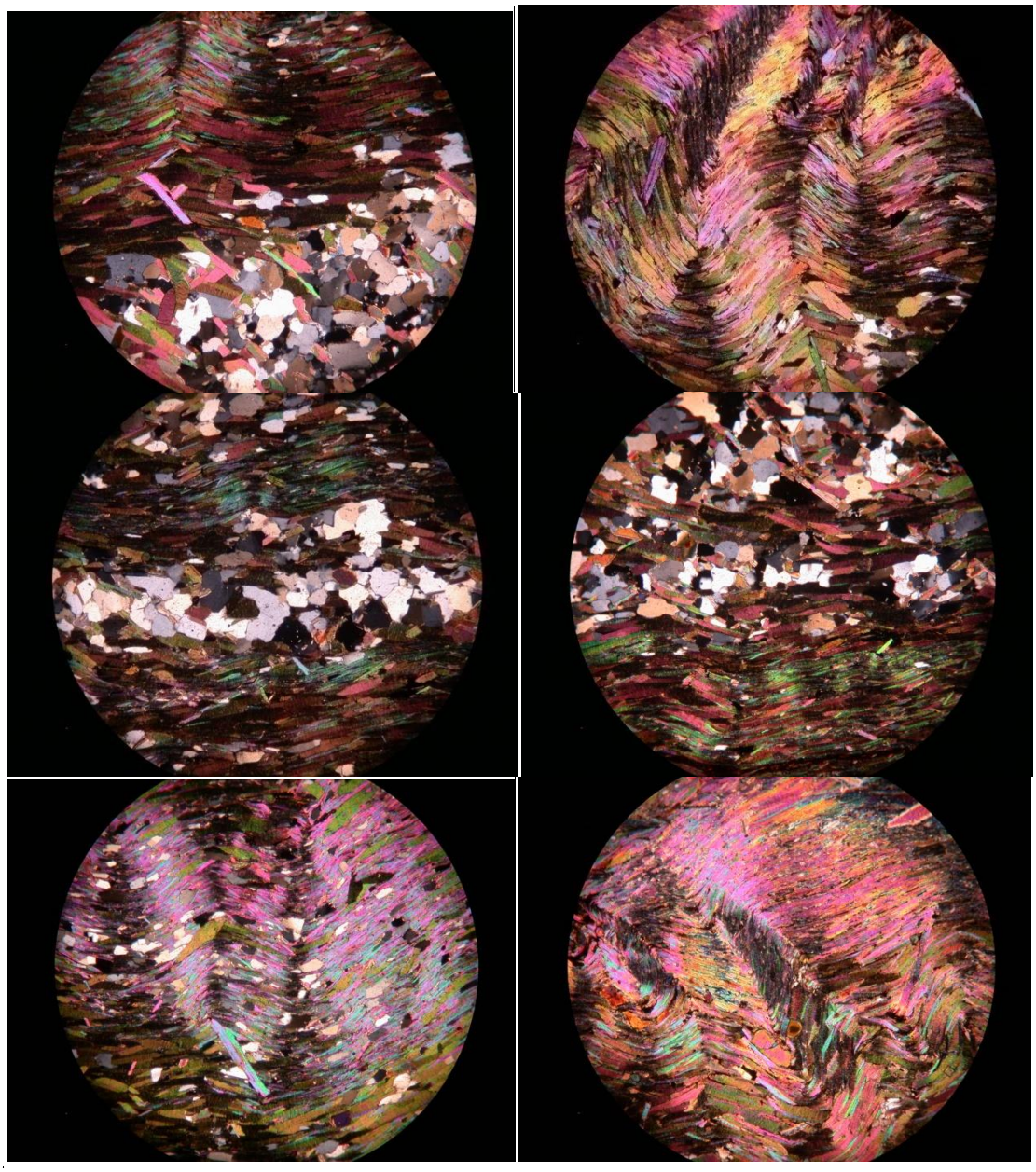

Photomicrographs for AARK07

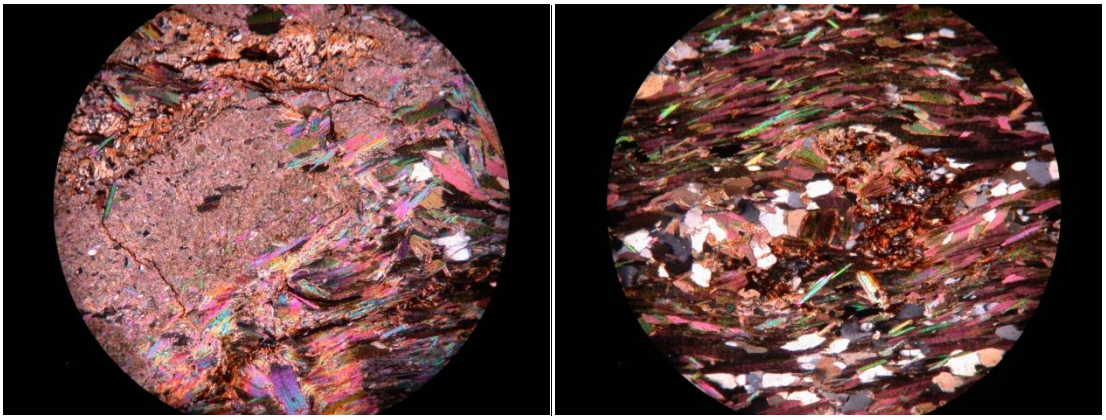

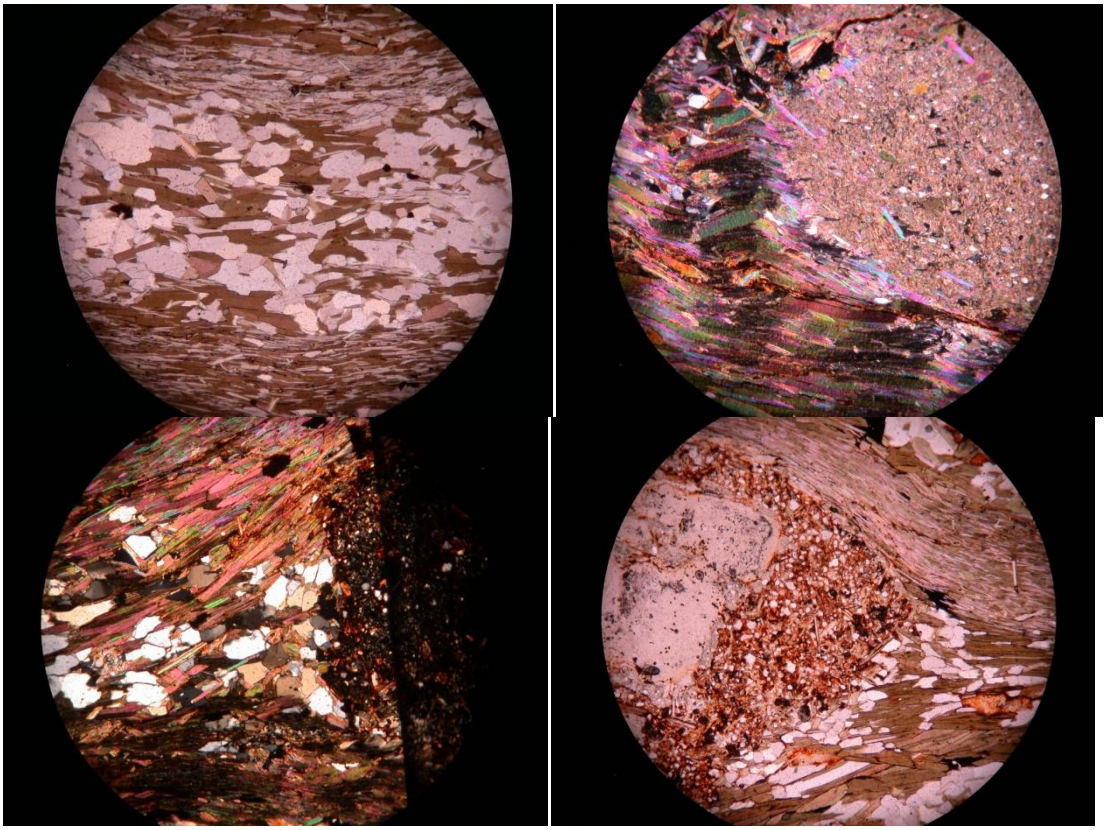

Appendix 3 – Detrital zircon data

Paralana Quartzite: Radiogenic ratios								
spot	207/206Pb	1s	206pb/238U	1s	207Pb/235U	1s	208Pb/232Th	1s
p1row101	0.10386	0.00128	0.2669	0.00326	3.82031	0.05304	0.08153	0.0009
p1row102	0.09785	0.00111	0.28498	0.00345	3.84303	0.05031	0.07634	0.00084
p1row103	0.10809	0.00124	0.29346	0.00356	4.37178	0.05768	0.07929	0.00086
p1row104	0.10263	0.00126	0.29902	0.00365	4.22928	0.05861	0.08323	0.00086
p1row105	0.10228	0.00136	0.31233	0.00385	4.4027	0.06467	0.0875	0.00098
p1row106	0.09646	0.00118	0.16563	0.00202	2.20194	0.03044	0.05031	0.00052
p1row107	0.10339	0.00141	0.31606	0.00391	4.50343	0.06749	0.08617	0.00101
p1row108	0.10685	0.00169	0.30639	0.00389	4.51197	0.07625	0.08768	0.00113
p1row109	0.09789	0.00125	0.2847	0.00349	3.84088	0.05498	0.07904	0.00088
p1row110	0.10478	0.00131	0.24609	0.00301	3.55364	0.04988	0.07653	0.00089
p1row111	0.10186	0.00252	0.17128	0.00238	2.40453	0.05993	0.05128	0.00082
p1row112	0.09957	0.00124	0.26327	0.00322	3.61266	0.05067	0.07325	0.00076
p1row113	0.10022	0.00126	0.2653	0.00325	3.66447	0.05184	0.07478	0.00077
p1row115	0.0985	0.00166	0.28721	0.00388	3.89748	0.07122	0.08302	0.00114
p1row116	0.08469	0.00097	0.15295	0.00197	1.78467	0.02474	0.05619	0.00062
p1row117	0.0783	0.0011	0.20047	0.00262	2.16246	0.03435	0.05889	0.00067
p1row118	0.10733	0.00144	0.31826	0.00418	4.70614	0.07241	0.09238	0.00129
p1row119	0.15576	0.00173	0.38441	0.00497	8.24897	0.11171	0.10207	0.00109
p1row120	0.09383	0.00147	0.28037	0.00374	3.6243	0.06249	0.08262	0.0011
p1row121	0.09848	0.00147	0.28899	0.00384	3.92073	0.06521	0.08227	0.00102

p1row122	0.097	0.00131	0.24219	0.00317	3.23653	0.05006	0.07391	0.00089
p1row123	0.0954	0.00115	0.21861	0.00283	2.8731	0.04102	0.05593	0.00061
p1row124	0.09976	0.0012	0.30098	0.0039	4.13653	0.05904	0.08659	0.00101
p1row125	0.09873	0.00114	0.16799	0.00216	2.28498	0.03167	0.04745	0.00052
p1row126	0.10074	0.0019	0.30306	0.00419	4.20601	0.08399	0.08983	0.00122
p1row127	0.10022	0.00132	0.2406	0.00314	3.32204	0.05048	0.07854	0.00088
p1row128	0.09686	0.00162	0.29489	0.00398	3.93487	0.07131	0.08523	0.00103
p1row129	0.09873	0.00145	0.29469	0.0039	4.00831	0.066	0.0857	0.00104
p1row130	0.10758	0.0013	0.31548	0.00409	4.67563	0.0668	0.09134	0.00107
p1row131	0.09868	0.00155	0.27978	0.00374	3.80339	0.0657	0.08122	0.00102
p1row132	0.08368	0.00154	0.19171	0.0026	2.21022	0.04347	0.0594	0.0007
p1row133	0.09985	0.00121	0.25542	0.00331	3.51366	0.05044	0.07303	0.00085
p1row134	0.11234	0.00127	0.32802	0.00423	5.07658	0.06966	0.0948	0.00104
p1row135	0.09934	0.00138	0.28255	0.00371	3.87034	0.06137	0.07859	0.00091
p1row136	0.11491	0.00125	0.23728	0.00304	3.75933	0.05052	0.06271	0.00067
p1row137	0.11446	0.00126	0.29758	0.00382	4.69626	0.06356	0.05204	0.0007
p1row138	0.09238	0.001	0.22156	0.00283	2.82211	0.03773	0.06246	0.00066
p1row139	0.09154	0.00102	0.22099	0.00283	2.7894	0.03805	0.04262	0.00049
p1row140	0.09565	0.00107	0.19113	0.00245	2.52063	0.03454	0.04808	0.00051
p1row141	0.10134	0.00143	0.28628	0.00376	4.00018	0.06397	0.08114	0.00096
p1row142	0.09963	0.00141	0.26649	0.0035	3.66081	0.05866	0.07765	0.00094
p1row143	0.09518	0.00123	0.24388	0.00317	3.20042	0.04807	0.07082	0.00081
p1row144	0.0919	0.00128	0.24941	0.00326	3.16026	0.05009	0.07466	0.00087
p1row145	0.10229	0.00115	0.18835	0.00242	2.65643	0.03633	0.05042	0.00055
p1row146	0.09363	0.00105	0.17992	0.00231	2.32281	0.03179	0.05537	0.0006
p1row147	0.09555	0.00126	0.25642	0.00334	3.37823	0.05154	0.07466	0.00083
p1row201	0.09681	0.00209	0.26508	0.00376	3.53697	0.07934	0.07119	0.00107
p1row202	0.10356	0.00222	0.28707	0.00409	4.09749	0.09119	0.0665	0.00139
p1row203	0.1051	0.00218	0.27285	0.00386	3.95236	0.08569	0.0764	0.00101
p1row204	0.08016	0.0015	0.19775	0.00268	2.18485	0.0436	0.05297	0.00065
p1row205	0.096	0.00194	0.26854	0.00375	3.55307	0.07539	0.07097	0.00094
p1row206	0.0958	0.00253	0.26912	0.00404	3.55355	0.09535	0.06601	0.00117
p1row206	0.09383	0.00104	0.18419	0.00236	2.38193	0.03233	0.04092	0.00041
p1row207	0.0923	0.00144	0.26751	0.00355	3.40328	0.05848	0.07087	0.00108
p1row208	0.10666	0.00188	0.30043	0.0041	4.41646	0.08354	0.08534	0.00114
p1row209	0.10176	0.00176	0.29307	0.00398	4.11037	0.07668	0.07744	0.001
p1row210	0.10098	0.00167	0.29999	0.00404	4.17518	0.07505	0.07856	0.00097

Paralana	Quartzite:	Age (Ma)						
207/206Pb	1s	206Pb/238U	1s	207/235Pb	1s	208Pb/232Th	1s	% conc
1694.2	22.52	1525.1	16.59	1597	11.17	1584.2	16.91	90
1583.5	21.04	1616.4	17.3	1601.8	10.55	1486.9	15.87	102
1767.4	20.83	1658.8	17.74	1707	10.9	1542.3	16.18	94
1672.2	22.51	1686.4	18.12	1679.7	11.38	1615.9	16.06	101
1665.9	24.34	1752.2	18.92	1712.8	12.15	1695.3	18.29	105
1556.8	22.8	988	11.16	1181.7	9.65	992.1	9.95	63
1685.8	24.92	1770.4	19.17	1731.6	12.45	1670.8	18.71	105
1746.4	28.68	1722.9	19.19	1733.2	14.05	1698.7	20.96	99
1584.3	23.78	1615	17.52	1601.4	11.53	1537.6	16.43	102
1710.5	22.82	1418.3	15.58	1539.2	11.12	1490.5	16.8	83
1658.3	45.19	1019.2	13.11	1244	17.87	1010.9	15.69	61
1616	23.05	1506.6	16.42	1552.3	11.15	1428.8	14.23	93
1628.2	23.28	1516.9	16.55	1563.7	11.28	1457.7	14.42	93
1595.9	31.15	1627.6	19.44	1613.2	14.77	1612	21.19	74
1308.4	22.19	917.5	11	1039.9	9.02	1105	11.81	67
1154.5	27.53	1177.8	14.07	1169.1	11.03	1156.6	12.88	102
1754.6	24.31	1781.2	20.44	1768.3	12.89	1785.9	23.86	70
2410.2	18.75	2096.8	23.12	2258.7	12.26	1964.4	20.02	102
1504.7	29.27	1593.2	18.82	1554.9	13.72	1604.6	20.49	102
1595.5	27.61	1636.5	19.18	1618	13.46	1598	19.11	87
1567.2	25.13	1398.1	16.46	1466	12	1441.2	16.74	106
1535.9	22.48	1274.6	14.96	1374.9	10.75	1100	11.71	103
1619.6	22.21	1696.2	19.32	1661.5	11.67	1678.6	18.77	89
1600.3	21.32	1001	11.95	1207.7	9.79	937	10.1	83
1637.8	34.53	1706.5	20.72	1675.2	16.38	1738.8	22.71	105
1628.2	24.34	1389.8	16.34	1486.2	11.86	1528.2	16.52	63
1564.4	30.95	1665.9	19.8	1620.9	14.67	1653.2	19.2	104
1600.3	27.23	1664.9	19.44	1635.9	13.38	1661.9	19.36	85
1758.8	21.81	1767.6	20.05	1762.9	11.95	1766.7	19.77	106
1599.3	29.01	1590.2	18.83	1593.5	13.89	1578.5	19.06	104
1285.1	35.56	1130.6	14.05	1184.3	13.75	1166.3	13.36	101
1621.3	22.41	1466.4	16.99	1530.3	11.35	1424.7	16.1	99
1837.6	20.36	1828.8	20.54	1832.2	11.64	1830.6	19.15	88
1611.8	25.75	1604.2	18.63	1607.5	12.8	1529.2	17	90
1878.4	19.49	1372.5	15.84	1584.1	10.78	1229.3	12.79	100
1871.4	19.73	1679.3	18.97	1766.6	11.33	1025.3	13.5	100
1475.1	20.43	1290.1	14.95	1361.4	10.02	1224.6	12.61	73
1457.8	21.04	1287.1	14.96	1352.7	10.2	843.6	9.41	90
1540.8	20.96	1127.5	13.27	1278	9.96	949.2	9.85	87
1648.8	25.93	1622.9	18.86	1634.2	12.99	1577	17.92	88
1617.2	26.11	1523	17.83	1562.9	12.78	1511.4	17.7	73
1531.6	24.11	1406.8	16.42	1457.3	11.62	1383	15.36	98
1465.1	26.34	1435.5	16.84	1447.5	12.23	1455.4	16.34	94
1666.1	20.57	1112.4	13.11	1316.4	10.09	994.2	10.59	92

1500.7	21.03	1066.6	12.61	1219.3	9.71	1089.2	11.54	98
1539	24.63	1471.5	17.13	1499.4	11.95	1455.4	15.67	67
1563.6	39.94	1515.8	19.14	1535.5	17.76	1390	20.15	71
1688.9	38.99	1626.9	20.49	1653.8	18.17	1301.3	26.39	96
1716.1	37.73	1555.2	19.55	1624.5	17.57	1488	19	72
1201	36.5	1163.2	14.42	1176.2	13.9	1043.2	12.39	104
1547.7	37.51	1533.4	19.04	1539.1	16.81	1385.8	17.65	97
1543.9	48.87	1536.3	20.5	1539.2	21.26	1292.1	22.24	100
1504.6	20.83	1089.8	12.85	1237.2	9.71	810.6	7.97	103
1473.5	29.34	1528.2	18.07	1505.2	13.49	1384	20.42	97
1743.1	31.87	1693.5	20.35	1715.4	15.66	1655.3	21.28	96
1656.4	31.71	1656.9	19.84	1656.4	15.24	1507.5	18.69	91
1642.2	30.32	1691.3	20.02	1669.2	14.73	1528.5	18.16	97

Humanity Seat Formation: Radiogenic ratios								
spot	207/206Pb	1s	206pb/238U	1s	207Pb/235U	1s	208Pb/232Th	1s
HS102	0.09633	0.00112	0.28817	0.00372	0.05255	1598.3	0.00111	1734.3
HS103	0.09788	0.00317	0.09742	0.00174	0.04092	852	0.00119	907.3
HS104	0.09976	0.00129	0.22388	0.00294	0.0453	1427.4	0.00137	1695.6
HS105	0.09766	0.00167	0.29528	0.00415	0.07181	1629	0.00202	1725.7
HS106	0.1832	0.00201	0.56939	0.00736	0.18992	2775	0.00218	3197.8
HS107	0.10392	0.00134	0.33145	0.00437	0.0698	1775.7	0.00146	1891
HS108	0.15814	0.00185	0.47742	0.00625	0.14287	2471.6	0.00198	2569.9
HS109	0.12001	0.00154	0.35132	0.00466	0.085	1948.1	0.00168	2194.2
HS110	0.10604	0.00129	0.32718	0.00426	0.06744	1781.8	0.00135	1871.9
HS111	0.09999	0.00143	0.29417	0.00395	0.06394	1645.1	0.00141	1739.3
HS112	0.10106	0.00218	0.30008	0.00459	0.09126	1670.1	0.00235	1662.4
HS113	0.10353	0.00164	0.31997	0.00443	0.07768	1743	0.00135	1773
HS114	0.09977	0.00149	0.27863	0.00378	0.0624	1599.4	0.00133	1724.1
HS115	0.09782	0.00145	0.24597	0.00332	0.05351	1484.9	0.00116	1593.1
HS116	0.09611	0.00205	0.27634	0.00418	0.07933	1562.9	0.00158	1560.4
HS117	0.15973	0.00182	0.46927	0.00611	0.1396	2465	0.00184	2491.7
hs201	0.09893	0.00085	0.28881	0.00375	3.93657	0.06633	0.08539	0.00101
hs202	0.10463	0.00154	0.33863	0.00426	4.88153	0.06842	0.10118	0.00118
hs203	0.10826	0.00127	0.32739	0.00409	4.88288	0.06495	0.09489	0.00123
hs204	0.10441	0.00122	0.34245	0.0043	4.92625	0.06767	0.10149	0.00115
hs205	0.10269	0.00123	0.3151	0.00395	4.45804	0.06105	0.09093	0.00102
hs206	0.10071	0.0012	0.30527	0.00388	4.23557	0.06296	0.08948	0.00109
hs207	0.15664	0.00133	0.49697	0.00622	10.72466	0.14044	0.1297	0.00145
hs208	0.10101	0.00172	0.29458	0.00373	4.09955	0.06045	0.08909	0.00099
hs209	0.10351	0.00132	0.31115	0.00412	4.43718	0.08085	0.093	0.00121
hs210	0.1062	0.00177	0.30997	0.00388	4.53532	0.06072	0.09022	0.00101
hs211	0.09899	0.0012	0.29723	0.00375	4.05347	0.0578	0.0908	0.00116
hs212	0.11162	0.00123	0.33737	0.00425	5.18822	0.07285	0.09831	0.00114
hs213	0.10467	0.00136	0.3112	0.00388	4.48773	0.05917	0.09885	0.00115
hs214	0.1041	0.00116	0.30819	0.00401	4.42006	0.0744	0.09305	0.00111
hs215	0.10256	0.00161	0.29331	0.00371	4.14436	0.06024	0.08381	0.00092
hs216	0.08605	0.00131	0.10469	0.00196	1.24117	0.06317	0.03734	0.00072
hs217	0.10667	0.00448	0.33116	0.00444	4.8668	0.09261	0.09554	0.00127
hs218	0.11781	0.00192	0.36039	0.00464	5.84966	0.09113	0.10402	0.00125
hs219	0.10669	0.00165	0.2991	0.00376	4.39644	0.06064	0.08783	0.00097
hs220	0.13044	0.00126	0.35198	0.0044	6.3255	0.08328	0.09875	0.00108
hs221	0.10208	0.00144	0.29437	0.00372	4.13995	0.06006	0.08567	0.00095
hs222	0.10497	0.0013	0.28332	0.00363	4.09711	0.0636	0.09459	0.00118
hs223	0.09865	0.00147	0.28207	0.00356	3.83366	0.05537	0.08619	0.00101
hs224	0.10582	0.00125	0.302	0.00377	4.40267	0.05854	0.08857	0.00098
hs225	0.11447	0.00119	0.29163	0.00367	4.59912	0.06426	0.10651	0.00117
hs226	0.10527	0.00138	0.30762	0.00394	4.46161	0.06876	0.09119	0.00117
hs227	0.0956	0.00146	0.26993	0.00338	3.55519	0.04877	0.07902	0.00085
hs228	0.09836	0.00112	0.27125	0.00343	3.67559	0.05336	0.07796	0.00086
hs229	0.10851	0.00125	0.32407	0.0042	4.84458	0.07929	0.09399	0.00107

hs230	0.11643	0.00162	0.26996	0.00342	4.33041	0.06254	0.09974	0.00118
hs231	0.10019	0.00168	0.27944	0.00368	3.85737	0.06925	0.08174	0.001
hs232	0.11246	0.0013	0.28816	0.00361	4.46445	0.06055	0.07792	0.00086
hs233	0.10754	0.00135	0.32079	0.00406	4.75295	0.06828	0.09306	0.00121
hs234	0.09662	0.0013	0.27124	0.00345	3.61078	0.0545	0.08129	0.00097
hs235	0.10041	0.00148	0.2963	0.00382	4.09898	0.06619	0.09001	0.00112
hs236	0.13371	0.00235	0.30626	0.00415	5.64183	0.10452	0.11061	0.00149
hs237	0.09928	0.00141	0.27207	0.00349	3.72148	0.0586	0.0813	0.00092
hs238	0.1152	0.00142	0.32386	0.00409	5.14009	0.07286	0.09803	0.00116
hs239	0.09787	0.00139	0.27071	0.00347	3.65005	0.05747	0.08396	0.00095
hs240	0.0989	0.00155	0.27088	0.00352	3.69085	0.06269	0.08016	0.00106
hs241	0.11618	0.00132	0.3367	0.00422	5.38905	0.07233	0.09896	0.0011
hs242	0.10025	0.00127	0.2782	0.00351	3.84236	0.05549	0.08761	0.00098
hs243	0.09329	0.00119	0.19547	0.00246	2.51224	0.03645	0.06081	0.0007
hs115b	0.10168	0.00284	0.28661	0.00376	4.01761	0.11179	0.07372	0.0014
hs116b	0.09366	0.00114	0.20742	0.00234	2.67849	0.03476	0.05638	0.00063
hs117b	0.10814	0.00246	0.26709	0.00335	3.98195	0.09058	0.08825	0.00146
hs118b	0.10005	0.00176	0.27854	0.00332	3.84207	0.06899	0.0825	0.00099
hs201b	0.1015	0.00136	0.28825	0.00331	4.03361	0.05678	0.08259	0.00091
hs202b	0.10972	0.00138	0.30947	0.00353	4.68113	0.06227	0.08802	0.00107
hs203b	0.08236	0.00103	0.14669	0.00166	1.66557	0.02215	0.01305	0.00015
hs204b	0.15475	0.00175	0.45475	0.00515	9.70183	0.11837	0.12721	0.00161
hs205b	0.09472	0.00136	0.25503	0.00294	3.33035	0.04974	0.07596	0.0009
hs206b	0.10802	0.00157	0.33356	0.00388	4.96734	0.07517	0.09185	0.00114
hs207b	0.10504	0.0014	0.31134	0.00357	4.5086	0.06305	0.08863	0.00106
208b	0.09584	0.00156	0.27401	0.00322	3.62063	0.0604	0.07753	0.00102
209b	0.09653	0.00116	0.27145	0.00307	3.61255	0.04625	0.07776	0.00086
210b	0.15781	0.00175	0.49943	0.00564	10.8659	0.13057	0.13478	0.00152
211b	0.10607	0.0013	0.33691	0.00383	4.92685	0.06431	0.09469	0.00111
212b	0.09725	0.00127	0.28648	0.00327	3.84085	0.053	0.07966	0.00087
hs214b	0.09577	0.00131	0.27547	0.00316	3.6373	0.05219	0.08046	0.00095
hs215b	0.10298	0.00148	0.29634	0.00343	4.20738	0.06304	0.0833	0.00093
hs216b	0.10354	0.00133	0.30028	0.00343	4.28648	0.05826	0.08586	0.00101
hs217b	0.11095	0.00127	0.34943	0.00394	5.34513	0.06601	0.09899	0.00107
hs218b	0.10022	0.00106	0.30022	0.00335	4.14829	0.04806	0.08682	0.001
hs219b	0.10055	0.0014	0.29424	0.00339	4.07883	0.05937	0.08506	0.001
hs220b	0.11441	0.00145	0.33883	0.00387	5.34461	0.07162	0.09583	0.00132

Humanity Seat Formation: Age (Ma)								
207/206Pb	1s	206Pb/238U	1s	207/235Pb	1s	208Pb/232Th	is	% conc
1554.3	21.69	1632.4	18.6	1598.3	11.06	1734.3	20.51	102
1584.1	59.37	599.3	10.23	852	17.95	907.3	22.96	97
1619.6	23.95	1302.4	15.49	1427.4	11.28	1695.6	25.41	102
1579.8	31.68	1667.9	20.67	1629	14.66	1725.7	37.43	104
2682.1	17.99	2905.3	30.25	2775	12.54	3197.8	37.67	66
1695.2	23.64	1845.4	21.16	1775.7	12.33	1891	26.91	95
2435.8	19.65	2516	27.28	2471.6	12.72	2569.9	35.27	96
1956.3	22.75	1940.9	22.21	1948.1	12.67	2194.2	30.45	97
1732.4	22.12	1824.7	20.71	1781.8	11.84	1871.9	24.93	104
1623.9	26.35	1662.3	19.68	1645.1	12.85	1739.3	26.11	100
1643.6	39.5	1691.7	22.77	1670.1	17.89	1662.4	43.83	96
1688.3	28.96	1789.6	21.64	1743	14.17	1773	25.08	96
1619.8	27.58	1584.5	19.07	1599.4	13.11	1724.1	24.6	91
1583	27.38	1417.7	17.18	1484.9	12.59	1593.1	21.58	99
1549.9	39.6	1572.9	21.09	1562.9	17.28	1560.4	29.5	98
2452.8	19.12	2480.4	26.79	2465	12.51	2491.7	32.79	81
1604.1	28.66	1635.6	18.75	1621.2	13.64	1656.1	18.9	86
1707.9	22.14	1880.1	20.53	1799.1	11.81	1948.2	21.63	97
1770.2	20.4	1825.7	19.87	1799.3	11.21	1832.3	22.8	99
1704	21.52	1898.5	20.64	1806.8	11.59	1953.7	21.18	106
1673.4	21.51	1765.7	19.37	1723.2	11.36	1759.2	18.81	102
1637.2	24.24	1717.4	19.14	1680.9	12.21	1732.1	20.15	106
2419.7	18.5	2600.7	26.79	2499.6	12.16	2464.9	25.93	104
1642.8	23.97	1664.4	18.6	1654.2	12.04	1725	18.36	102
1688	31.23	1746.4	20.25	1719.3	15.1	1797.4	22.4	103
1735.2	20.65	1740.6	19.07	1737.5	11.14	1746	18.69	95
1605.1	22.99	1677.6	18.62	1645	11.61	1756.7	21.47	103
1826	21.89	1874	20.51	1850.7	11.95	1895.4	21.07	103
1708.6	20.24	1746.6	19.08	1728.7	10.95	1905.3	21.12	102
1698.5	28.3	1731.8	19.76	1716.1	13.94	1798.4	20.59	101
1670.9	23.42	1658.1	18.5	1663.1	11.89	1626.8	17.2	97
1339.3	97.26	641.8	11.44	819.4	28.62	740.9	14.11	45
1743.3	32.61	1844	21.52	1796.5	16.03	1844.3	23.37	104
1923.3	24.96	1984	22.01	1953.8	13.51	2000.2	22.85	102
1743.7	21.56	1686.8	18.64	1711.7	11.41	1701.5	18.03	97
2103.9	19.3	1944.1	20.98	2022	11.54	1903.4	19.82	95
1662.3	23.38	1663.3	18.54	1662.2	11.87	1661.4	17.67	100
1713.7	25.47	1608	18.22	1653.7	12.67	1826.8	21.88	94
1598.8	23.42	1601.8	17.91	1599.8	11.63	1671	18.8	100
1728.6	20.46	1701.2	18.67	1712.8	11	1715.3	18.27	99
1871.6	21.64	1649.6	18.34	1749.1	11.65	2045.7	21.46	89
1719.1	25.2	1729	19.4	1723.9	12.78	1763.8	21.72	100
1539.9	21.93	1540.4	17.17	1539.6	10.87	1537.1	15.9	99
1593.2	23.61	1547.1	17.38	1566.1	11.59	1517.4	16.05	99

1774.5	27.11	1809.6	20.46	1792.7	13.77	1815.7	19.79	100
1902.1	22.61	1540.6	17.37	1699.2	11.91	1921.7	21.61	87
1627.7	30.92	1588.6	18.52	1604.8	14.48	1588.1	18.61	98
1839.5	20.8	1632.3	18.08	1724.4	11.25	1516.5	16.1	89
1758.2	22.74	1793.6	19.8	1776.6	12.05	1798.6	22.34	102
1559.9	25	1547.1	17.48	1551.9	12	1579.7	18.17	99
1631.7	27.07	1672.9	18.98	1654.1	13.18	1742	20.71	103
2147.3	30.38	1722.3	20.47	1922.5	15.98	2120.5	27.18	80
1610.7	26.28	1551.3	17.66	1576	12.6	1579.8	17.23	96
1883	22.06	1808.6	19.93	1842.8	12.05	1890.2	21.36	96
1583.9	26.36	1544.4	17.59	1560.5	12.55	1629.5	17.77	98
1603.5	28.97	1545.3	17.85	1569.4	13.57	1558.5	19.9	96
1898.2	20.33	1870.8	20.33	1883.1	11.49	1907.4	20.21	99
1628.7	23.33	1582.3	17.72	1601.7	11.64	1697.4	18.26	97
1493.7	23.91	1150.9	13.29	1275.6	10.54	1193.1	13.4	77
1654.9	50.9	1624.6	18.85	1637.8	22.62	1437.6	26.39	100
1501.4	22.86	1215.1	12.52	1322.5	9.59	1108.7	12.1	100
1768.2	40.98	1526	17.05	1630.5	18.46	1709.4	27.07	106
1625	32.45	1584	16.76	1601.6	14.47	1602.4	18.51	104
1651.7	24.66	1632.8	16.54	1641	11.45	1604.1	16.98	99
1794.7	22.71	1738.1	17.36	1763.9	11.13	1705.1	19.94	97
1254	24.14	882.4	9.32	995.5	8.44	262.1	2.95	70
2399.1	19.1	2416.3	22.82	2406.9	11.23	2420.3	28.79	101
1522.5	26.83	1464.4	15.1	1488.2	11.66	1479.7	16.84	96
1766.2	26.45	1855.6	18.77	1813.8	12.79	1776	21.15	105
1715	24.28	1747.3	17.56	1732.6	11.62	1716.3	19.6	102
1544.7	30.23	1561.1	16.27	1554.1	13.27	1509.3	19.22	101
1558.1	22.31	1548.1	15.55	1552.3	10.18	1513.5	16.22	99
2432.3	18.67	2611.4	24.25	2511.7	11.17	2555.6	27.16	107
1732.9	22.33	1871.8	18.46	1806.9	11.02	1828.7	20.45	108
1572	24.33	1623.9	16.39	1601.4	11.12	1549.2	16.35	103
1543.4	25.55	1568.5	15.98	1557.7	11.43	1564.2	41.12	102
1678.6	26.4	1673.1	17.07	1675.5	12.29	1617.3	17.33	100
1688.6	23.57	1692.7	16.99	1690.8	11.19	1664.8	18.85	100
1815.1	20.68	1931.9	18.82	1876.1	10.56	1907.8	19.73	106
1628.3	19.54	1692.4	16.61	1663.9	9.48	1682.7	18.58	104
1634.2	25.68	1662.7	16.89	1650.1	11.87	1650	18.68	102
1870.6	22.68	1881.1	18.65	1876	11.46	1849.7	24.28	101

Blue Mine Conglomerate			Radiogenic	ratios				
spot	207/206Pb	1s	206pb/238U	1s	207Pb/235U	1s	208Pb/232Th	1s
bmrow11	0.0963	0.00115	0.2674	0.00319	3.5567	0.04761	0.07878	0.00084
bmrow102	0.10971	0.00172	0.29204	0.00363	4.42528	0.07311	0.11217	0.00156
bmrow103	0.09585	0.00164	0.27724	0.00347	3.67031	0.06548	0.0811	0.00104
bmrow104	0.10453	0.00132	0.29805	0.00358	4.30295	0.05981	0.0881	0.00101
bmrow105	0.10731	0.00134	0.30692	0.00368	4.54887	0.06295	0.09084	0.00109
bmrow106	0.10298	0.00136	0.31219	0.00377	4.44033	0.06403	0.10153	0.00126
bmrow107	0.09912	0.00126	0.27857	0.00334	3.81362	0.05338	0.07262	0.00079
bmrow108	0.10895	0.00137	0.31209	0.00375	4.69649	0.06522	0.07639	0.00094
bmrow109	0.09827	0.00128	0.29081	0.0035	3.94707	0.05644	0.08419	0.00096
bm110	0.09787	0.00172	0.27358	0.00345	3.69811	0.06763	0.08313	0.00109
bm111	0.09708	0.00133	0.25215	0.00305	3.38098	0.05021	0.06161	0.00067
bm112	0.09175	0.00108	0.19455	0.00231	2.46543	0.03252	0.05544	0.00062
bm113	0.09421	0.00115	0.20222	0.00241	2.63127	0.03581	0.05148	0.00059
bm114	0.09857	0.0013	0.22934	0.00276	3.12233	0.04488	0.066	0.00071
bm115	0.09768	0.00124	0.26803	0.00321	3.61606	0.05056	0.07494	0.00089
bm116	0.09687	0.00114	0.23611	0.00281	3.15922	0.04159	0.06434	0.00072
bm117	0.10058	0.00128	0.27054	0.00325	3.75844	0.05266	0.0627	0.00078
bm118	0.09905	0.0013	0.27524	0.00332	3.76558	0.05399	0.08432	0.00102
bm119	0.09592	0.00173	0.27132	0.00343	3.59441	0.06714	0.08207	0.00119
bm120	0.09823	0.00144	0.26834	0.00328	3.64049	0.05716	0.07746	0.00109
bm121	0.09692	0.00162	0.19803	0.00246	2.6509	0.04639	0.06283	0.00076
bm122	0.1007	0.00138	0.26215	0.00318	3.64601	0.05411	0.07493	0.00083
bm123	0.09897	0.00127	0.27198	0.00327	3.71761	0.05246	0.08022	0.00102
bm124	0.09804	0.00114	0.2746	0.00326	3.7182	0.0486	0.08041	0.00091
bm125	0.0984	0.00179	0.26434	0.00335	3.59256	0.06778	0.07527	0.00093
bm126	0.08592	0.00107	0.13459	0.0016	1.59713	0.02204	0.05403	0.0006
bmrow127	0.09552	0.00124	0.25827	0.0031	3.40753	0.0484	0.07567	0.00085
bmrow129	0.11267	0.00145	0.32313	0.0039	5.02839	0.07108	0.09057	0.00109
bmrow130	0.10126	0.00159	0.27118	0.00336	3.79272	0.06302	0.07845	0.00095
bmrow131	0.09862	0.00125	0.26541	0.00318	3.61511	0.05054	0.07457	0.00091
bmrow132	0.11007	0.00234	0.31237	0.00415	4.74893	0.10261	0.09404	0.00151
bmrow133	0.09534	0.00123	0.18596	0.00223	2.44873	0.03467	0.01851	0.00022
bmrow134	0.09672	0.00202	0.27264	0.00356	3.6421	0.07776	0.07862	0.00135
bmrow136	0.09482	0.00134	0.22062	0.00268	2.88937	0.0439	0.07158	0.00094
bmrow137	0.08528	0.00146	0.13004	0.00161	1.53173	0.02739	0.05418	0.00071
bmrow138	0.08818	0.00104	0.1496	0.00177	1.82208	0.02402	0.04437	0.00047
bmrow139	0.10295	0.00122	0.23479	0.0028	3.3384	0.04427	0.05603	0.00061
bmrow140	0.09642	0.00134	0.23736	0.00288	3.16106	0.04739	0.05338	0.00057
bmrow141	0.07856	0.00117	0.1952	0.00237	2.11807	0.03375	0.0579	0.00066
bmrow142	0.09227	0.00125	0.21897	0.00264	2.79054	0.04095	0.05806	0.0007
bmrow143	0.09924	0.00149	0.23336	0.00286	3.19869	0.05123	0.06637	0.00079
bmrow144	0.0839	0.00112	0.08365	0.001	0.96926	0.01406	0.01371	0.00016
bmrow145	0.09717	0.00163	0.26064	0.00325	3.498	0.0613	0.07498	0.00109
bmrow146	0.07817	0.00102	0.10398	0.00124	1.12273	0.01609	0.0283	0.00029

bmrow147	0.1	0.00193	0.27122	0.00348	3.74591	0.07433	0.07877	0.00124
bmrow148	0.09788	0.00139	0.25706	0.00313	3.47519	0.05323	0.07586	0.00088
bmrow149	0.09889	0.00163	0.21509	0.00268	2.93782	0.05079	0.0304	0.00044
bmrow150	0.09873	0.00123	0.24954	0.00299	3.40285	0.04682	0.0572	0.00066
bmrow151	0.09622	0.00115	0.21614	0.00257	2.87238	0.0384	0.04866	0.0005
bmrow152	0.09488	0.00112	0.23013	0.00274	3.01566	0.03984	0.05182	0.00058
bmrow201	0.09848	0.00124	0.22966	0.00275	3.12375	0.04328	0.05495	0.00062
bmrow202	0.09866	0.00115	0.27414	0.00326	3.73558	0.04891	0.0818	0.00093
bmrow203	0.09349	0.00145	0.26801	0.0033	3.46061	0.05685	0.08058	0.00105
bmrow204	0.09689	0.0014	0.26825	0.00327	3.5898	0.05575	0.07834	0.00093
bmrow205	0.1014	0.0017	0.26814	0.00335	3.75536	0.06578	0.08163	0.00115
bmrow206	0.09227	0.00115	0.21985	0.00263	2.80167	0.03867	0.05217	0.00054
bmrow207	0.09463	0.00124	0.19982	0.0024	2.61149	0.03739	0.05802	0.00065
bmrow208	0.09893	0.00119	0.22864	0.00273	3.12423	0.04202	0.04967	0.00057
bmrow209	0.09769	0.0012	0.24515	0.00293	3.30761	0.04515	0.07218	0.00077
bmrow210	0.10164	0.00126	0.27411	0.00328	3.84795	0.05299	0.08276	0.00089
bmrow211	0.09611	0.00137	0.27085	0.0033	3.59555	0.05509	0.08129	0.00091
bmrow212	0.1122	0.00127	0.32314	0.00383	5.0076	0.06417	0.09294	0.00102
bmrow213	0.09631	0.00126	0.2501	0.00301	3.32685	0.04766	0.07273	0.00084
bmrow214	0.08992	0.00135	0.15259	0.00186	1.89519	0.03021	0.03386	0.00035
bmrow215	0.09839	0.00126	0.26842	0.00322	3.64783	0.05146	0.08126	0.00089
bmrow216	0.09548	0.00139	0.2461	0.003	3.24549	0.05055	0.07923	0.00103
bmrow217	0.0973	0.00143	0.25746	0.00315	3.45997	0.05437	0.08141	0.00097
bmrow218	0.09431	0.00125	0.20593	0.00248	2.6825	0.03876	0.05884	0.0007
bmrow219	0.09811	0.00135	0.26364	0.0032	3.57265	0.05333	0.07968	0.00084
bmrow220	0.13473	0.00198	0.32754	0.00407	6.09533	0.09523	0.14132	0.00186
bmrow221	0.16897	0.00266	0.10245	0.00129	2.39086	0.03914	0.14167	0.0017
bmrow222	0.09717	0.00229	0.28638	0.00384	3.84349	0.09175	0.08253	0.00183
bmrow223	0.10421	0.00148	0.3035	0.00371	4.36825	0.06682	0.08773	0.0011
bmrow224	0.10206	0.00248	0.26396	0.00362	3.72086	0.09104	0.07961	0.00144
bmrow225	0.09323	0.00116	0.15799	0.00189	2.03454	0.02805	0.04732	0.00053
bmrow226	0.09759	0.00199	0.28575	0.00372	3.85175	0.08015	0.08488	0.00152
bmrow227	0.09766	0.00125	0.26034	0.00312	3.5115	0.04935	0.07367	0.0008
bmrow228	0.0977	0.00155	0.17524	0.00216	2.36466	0.03957	0.07297	0.00094
bmrow229	0.09802	0.0012	0.27117	0.00324	3.67126	0.04984	0.07866	0.00096
bmrow230	0.09703	0.00115	0.14062	0.00167	1.88451	0.02507	0.04706	0.0005
bmrow231	0.07553	0.00163	0.1871	0.00238	1.95166	0.04306	0.05467	0.00077
bmrow232	0.10151	0.00119	0.28584	0.0034	4.00777	0.05281	0.08026	0.00084
bmrow233	0.09396	0.00142	0.26519	0.00324	3.4413	0.0555	0.07902	0.00094
bmrow234	0.08257	0.00217	0.11915	0.00161	1.35881	0.03572	0.05363	0.00106
bmrow235	0.09734	0.00124	0.27776	0.00333	3.73436	0.05244	0.07958	0.00085
bmrow236	0.174	0.00187	0.30313	0.00359	7.28511	0.09002	0.06997	0.00077
bmrow237	0.10784	0.00131	0.29887	0.00357	4.45174	0.06018	0.08611	0.00101
bmrow238	0.09662	0.00121	0.28118	0.00336	3.75237	0.05193	0.07997	0.00088
bmrow239	0.09874	0.0016	0.26092	0.00322	3.5585	0.06079	0.07537	0.00095
bmrow240	0.09821	0.00142	0.28368	0.00346	3.84809	0.05955	0.08002	0.00095

bmrow241	0.09679	0.00109	0.2174	0.00257	2.9061	0.03711	0.0487	0.00052
bmrow242	0.09952	0.00117	0.25712	0.00306	3.53436	0.04661	0.06936	0.00076
bmrow243	0.09775	0.00107	0.26963	0.00318	3.64019	0.04568	0.07776	0.00082
bmrow244	0.11643	0.0013	0.33695	0.00399	5.41831	0.06871	0.09479	0.00103
bmrow245	0.0924	0.00132	0.13538	0.00164	1.7276	0.0265	0.05133	0.00065
bmrow246	0.09986	0.00139	0.28806	0.0035	3.97321	0.05973	0.08024	0.00089
bmrow247	0.09705	0.00133	0.27094	0.00328	3.63175	0.05381	0.07989	0.00087
bmrow248	0.09513	0.00192	0.24752	0.00315	3.2523	0.06729	0.07181	0.00102
bmrow249	0.10537	0.00121	0.28655	0.0034	4.17045	0.05405	0.06389	0.00071

Blue Mine Conglomerate: Age (Ma)								
207/206Pb	1s	206Pb/238U	1s	207/235Pb	1s	208Pb/232Th	1s	% conc
1553.7	22.33	1527.6	16.2	1539.9	10.61	1532.7	15.65	101
1794.6	28.22	1651.7	18.1	1717.1	13.68	2148.8	28.26	100
1544.9	31.76	1577.4	17.52	1564.9	14.24	1576.2	19.36	116
1706	23.01	1681.6	17.77	1693.9	11.45	1706.5	18.77	106
1754.2	22.69	1725.6	18.17	1740	11.52	1757.5	20.23	105
1678.5	24.2	1751.5	18.52	1719.9	11.95	1954.6	23.2	105
1607.6	23.51	1584.2	16.85	1595.6	11.26	1416.9	14.87	97
1782	22.81	1751	18.43	1766.6	11.63	1487.9	17.6	103
1591.5	24.2	1645.6	17.49	1623.4	11.58	1633.9	17.87	107
1583.9	32.52	1559	17.44	1571	14.62	1614	20.28	73
1568.8	25.47	1449.5	15.71	1500	11.64	1208.5	12.69	96
1462.2	22.15	1146	12.47	1262	9.53	1090.5	11.96	86
1512.3	22.96	1187.2	12.93	1309.4	10.01	1014.7	11.39	84
1597.3	24.36	1331	14.48	1438.2	11.05	1291.8	13.38	80
1580.3	23.55	1530.8	16.34	1553.1	11.12	1460.7	16.72	100
1564.8	21.81	1366.5	14.63	1447.3	10.15	1260.3	13.6	87
1634.9	23.46	1543.6	16.47	1583.9	11.24	1229.1	14.83	94
1606.4	24.25	1567.3	16.76	1585.4	11.5	1636.2	18.96	100
1546.2	33.47	1547.5	17.39	1548.3	14.84	1594.3	22.32	104
1590.7	27.18	1532.4	16.67	1558.4	12.51	1507.9	20.51	99
1565.7	31.04	1164.7	13.25	1314.9	12.9	1231.6	14.47	77
1637	25.23	1500.8	16.22	1559.6	11.83	1460.4	15.63	94
1604.7	23.76	1550.8	16.56	1575.2	11.29	1559.8	19.05	99
1587.1	21.54	1564.1	16.5	1575.3	10.46	1563.3	17.09	101
1594	33.66	1512	17.09	1547.9	14.98	1466.8	17.4	96
1336.3	23.99	814	9.12	969.1	8.62	1063.6	11.48	62
1538.4	24.16	1538.4	15.9	1506.1	11.15	1474.3	15.95	97
1842.9	23.14	1842.9	19	1824.1	11.97	1752.4	20.27	95
1647.3	28.89	1647.3	17.02	1591.2	13.35	1526.6	17.82	98
1598.2	23.5	1598.2	16.22	1552.9	11.12	1453.7	17.1	99
1800.6	38.16	1800.6	20.4	1775.9	18.12	1816.6	27.83	73
1534.8	24.1	1534.8	12.12	1257.1	10.21	370.8	4.33	103
1561.8	38.74	1561.8	18.02	1558.8	17.01	1529.6	25.22	93

1524.5	26.35	1285.2	14.13	1379.1	11.46	1397.4	17.68	60
1321.9	32.93	788.1	9.18	943.2	10.98	1066.5	13.68	67
1386.4	22.33	898.7	9.95	1053.4	8.64	877.4	9.09	84
1677.9	21.72	1359.5	14.59	1490.1	10.36	1101.8	11.63	91
1556	25.81	1373	14.98	1447.7	11.56	1051.2	10.88	101
1161.1	29.29	1149.5	12.78	1154.7	10.99	1137.7	12.66	88
1472.8	25.52	1276.4	13.96	1353	10.97	1140.8	13.28	88
1609.9	27.8	1352.1	14.96	1456.8	12.39	1298.8	14.91	37
1290.1	25.72	517.8	5.96	688.1	7.25	275.3	3.2	40
1570.5	31.03	1493.1	16.62	1526.8	13.84	1461.4	20.48	93
1151.3	25.78	637.7	7.26	764.3	7.7	564.1	5.74	98
1624	35.48	1547	17.67	1581.2	15.9	1532.5	23.26	55
1584.1	26.41	1474.8	16.04	1521.6	12.08	1478	16.45	60
1603.3	30.47	1255.9	14.19	1391.7	13.1	605.2	8.58	91
1600.3	23.02	1436.1	15.4	1505.1	10.8	1124.4	12.65	92
1552.1	22.31	1261.4	13.64	1374.7	10.07	960.4	9.72	71
1525.6	22.02	1335.2	14.33	1411.6	10.07	1021.2	11.14	88
1595.5	23.25	1332.7	14.41	1438.6	10.66	1081.1	11.84	78
1599	21.55	1561.8	16.48	1579	10.49	1589.2	17.35	85
1497.8	29.03	1530.7	16.76	1518.3	12.94	1566.3	19.6	83
1565.1	26.91	1531.9	16.63	1547.3	12.33	1524.6	17.36	97
1649.9	30.72	1531.3	17.05	1583.3	14.05	1586	21.52	97
1472.8	23.61	1281.1	13.88	1356	10.33	1027.9	10.44	96
1520.6	24.49	1174.3	12.9	1303.9	10.51	1139.9	12.37	92
1604.1	22.34	1327.4	14.3	1438.7	10.35	979.8	11.06	86
1580.5	22.84	1413.4	15.16	1482.8	10.64	1408.7	14.53	75
1654.3	22.89	1561.6	16.61	1602.8	11.1	1607.1	16.6	82
1550	26.52	1545.1	16.71	1548.5	12.17	1579.7	17.09	86
1835.3	20.33	1805.1	18.68	1820.6	10.85	1796.3	18.87	93
1553.9	24.39	1439	15.52	1487.4	11.18	1419	15.8	99
1423.8	28.3	915.5	10.4	1079.4	10.59	673.1	6.87	95
1593.9	23.79	1532.8	16.39	1560	11.24	1579	16.57	92
1537.6	27.11	1418.3	27.11	1468.1	12.09	1468.1	19.32	63
1573	27.28	1476.8	27.28	1518.1	12.38	1518.1	18.1	105
1514.4	24.79	1207.1	24.79	1323.6	10.69	1323.6	13.39	92
1588.6	25.57	1508.4	25.57	1543.5	11.84	1543.5	15.64	94
2160.6	25.36	1826.5	25.36	1989.6	13.63	1989.6	32.95	80
2547.4	26.15	628.7	26.15	1239.9	11.72	1239.9	30.06	95
1570.5	43.58	1623.4	43.58	1601.9	19.23	1601.9	34.14	85
1700.4	25.98	1708.6	25.98	1706.4	12.64	1706.4	20.49	25
1661.9	44.39	1510.1	44.39	1575.9	19.58	1575.9	27.02	103
1492.7	23.42	945.6	23.42	1127.1	9.39	1127.1	10.24	100
1578.6	37.61	1620.3	37.61	1603.6	16.77	1603.6	28.27	91
1579.9	23.71	1491.6	23.71	1529.8	11.11	1529.8	15.14	63
1580.7	29.45	1040.9	29.45	1232	11.94	1232	17.62	103
1586.8	22.65	1546.7	22.65	1565.1	10.83	1565.1	17.96	94

1567.8	22.14	848.2	22.14	1075.7	8.83	929.5	9.66	66
1082.5	42.69	1105.6	42.69	1099	14.81	1075.9	14.8	97
1652	21.58	1620.7	21.58	1635.8	10.71	1560.5	15.68	54
1507.2	28.34	1516.3	28.34	1513.9	12.69	1537.2	17.53	102
1259	50.41	725.7	50.41	871.4	15.37	1056	20.26	98
1573.8	23.69	1580.1	23.69	1578.8	11.25	1547.6	15.88	101
2596.5	17.83	1706.8	17.83	2147	11.03	1367	14.52	58
1763.3	21.98	1685.7	21.98	1722	11.21	1669.6	18.79	100
1559.9	23.29	1597.3	23.29	1582.6	11.09	1555	16.41	66
1600.5	29.95	1494.6	29.95	1540.3	13.54	1468.8	17.9	96
1590.5	26.7	1609.9	17.37	1602.9	12.47	1556	17.77	102
1563.1	20.93	1268.1	13.62	1383.5	9.65	961.2	10.05	93
1615.2	21.72	1475.1	15.68	1534.9	10.44	1355.5	14.36	101
1581.6	20.37	1538.9	16.17	1558.4	10	1513.7	15.46	81
1902.1	19.88	1872	19.25	1887.8	10.87	1830.4	19.06	91
1475.4	26.99	818.5	9.32	1018.9	9.86	1011.7	12.55	97
1621.5	25.66	1631.8	17.49	1628.7	12.19	1560	16.62	98
1568.2	25.37	1545.6	16.62	1556.5	11.8	1553.5	16.24	55
1530.7	37.45	1425.7	16.26	1469.7	16.07	1401.7	19.22	101
1720.9	20.93	1624.3	17.04	1668.2	10.61	1251.8	13.54	99

KEY

- Lithological boundary
- Unconformable lithological boundary
- Inferred lithological boundary
- Synclinal axial trace
- Anticlinal axial trace
- Fault
- Inferred fault
- Bedding
- S_z foliation
- L_z lineation
- Fold plunge

LEGEND

PALAEOZOIC

ORDOVICIAN INTRUSIVES

PEGMATITIC INTRUSIVES: coarsely crystalline sodic leucogranites and granitic pegmatites.

NEOPROTEROZOIC

ADELAIDEAN

TORRENSIAN

UPPER BURRA GROUP

OPAMINDA FORMATION: Fine-grained green, actinolitic shales, dolomites and interbeds of dark grey silts and fine sands preserving mudcracks and ripple marks.

WILLOURAN

LOWER BURRA GROUP

BLUE MINE CONGLOMERATE: Medium-grained, arkosic conglomerate with occasional heavy mineral laminations and cross-stratification. Heterogeneous, coarse sand-cobble size, sub-rounded clasts derived from underlying lithologies. Transitional package of gritty, clast poor micaceous arenite in underlying sedimentary contact.

WOODNAMOKA FORMATION: Highly variable meta-sedimentary unit of well laminated silty phyllites, biotite-andalusite-schists, medium-grained sandstones and micaceous arenites. Variable metamorphic grade with coarse, low-grade units displaying heavy mineral laminations and cross-stratification.

OLIPHANT ARKOSE MEMBER: Sub-basal member of medium- to coarse-grained pink-red weathering arkosic sandstone. Extensive heavy mineral laminations and cross-

ARKAROOLA CREEK BRECCIA MEMBER: Polymictic sedimentary breccia; pebble-cobble size clasts with a medium grained, quartzose, sandstone matrix.

HUMANITY SEAT FORMATION: Medium-grained, heavy mineral laminated meta-sandstone with interbedded massive quartzites and purple-grey shales. Extensive cross-stratification, scour & fills and ripple marks.

CALLANNA GROUP

WOOLTANA VOLCANICS: Grey-green to red-purple weathering basalts with porphyroblastic, vesicular and amygdaloidal textures in flows with minor meta-sedimentary interbeds. Abundance of metasomatic actinolite and epidote with minor anhydrite and tremolite.

WYWYWANA FORMATION: Actinolitic marbles, minor calc-silicate rocks and meta-siltstones. Fault related metasomatism to massive, actinolite rubbles.

PARALANA QUARTZITE: Medium-grained, massive, pink to grey weathering orthoquartzites, with argillaceous interbeds. Rare ripple marks and heavy mineral laminations. Basal sub-unit of poorly-sorted, grey-red weathering arkosic arenite. Fine sericite-kaolinite matrix between coarse, predominantly felspathic grit.

MESOPROTEROZOIC

CARPENTARIAN

MT. PAINTER BASEMENT COMPLEX

MOUNT NEIL GRANITE PORHYRY: Granite porphyry with phenocrysts of blue-quartz. Locally mylonotised at contact with Adelaidean cover sequence.

500 m

Geological map of the Arkaroola area

A.Job, R. Hansberry, 2011